

AN ANALYZING MODEL OF STRESS-RELATED WELLBORE STRENGTHENING
TECHNIQUES

A Thesis

by

HUSSAIN IBRAHIM H ALBAHRANI

Submitted to the Office of Graduate and Professional Studies of
Texas A&M University
in partial fulfillment of the requirements for the degree of

MASTER OF SCIENCE

Chair of Committee,	Samuel F. Noynaert
Committee Members,	Jerome J. Schubert
	Marcelo Sanchez
Head of Department,	A. Daniel Hill

August 2015

Major Subject: Petroleum Engineering

Copyright 2015 Hussain Ibrahim H AlBahrani

ABSTRACT

One of the major causes of nonproductive time (NPT) and the resulting additional costs during drilling operations is lost circulation. The problem of lost circulation is an ever growing concern to the operators for several reasons, including the continuous depletion of reservoirs and the naturally occurring narrow drilling window due to an abnormally pressured interval or simply the low fracture pressure gradient of the formation rock. To deal with the issue of lost circulation, the concept of wellbore strengthening was introduced. The ultimate goal of this concept is to increase the drilling fluid pressure required to fracture the formation; thus, eliminating lost circulation and NPT and reducing the costs. Numerous wellbore strengthening techniques were created for this purpose over the years. Those techniques vary in their applicability to different scenarios and their effectiveness. Therefore, there is a clear need for a tool that will help to define the most suitable wellbore strengthening technique for a well-defined scenario.

The model described in this study aims to provide a practical tool that evaluates and predicts the performance of wellbore strengthening techniques in practical situations. The wellbore strengthening techniques covered by the model use stress changes around the wellbore as the primary criteria for enhancing the fracture pressure and effectively enlarging the drilling window. The model uses geometric principles, basic rock mechanics data, linear elasticity plane stress theory, drilling fluid data, and geological data to evaluate and predict the performance of a wellbore strengthening

technique. Another important objective of the model is the proper selection of candidates for wellbore strengthening. To achieve that goal, the model creates all of the possible scenarios in terms of well placement, surface location, and trajectory based on the input data to emphasize the scenario that will yield maximum results using a specific wellbore strengthening technique.

The use of the model is illustrated through the use of a case study. The results of the case study show practical advantages of applying the model in the well planning phase. The analysis performed using the model will demonstrate the applicability of a certain wellbore strengthening technique, the effectiveness of the technique, and the best parameters for the technique. Therefore, the analysis shows not only the best case scenario for applying a wellbore strengthening technique, but it also illustrates the cases where applying the technique should be avoided due to an expected unsatisfactory performance.

DEDICATIONS

I would like to dedicate this work to my family, especially my father for passing his work ethics on to me and my mother for all her devotion and sacrifice. I would also like to dedicate this work to my fiancée Sara, who remained patient and supportive of this endeavor from overseas for two long years.

ACKNOWLEDGEMENTS

I would like to acknowledge the following for their invaluable contributions to the process of completing this work and for supporting me throughout this undertaking.

I would first like to acknowledge my committee chair, Dr. Samuel F. Noynaert, for his support, guidance, and most importantly for providing me with the best possible environment to do this work. I would also like to thank my committee members, Dr. Jerome J. Schubert and Dr. Marcelo Sanchez, for being the source for many of the ideas used to accomplish this work through their taught courses and for their time and effort spent in making sure this research is accurate.

I would also like to express my deep appreciation for Mr. Fred Dupriest for inspiring me the main idea of this research and for his instrumental contributions that followed.

I would be remiss if I did not acknowledge my sponsor and my employers, Saudi Aramco, especially my supervisor, Mr. Nasser Khanferi, for believing in me and giving me this tremendous opportunity to expand my knowledge and improve my skills as a researcher.

Finally, my sincere and everlasting gratitude for all the help I received from all the faculty, students, and staff in the Texas A&M University Petroleum Engineering Department, especially my great friend Zuhair Al-yousef.

TABLE OF CONTENTS

	Page
ABSTRACT	ii
DEDICATIONS	iv
ACKNOWLEDGEMENTS	v
TABLE OF CONTENTS	vi
LIST OF FIGURES	viii
LIST OF TABLES	xiii
 1. INTRODUCTION.....	 1
1.1 Wellbore Strengthening Definition	1
1.2 Objectives	4
 2. MODEL DESCRIPTION	 6
2.1 Model Introduction	6
2.2 In-Situ Stress Transformation	7
2.2.1 In-Situ Stress Description	7
2.2.2 The Transformation to the Wellbore Coordinates	11
2.3 Induced Borehole Stresses	16
2.4 Plane Stress Transformation	20
2.5 Model Assumptions and the Corresponding Implications and Corrections	31
2.6 The Evaluation of Fracture-Pressure Gradient Enhancement	41
2.6.1 Evaluation of Wellbore Strengthening Techniques from Basic Rock Mechanics	44
2.7 Model Interface	52
 3. MODEL RESULTS AND ANALYSIS (CASE STUDY SCENARIO).....	 63
3.1 The Case Study Setup	63
3.2 The Preliminary Results	66
3.3 Wellbore Strengthening Evaluation Data and Preliminary Results	68
3.4 Parametric Analysis	70
3.4.1 First Stage Parametric Analysis	72

3.4.1.1 First stage Poisson's ratio analysis.....	73
3.4.1.2 First stage Young's modulus analysis.....	75
3.4.1.3 First stage wellbore azimuth analysis.....	78
3.4.1.4 First stage wellbore inclination analysis	79
3.4.2 Second Stage Parametric Analysis.....	83
3.4.2.1 Second stage Poisson's ratio analysis	83
3.4.2.2 Second stage Young's modulus analysis.....	87
3.4.2.3 Second stage wellbore inclination analysis	89
3.4.2.4 Second stage wellbore diameter analysis	92
3.4.2.5 Second stage fracture aperture analysis.....	94
3.4.2.6 Second stage fracture toughness analysis.....	97
3.4.2.7 Second stage fracture plug placement analysis	99
3.4.2.8 Second stage fracture-pressure buildup analysis.....	101
3.4.3 Well Placement Evaluation	104
4. CONCLUSIONS	118
NOMENCLATURE.....	120
REFERENCES	126

LIST OF FIGURES

	Page
Fig. 1 - A general illustration of a drilling window (Mitchell et al. 2011).	2
Fig. 2 - The world in-situ stress map showing direction and magnitude of stresses (Tingay et al 2006).	8
Fig. 3 - The pattern of borehole breakout and induced fractures on reference to the direction of the earth in-situ stresses direction (Dupreist et al. 2008).....	9
Fig. 4 - The estimation of the maximum horizontal stress based on the shape of the borehole (Duffadar et al. 2013).	10
Fig. 5 - The relationship between the in-situ stresses reference frame and the defined wellbore section reference frame (Watson et al. 2003).....	12
Fig. 6 - The concentration of stress due to the presence of a wellbore.	16
Fig. 7 - The illustration of the resulting induced stress acting on an element of the wellbore (Amadei et al. 1997b).....	20
Fig. 8 - The contrast between determining the direction of the fracture in a vertical section and in a horizontal section.	22
Fig. 9 - The relationship between the induced stresses reference frame and the plane stresses reference frame.	24
Fig. 10 - Illustration of the resulting principle stresses acting on the plane of zero shears containing the induced fractures.	27
Fig. 11 - The geometry used to derive the equation for the principle stresses acting directly on the fracture plane.....	28
Fig. 12 - The location of the critical angle θ_c	31
Fig. 13 - The effect of in-situ earth stress field on the shape of the borehole (Duffadar et al. 2013).....	34

Fig. 14 - The local change to the pore pressure due to mud filtration (Watson et al. 2003).....	35
Fig. 15 - Illustration of the change undergone by the effective hoop stress as a result of wellbore wall flow due to overbalance.	37
Fig. 16 - Illustration of the effect of the buildup of filter-cake as a drop in pressure from the wellbore to the sand face due to its impermeable nature.	38
Fig. 17 -The contrast between the bottomhole formation and bottomhole fluid temperatures and the temperature of the drilling fluid (Raymond 1969).....	39
Fig. 18 - The resulting narrower drilling window due to reservoir depletion.	42
Fig. 19 - The three mode of fracture loadings or openings according to fracture mechanics (Jaeger et al. 2007).	45
Fig. 20 - The description of the sealed fracture scenario of particle and fracture interaction in wellbore strengthening (Morita et al. 2012).....	47
Fig. 21 - The description of the plugged fracture scenario of particle and fracture interaction in wellbore strengthening (Morita et al. 2012).....	50
Fig. 22 - The command buttons used in the model to obtain the initial results.	53
Fig. 23 - The user form that enables the model to select the particle and fracture interaction scenario and input the data for each scenario.....	55
Fig. 24 - The user form that enables selecting the base variable for the initial parametric analysis.	56
Fig. 25 - The user form that enables selecting the base variable for the final parametric analysis.	58
Fig. 26 - Ease of drilling data user form.	60
Fig. 27 - Samples of the produced polar plots highlighting the differences between them each type.....	62
Fig. 28 - Description of the case study well trajectory and position with respect to the in-situ stresses (Watson et al. 2003).....	65
Fig. 29 - The results of the Poisson's ratio first stage parametric analysis showing a decrease in the fracture gradient with the increasing Poisson's ratio values.	74

Fig. 30 - The definition of the Young's modulus as the slope of the stress versus strain plot (Watson et al. 2003).	76
Fig. 31 - The results of the Young's modulus first stage parametric analysis showing an increase in the fracture gradient with the increasing Young modulus values. 77	
Fig. 32 - The results of the wellbore azimuth angle first stage parametric analysis.	78
Fig. 33 - The results of the wellbore inclination angle first stage parametric analysis showing a decrease in the fracture gradient with the increasing inclination angle.	79
Fig. 34 - A magnified section of the graph of the results of the wellbore inclination angle first stage parametric analysis showing a slight increase in the fracture gradient with the increasing inclination angle.....	81
Fig. 35 - The results of the Poisson's ratio second stage sealed fracture strengthening parametric analysis showing an increase in the fracture gradient with the increasing Poisson's ratio values.....	84
Fig. 36 - The results of the Poisson's ratio second stage plugged fracture strengthening parametric analysis showing an increase in the fracture gradient with the increasing Poisson's ratio values.....	84
Fig. 37 - The illustration of the load reversal after applying the wellbore strengthening technique due to the action of the Poisson ratio.	86
Fig. 38 - The results of the Young's modulus second stage sealed fracture strengthening parametric analysis showing an increase in the fracture gradient with the increasing Young modulus values.....	87
Fig. 39 - The results of the Young's modulus second stage plugged fracture strengthening parametric analysis showing an increase in the fracture gradient with the increasing Young modulus values.....	88
Fig. 40 - The results of the wellbore inclination angle second stage sealed fracture strengthening parametric analysis.	90
Fig. 41 - The results of the wellbore inclination angle second stage plugged fracture strengthening parametric analysis.	90

Fig. 42 - The results of the wellbore diameter second stage sealed fracture strengthening parametric analysis showing a decrease in the fracture gradient with the increasing wellbore diameter.	92
Fig. 43 - The results of the wellbore diameter second stage plugged fracture strengthening parametric analysis showing a decrease in the fracture gradient with the increasing wellbore diameter.	93
Fig. 44 - The results of the fracture aperture second stage sealed fracture strengthening parametric analysis showing an increase in the fracture gradient with the increasing fracture aperture.	94
Fig. 45 - The results of the fracture aperture second stage plugged fracture strengthening parametric analysis showing an increase in the fracture gradient with the increasing fracture aperture.	95
Fig. 46 - The effect of fracture aperture and particle size on the enhancement of tangential stress.	96
Fig. 47 - The effect of fracture aperture and particle size on the enhancement of tangential stress illustrated by finite element analysis (Duffadar et al. 2013).	97
Fig. 48 - The results of the fracture toughness second stage sealed fracture strengthening parametric analysis showing an increase in the fracture gradient with the increasing fracture toughness.	98
Fig. 49 - The results of the fracture toughness second stage plugged fracture strengthening parametric analysis showing an increase in the fracture gradient with the increasing fracture toughness.	98
Fig. 50 - The results of the fracture plug placement second stage plugged fracture strengthening parametric analysis showing a decrease in the fracture gradient with the increasing fracture plug placement.....	99
Fig. 51 - The results of the fracture pressure buildup second stage sealed fracture strengthening parametric analysis showing a decrease in the fracture gradient with the increasing fracture pressure buildup.	102
Fig. 52 - The results of the fracture pressure buildup second stage plugged fracture strengthening parametric analysis showing a decrease in the fracture gradient with the increasing fracture pressure buildup.	102
Fig. 53 - The resulting ease of drilling plot based on a maximum gradient for the initial fracture pressure gradient.....	106

Fig. 54 - The resulting ease of drilling plot based on a constant reference value for the initial fracture pressure gradient.....	108
Fig. 55 - The resulting ease of drilling plot based on a maximum gradient for the mud filtrate and temperature affected fracture pressure gradient.....	109
Fig. 56 - The resulting ease of drilling plot based on a constant reference value for the mud filtrate and temperature affected fracture pressure gradient.....	110
Fig. 57 - The resulting ease of drilling plot based on a maximum gradient for the fracture pressure gradient after applying sealed fracture wellbore strengthening.	111
Fig. 58 - The resulting ease of drilling plot based on a constant reference value for the fracture pressure gradient after applying sealed fracture wellbore strengthening.	112
Fig. 59 - The resulting ease of drilling plot based on a maximum gradient for the fracture pressure gradient after applying plugged fracture wellbore strengthening.	114
Fig. 60 - The resulting ease of drilling plot based on a constant reference value for the fracture pressure gradient after applying plugged fracture wellbore strengthening.	115
Fig. 61 - A comparison to illustrate the varying fracture wellbore strengthening performance in different drilling directions.	117

LIST OF TABLES

	Page
Table 1 - The initial input values for the model case study.	64
Table 2 - The model preliminary results.	67
Table 3 - Input data describing the interaction between the induced fractures and the solid particles for the wellbore strengthening part of the model case study.	69
Table 4 - The initial result of the wellbore strengthening performance evaluation from the model case study.....	70
Table 5 - The range of Young's modulus and Poisson's ratio used for the parametric analysis (Fjaer et al. 2008).	74
Table 6 - A comparison to illustrate the varying sealed fracture wellbore strengthening performance in varying wellbore positions.	113
Table 7 - A comparison to illustrate the varying plugged fracture wellbore strengthening performance in varying wellbore positions.	116

1. INTRODUCTION

1.1 Wellbore Strengthening Definition

The continuous depletion of hydrocarbon-bearing reservoirs coupled with the ever increasing depth of well target zones has led to new drilling challenges in the form of narrow drilling windows as illustrated in **Fig. 1**. The drilling window being referred to here is defined as the range of the drilling fluid pressure that is equal to or greater than the formation pore pressure to prevent flow from the reservoir, and less than the formation fracture pressure to avoid fracturing the formation. Abnormally pressured zones, fractured formations, and low-fracture-pressure gradient zones are all leading causes of the narrow drilling windows. Faced with this challenge, drillers are forced to restrict the wellbore pressure values to a small range with negligible margin for error. A number of techniques were created to help achieve this goal such as managed pressure drilling (Nas 2010). However, employing such techniques require additional equipment, additional personnel training and, as a result, additional costs. While these techniques are well proven, employing them is not economically viable in certain situations.

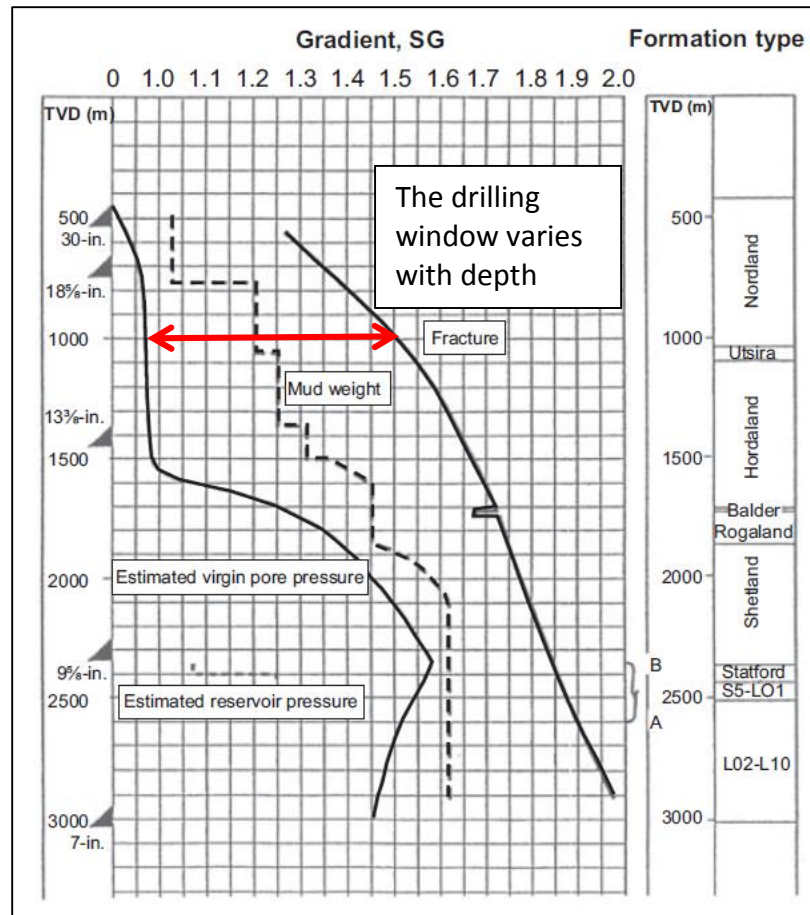


Fig. 1 - A general illustration of a drilling window (Mitchell et al. 2011).

Wellbore strengthening is a concept encompassing various techniques aimed at dealing with wellbore instability and lost circulation and intended to eliminate the problem of a narrow drilling window instead of working around it and managing it. The basic idea behind this concept is to increase the fracture resistance of the formation rock being drilled. The result is an additional margin in the drilling window to ensure that the fracture gradient limit of the drilling window is not exceeded by the equivalent circulating density (ECD) of the fluid in dynamic conditions. If successful, the fracture

gradient is sufficiently enhanced to allow for employing drilling fluid with a higher mud weight.

Over the years, many different wellbore strengthening techniques have been developed. These techniques are based on a variety of concepts and can be classified according to (Soroush et al. 2006) as follows:

- A. Bridging agents— increase the fracture resistance of the rock by sealing and plugging the fine fractures and consolidating the formation, including:
 - 1. Lost prevention material (LPM) with specific particle size
 - 2. Lost circulation material (LCM) blend 15/15/10 (Attong et al. 1995)
 - 3. Nanoparticles
- B. Cementing agents— increase the shear strength of the rock and include:
 - 1. Chemical grout
 - 2. Deformable, viscous, and cohesive systems (DVC)
- C. Gelling agents— create a membrane seal instead of bridging the pores by using noninvasive fluids (NIF), which are ultralow in solids
- D. Stress cage—enhance the wellbore tangential stress and increase the fracture gradient by employing a specially designed drilling fluid
- E. Resin treatments—consolidate weak rocks including:
 - 1. Formation consolidation and chemical casing method
 - 2. Water dispersible, aliphatic epoxy-resin system (WDR)
- F. Other emerging technologies—micro flux control and high-power laser.

1.2 Objectives

This work focuses on a certain range of wellbore strengthening techniques. This range includes all of the wellbore strengthening techniques that use the stress state around the wellbore as the main criteria for enhancing the fracture gradient. These wellbore strengthening techniques include bridging agents and LCM, the stress cage concept, and wellbore drilling fluid temperature variations.

The main goal of this work is to examine the performance of the defined wellbore strengthening techniques and predict the final results from implementing these techniques. The evaluation of their performance is based on geometric principles, basic rock mechanics data, linear elasticity plane stress theory, drilling fluid data, and geological data. A code and a user-friendly interface is created in VBA Excel® programming language based on the sets of data and principles listed previously in addition to the use of a recent and reputable numerical solution.

The secondary objective in this work is to provide a practical and accessible tool to be used in evaluating and predicting the performance of a specific wellbore strengthening technique in a particular section of a well. The tool is intended to be used in the well planning phase on a well section expected to cause drilling troubles such as lost circulation and hole stability issues due to a narrow drilling window. It will help to determine the applicability of a particular wellbore strengthening technique. Another important goal is reducing the cost of drilling problems either by defining the most

applicable wellbore strengthening technique for the situation or by avoiding the use of a particular wellbore strengthening technique due to predicted poor performance.

The final goal is to enable the proper selection of well candidates for wellbore strengthening based on a thorough study of different scenarios. These scenarios are created to reveal the best well candidate for wellbore strengthening in a certain field based on its placement, trajectory, and surface location. This method will help to obtain the maximum possible performance out of the selected wellbore strengthening techniques.

2. MODEL DESCRIPTION

2.1 Model Introduction

The purpose of this model is to combine the use of geometric principles, rock mechanics, linear elasticity plane stress theory and geological data to estimate the initial virgin fracture-pressure gradient in a certain section of a well. The model is then extended to evaluate the stress state and stress-related wellbore strengthening techniques through the use of recently available and reputable numerical solutions.

This model relies primarily on the tangential (hoop stress) concept first described by (Kirsch 1898). The model is based on the concept that a fracture in a wellbore is first initiated when the effective tangential stress or hoop stress is reduced to zero by the wellbore pressure, provided the wellbore pressure overcomes the additional and usually marginal rock tensile strength. This concept is the main principle used to estimate the initial virgin fracture-pressure gradient and the affect. In the next step, fundamental wellbore parameters, including change in temperature due to the drilling fluid and wellbore rock contact and change in local pore pressure due to filtration are examined to illustrate their effect on tangential stress and, consequently, on the fracture-pressure gradient.

Another concept used in the model is the fracture propagation concept. According to this concept, an already initiated fracture can propagate when the wellbore pressure exceeds the minimum field stress and the additional fracture toughness. This is the main basis for the wellbore strengthening techniques evaluation portion of the model.

A programming code is created to combine these concepts into a single model that can be used to evaluate the wellbore strengthening (fracture-pressure gradient enhancement) potential and applicability in a particular section of a well specifically defined by its depth, pore pressure, in-situ stress, rock properties, inclination, azimuth, and position with respect to the in-situ stress field.

2.2 In-Situ Stress Transformation

2.2.1 In-Situ Stress Description

For the purpose of quantifying the initial or virgin fracture-pressure gradient, the earth in-situ stresses are transformed to the wellbore coordinate system. First, the earth in-situ stresses need to be measured or estimated and described. Due to the fact that rock masses are rarely homogeneous as well as the fact that the state of the stress is the result of consequential past geological events, in-situ stresses are almost impossible to measure precisely and are always changing with time (Amadei et al. 1997a). Therefore,

estimating those stresses from stress versus depth relationships is a more common process than actually measuring them.

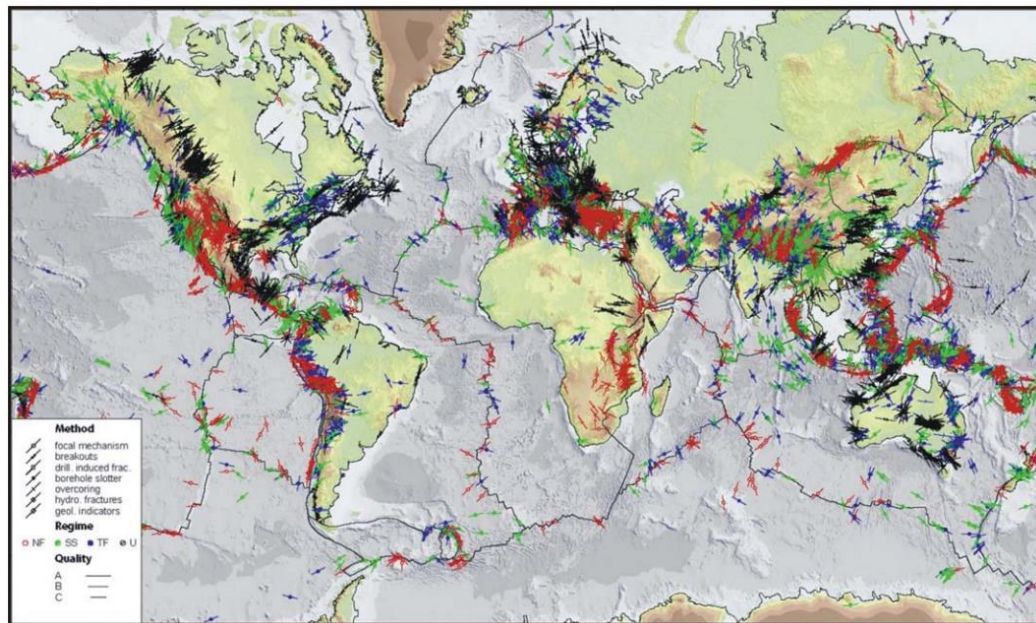


Fig. 2 - The world in-situ stress map showing direction and magnitude of stresses (Tingay et al 2006).

A good starting point for achieving the goal of describing in-situ stresses is to use a stress map of the region of interest. Through a stress map similar to the one shown in **Fig. 2**, the orientation of the horizontal stresses can be identified. Another good indication of the in-situ stress orientation is the direction of borehole breakout from well offset data. As shown in **Fig. 3**, breakouts in the borehole occur in the direction of the minimum horizontal stress while the induced fractures occur in the direction of the maximum horizontal stress. The location of such breakouts in the wellbore can be

obtained using various types of caliper logs and image logs. Well logs perform an important role in determining the magnitude of the in-situ stresses in addition to the orientation. Density logs provide useful data for estimating the vertical or overburden stress by calculating the vertical weight above the zone of interest. As for the magnitude of the two horizontal stresses, there are countless methods available for obtaining the magnitude of the two horizontal stresses. One method uses the overburden stress, pore pressure, and the Poisson's ratio to calculate a single and theoretical nominal value for the horizontal stress as follows according to (Watson et al. 2003):

$$\sigma_H = \frac{\nu}{1-\nu} (\sigma_V - P_p) + P_p \dots \dots \dots (\text{Eq. 2.1})$$

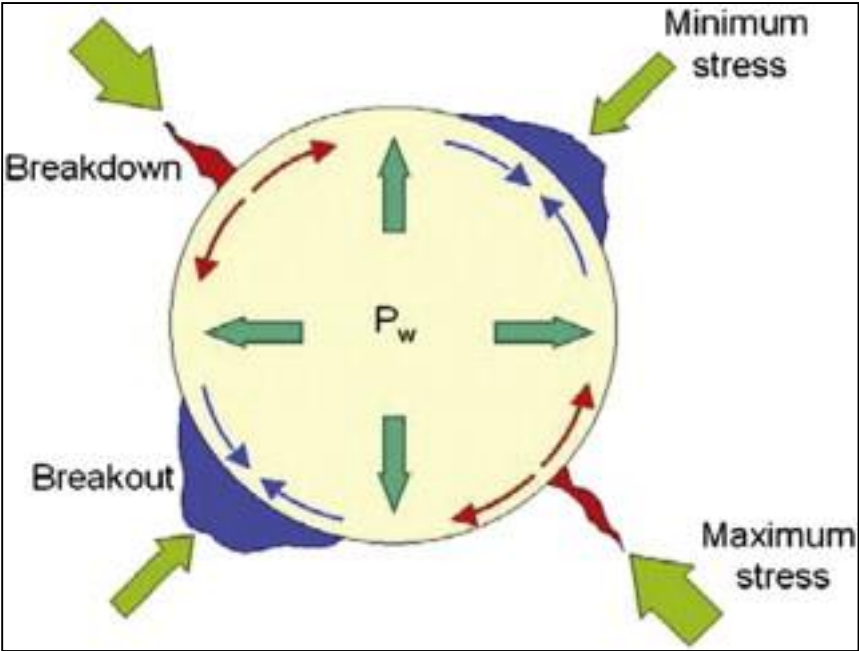


Fig. 3 - The pattern of borehole breakout and induced fractures on reference to the direction of the earth in-situ stresses direction (Dupreist et al. 2008).

However, the method which uses equation 2.1 is insufficient, particularly in fields with high-horizontal stress anisotropy. A more accurate and practical method involves using borehole opening pressure from the available leakoff test data to estimate the minimum horizontal stress. It is noteworthy that the magnitude of the maximum horizontal stress is the one that usually has the highest uncertainty of the three in-situ stresses, especially when estimated from the hole ovality (deviation from a circular shape to an oval shape) and the degrees of breakout as illustrated in **Fig. 4**. This is important because, considering the role of the maximum horizontal stress in the model that is going to be discussed later on, the uncertainty of its magnitude could be a major source of errors.

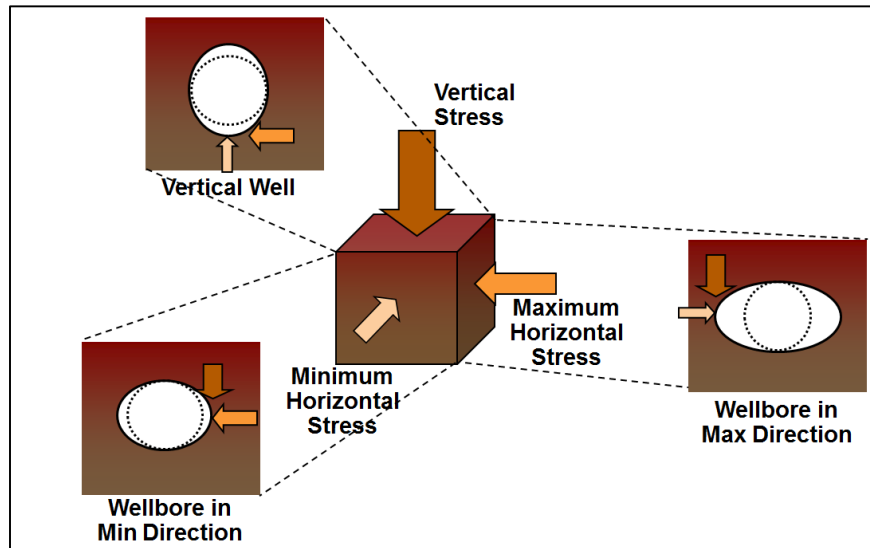


Fig. 4 - The estimation of the maximum horizontal stress based on the shape of the borehole (Duffadar et al. 2013).

All of the aforementioned methods should suffice for the purpose of this model. However, it should be noted that the in-situ stress values supplied for the model are expected to be major sources of error and deviation from the actual field values for the simulated fracture-pressure gradient and the estimation of its enhancement. For the purpose of this model, the magnitude and orientation of the earth in-situ stresses are assumed to be provided.

2.2.2 The Transformation to the Wellbore Coordinates

The simplest case that the model considers is when the wellbore axis is parallel to the maximum in-situ stress, which in most cases is the vertical overburden pressure. In this case, the section of the well being considered is vertical and no in-situ stress transformation is required because all of the stresses, vertical and horizontal, are aligned conveniently with the wellbore axis. However, for the more common cases where the wellbore axis in the section being considered deviates at an angle of inclination from the maximum in-situ stress or the less common cases where the maximum in-situ stress is not the vertical overburden as in the shallower sections of the well, the stresses need to be converted or transformed to the wellbore coordinate system. This transformation enables the model to quantify the principle in-situ stress components in the direction of the wellbore axis in the form of converted stresses acting orthogonally to the wellbore. **Fig. 5** shows the earth in-situ stresses on their original axis and transformed wellbore normal stresses on the wellbore axis. The figure also shows the specified location of the

wellbores with respect to the in-situ stress orientation. The angle γ describes the inclination of the wellbore as a deviation from the maximum in-situ stress and the angle β specifies the relationship between the maximum horizontal stress and the wellbore projection on the two horizontal stresses plane. Finally, the angle θ defines the circumferential position in the wellbore.

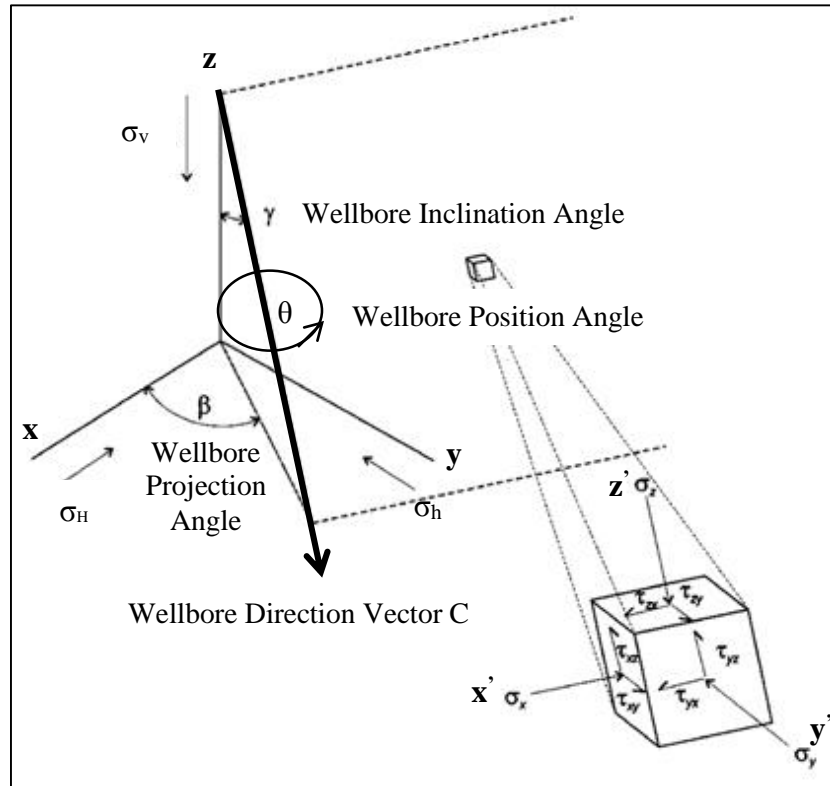


Fig. 5 - The relationship between the in-situ stresses reference frame and the defined wellbore section reference frame (Watson et al. 2003).

There are numerous techniques used to transform the stress to the desired coordinates. The technique that is related to the model is best described by (Daneshy

1973) and (Richardson 1983). Using the angles and the coordinate systems described in **Fig. 5**, the relationship between the in-situ stress coordinates (x, y, z) and the wellbore coordinates (x', y', z') can be established. C is the unit vector acting along the wellbore axis. The matrix $[\sigma]$ defines the in-situ stress components to be transformed. What follows is Richardson's transformation, slightly modified and applied to fit the purpose of the model.

Considering that the transformation required here is for a nonbasic rotation, meaning there is more than one axis that needs to be shifted at an angle from the original coordinate system, the rotation matrices that are going to be used are as follows:

$$C_x(\gamma) = \begin{bmatrix} \cos \gamma & 0 & -\sin \gamma \\ 0 & 1 & 0 \\ \sin \gamma & 0 & \cos \gamma \end{bmatrix} \dots\dots\dots (\text{Eq. 2.2})$$

$$C_z(\beta) = \begin{bmatrix} \cos \beta & \sin \beta & 0 \\ -\sin \beta & \cos \beta & 0 \\ 0 & 0 & 1 \end{bmatrix} \dots\dots\dots (\text{Eq. 2.3})$$

$$C_y(0) = \begin{bmatrix} \cos 0 & \sin 0 & 0 \\ -\sin 0 & \cos 0 & 0 \\ 0 & 0 & 1 \end{bmatrix} \dots\dots\dots (\text{Eq. 2.4})$$

The matrix $[C_x]$ rotates about the x-axis and away from the z-axis by an angle of γ , the matrix $[C_z]$ rotates about the z-axis and away from the x-axis by an angle of β , and the matrix $[C_y]$ shows that no additional rotation is occurring about the y-axis. The resultant transformation matrix is obtained by multiplying the three previous rotating matrices as follows:

$$[C] = [C_y][C_z][C_x] \dots \dots \dots (\text{Eq. 2.5})$$

Therefore:

$$\begin{bmatrix} \cos 0 & \sin 0 & 0 \\ -\sin 0 & \cos 0 & 0 \\ 0 & 0 & 1 \end{bmatrix} \begin{bmatrix} \cos \gamma & 0 & -\sin \gamma \\ 0 & 1 & 0 \\ \sin \gamma & 0 & \cos \gamma \end{bmatrix} \begin{bmatrix} \cos \beta & \sin \beta & 0 \\ -\sin \beta & \cos \beta & 0 \\ 0 & 0 & 1 \end{bmatrix} =$$

$$\begin{bmatrix} \cos \gamma \cos \beta & \cos \gamma \sin \beta & -\sin \gamma \\ -\sin \beta & \cos \beta & 0 \\ \sin \gamma \cos \beta & \sin \gamma \sin \beta & \cos \gamma \end{bmatrix} \dots \dots \dots (\text{Eq. 2.6})$$

The matrix $[C]$ is the second-order transformation for a Cartesian tensor. The final resultant matrix is $[\sigma_c]$, which defines the normal wellbore transformed stresses. This matrix can be determined using Cauchy's transformation rule of the stress tensor. According to this rule, the stress component in the secondary coordinate system, the wellbore coordinate, can be calculated by multiplying the required transformation matrix $[C]$ by the stress in the original coordinate system matrix, the in-situ stress matrix $[\sigma]$, and by the transpose of the transformation matrix $[C]^T$ as shown in the following equation:

$$[\sigma_c] = [C][\sigma][C]^T \dots \dots \dots (\text{Eq. 2.7})$$

Therefore:

$$\begin{bmatrix} \sigma_x & \tau_{xy} & \tau_{xz} \\ \tau_{xy} & \sigma_y & \tau_{yz} \\ \tau_{xz} & \tau_{yz} & \sigma_z \end{bmatrix} = \begin{bmatrix} \cos \gamma \cos \beta & \cos \gamma \sin \beta & -\sin \gamma \\ -\sin \beta & \cos \beta & 0 \\ \sin \gamma \cos \beta & \sin \gamma \sin \beta & \cos \gamma \end{bmatrix} \cdot \begin{bmatrix} \sigma_H & 0 & 0 \\ 0 & \sigma_h & 0 \\ 0 & 0 & \sigma_v \end{bmatrix}.$$

$$\begin{bmatrix} \cos \gamma \cos \beta & -\sin \beta & \sin \gamma \cos \beta \\ \cos \gamma \sin \beta & \cos \beta & \sin \gamma \sin \beta \\ -\sin \gamma & 0 & \cos \gamma \end{bmatrix} \dots \dots \dots (\text{Eq. 2.8})$$

The resulting equations from Cauchy's transformation for each stress term are as follows:

$$\sigma_x = \sigma_v \sin^2 \gamma + (\sigma_H \cos^2 \beta + \sigma_h \sin^2 \beta) \cos^2 \gamma \dots\dots\dots (\text{Eq. 2.9})$$

$$\sigma_y = \sigma_H \sin^2 \beta + \sigma_h \cos^2 \beta \dots\dots\dots (\text{Eq. 2.10})$$

$$\sigma_z = \sigma_v \cos^2 \gamma + (\sigma_H \cos^2 \beta + \sigma_h \sin^2 \beta) \sin^2 \gamma \dots\dots\dots (\text{Eq. 2.11})$$

$$\tau_{yz} = \frac{\sigma_H - \sigma_h}{2} \sin(2\beta) \sin \gamma \dots\dots\dots (\text{Eq. 2.12})$$

$$\tau_{xz} = \frac{1}{2} (\sigma_H \cos^2 \beta + \sigma_h \sin^2 \beta) \sin(2\gamma) \dots\dots\dots (\text{Eq. 2.13})$$

$$\tau_{xy} = \frac{\sigma_H - \sigma_h}{2} \sin(2\beta) \cos^2 \gamma \dots\dots\dots (\text{Eq. 2.14})$$

These equations do not take into account the effect of rock excavation and the existence of a borehole, they merely transform the in-situ stresses into normal stresses in the direction of the section of interest in the borehole. The removal of the rock through the drilling process causes a concentration of these wellbore normal stresses in the rock surrounding the borehole. Therefore, these stresses are not sufficient for the model to quantify the fracture-pressure gradient.

2.3 Induced Borehole Stresses

As a result of rock excavation and the formation of a borehole, stress is concentrated in the rock surrounding the borehole at values significantly greater than those of the far-field in-situ stress as shown in **Fig. 6**. As the radial distance from the center of the wellbore increases, the concentration of the stresses around wellbore decrease until it reaches a constant value that is the normal and undisturbed far field in-situ stress value. This is the effect that essentially defines the initial fracture-pressure gradient of the borehole.

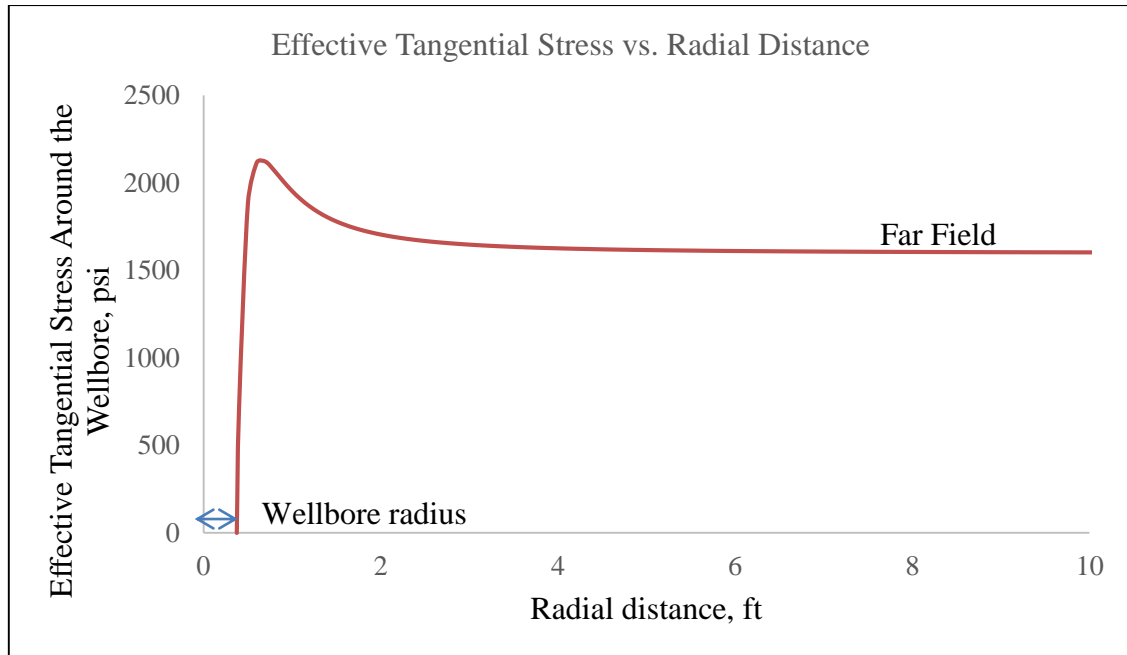


Fig. 6 - The concentration of stress due to the presence of a wellbore.

For the purpose of the model, these induced stresses need to be quantified based on the previously determined transformed normal wellbore stresses. There are numerous solutions available for quantifying the induced stresses; however, the solution required for this model should agree with its most important rock mechanics assumption, which is linear elasticity. In his work published in 1987, Aadnoy provided such a solution (Aadnoy 1987). It should also be noted that the solution given by the model should yield a value of induced stresses at the wall of the borehole. This point is noteworthy because there are several solutions available that agree with the model assumption, yet, they slightly disagree with model's purpose because they aim to determine the induced stresses of various radial values rather than at the borehole wall. This justifies the selection of the Aadnoy's solution. Those solutions are similar to the one used to produce the plot in **Fig. 6** (Jaeger et al. 2007).

According to Aadnoy's derivation, the induced stress should be considered in three directions. It is very important that these directions agree with borehole coordinate system defined in the previous section for the in-situ stress transformation. As a result of this agreement, the value for the transformed stresses can now be used in the model to quantify the induced stresses instead of directly using the in-situ stresses which would prove to be substantially in error.

The first direction of induced stress is the radial stress, which acts on the borehole walls perpendicular from the center of the borehole. The radial stress results from the hydraulic forces exerted by the drilling fluid occupying the borehole. Therefore, the radial stress can be stated simply as the pressure of the wellbore:

$$\sigma_r = P_w \dots \dots \dots (Eq. 2.15)$$

The second induced stress direction is the axial stress, which acts in parallel to the wellbore axis (z' -axis). According to Aadnoy, this stress can be calculated as follows:

$$\sigma_{zz} = \sigma_z - 2\nu(\sigma_x - \sigma_y)\cos 2\theta - 4\nu\tau_{xy}\sin 2\theta \dots \dots \dots (Eq. 2.16)$$

The third induced stress is by far the most complicated and important of the three stresses. The importance of this particular induced stress stems from the statement mentioned previously declaring that the model's main principle for estimating the initial fracture-pressure gradient is the reduction of the effective tangential stress to zero. The tangential stress, also called hoop stress, can be broken down into three components. These components are the borehole pressure component, the normal stress component, and the shear stress component, expressed by the following equations:

$$\sigma_{t1} = \sigma_x + \sigma_y - P_w \dots \dots \dots (Eq. 2.17)$$

$$\sigma_{t2} = -2(\sigma_x - \sigma_y)\cos 2\theta \dots \dots \dots (Eq. 2.18)$$

$$\sigma_{t3} = -4\tau_{xy}\sin 2\theta \dots \dots \dots (Eq. 2.19)$$

$$\sigma_t = \sigma_{t1} + \sigma_{t2} + \sigma_{t3} \dots \dots \dots (Eq. 2.20)$$

Finally, the induced shear stresses that need to be discussed for the model are the tangential-axial finite shear stress, the radial-tangential shear stress, and the radial-axial shear stress acting on the wellbore. This tangential-axial finite shear stress acts on the

axial-tangential (σ_{zz} - σ_t) stress planes in the defined wellbore polar coordinate. This shear stress is given by the following equation:

$$\tau_{tzz} = 2(-\tau_{xz} \sin \theta + \tau_{yz} \cos \theta) \dots\dots\dots(\text{Eq. 2.21})$$

As for the two remaining shear stresses, due to the fact that the radial stress, σ_r , is always zero or positive, they are both equal to zero at all times as follows:

$$\tau_{rt} = \tau_{rzz} = 0 \dots\dots\dots(\text{Eq. 2.22})$$

An illustration of these induced stresses acting on an element of the wellbore is shown in **Fig. 7**. The function of these stresses in the model is adding the effect of the excavation and the existence of a wellbore; hence, the emergence of the wellbore pressure as a contributing factor. Therefore, these stresses function as a complementary addition to the normal transformed in-situ stresses. However, unlike the process for determining the transformed stresses, when defining the induced stresses, the knowledge of basic mechanical rock properties begins to come into play. Namely, as can be observed from the induced stresses governing equations, the required rock property at this step is Poisson's Ratio, ν . The angle required in these equations, θ , is the circumferential position in the wellbore as mentioned earlier. In this model, the angle is going to be measured from the normal stress in the y' -axis direction or σ_y direction.

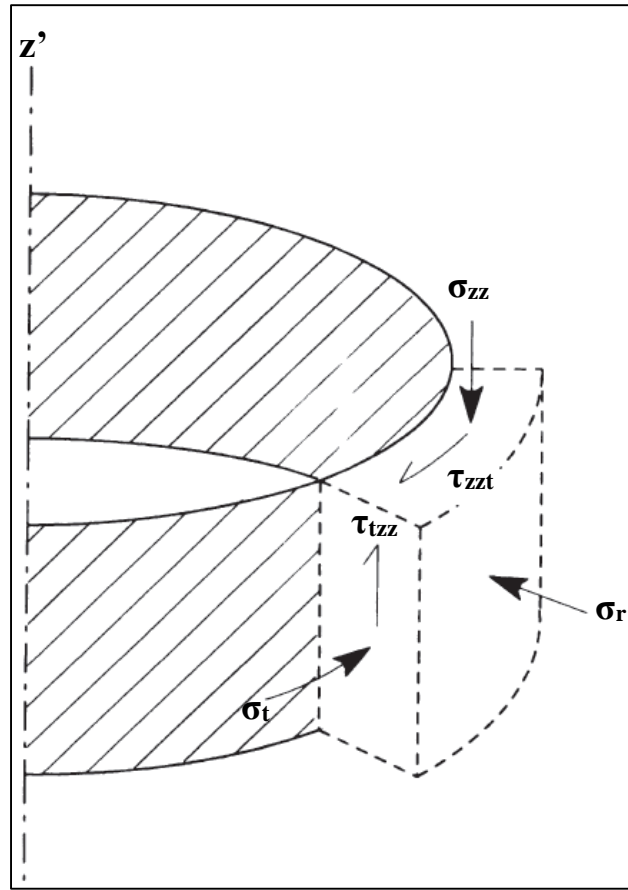


Fig. 7 - The illustration of the resulting induced stress acting on an element of the wellbore (Amadei et al. 1997b).

2.4 Plane Stress Transformation

The process of initial fracture-pressure gradient determination concludes in this section. The main objective here is to use the induced stress in determining the wellbore principle plane stresses, which will lead to the initial fracture-pressure gradient. By using the plane stress transformation, the model defines a specific plane at an angle from the

wellbore axis ($2\xi_p$). This plane is the plane of zero shear in the formation, which is the plane that will accommodate the two induced fractures. The advantage in adding this step to the model is that it enables the determination the two stresses (principle stresses mentioned previously) acting directly on the fracture plane. The first of the two stresses will act perpendicularly to the direction of the induced fractures on the fracture plane and the second stress will act in the same direction as the induced fractures. Recalling the simple approach undertaken to determine the direction or the position of the wellbore fracture and wellbore breakout based on the direction of the earth in-situ stresses, this condition can only exist in the case of a simple vertical wellbore with the overburden as the maximum in-situ stress. However, changing the wellbore inclination and changing its position with respect to the in-situ stress renders this approach as being inaccurate at best. This contrast between those two scenarios is illustrated in **Fig. 8**.

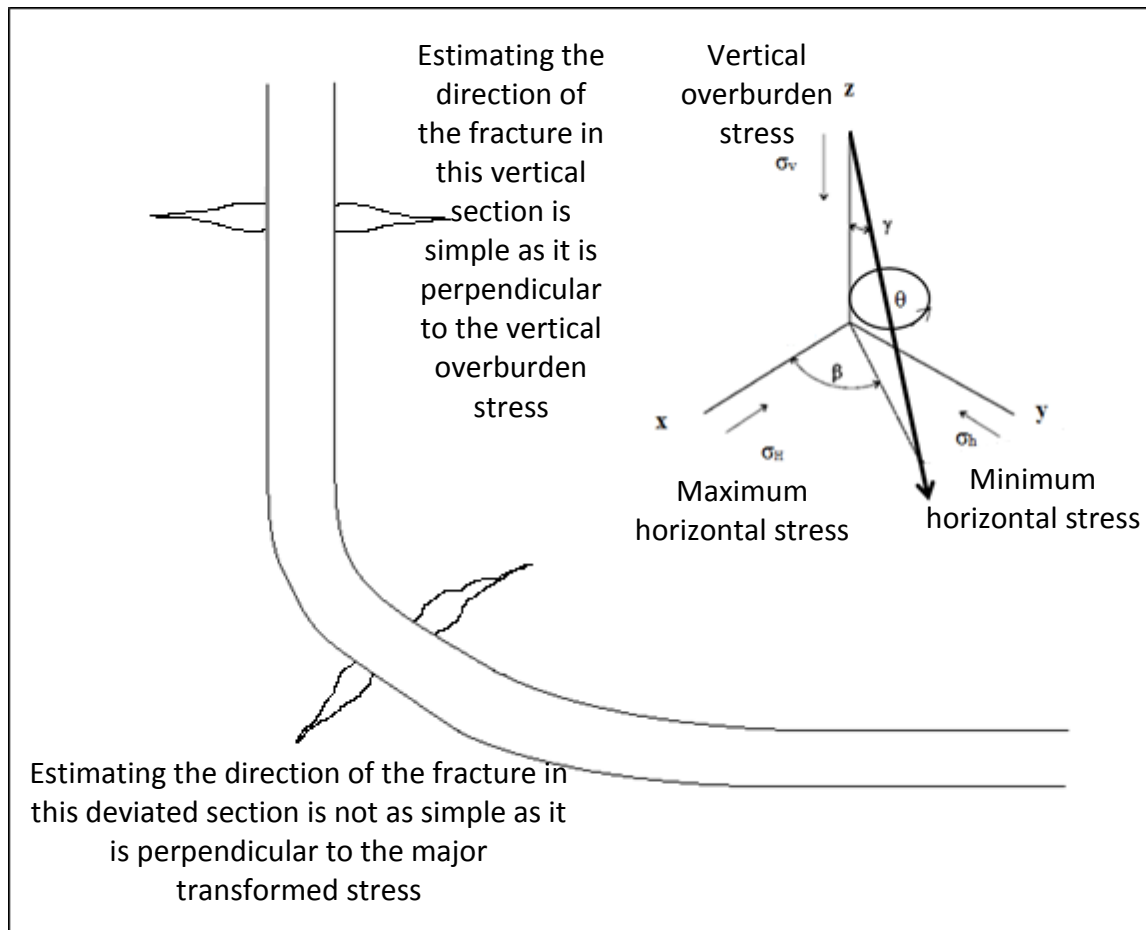


Fig. 8 - The contrast between determining the direction of the fracture in a vertical section and in a horizontal section.

In those more complex cases (deviated holes), using the in-situ stress directions and magnitudes to determine the expected location and the gradient of the fracture as described in **Fig. 3** will lead to erroneous results. Another advantage in determining the wellbore principle stresses acting on the specific fracture plane is the improvement in the wellbore strengthening evaluation. The value of those stresses can be used to evaluate the response of the wellbore to various stress-related wellbore strengthening techniques.

The general practice has been to simply use the values of the in-situ stresses to evaluate stress-related wellbore strengthening techniques. By including the principle stresses oriented to the failure plane, this model improves the process.

The mathematical representation of the plane stresses used for the model begins by considering the essential stresses acting on an element of the wellbore as described in **Fig. 9**. By applying Hibbler's plane stress transformation adjusted for the purpose of this model to represent a wellbore, the sum of the forces on the wellbore element in **Fig. 7** in the direction of x_1 and y_1 at equilibrium is as follows (Hibbler 2011):

$$\sum F_{x_1} = (\sigma_{x_1} A) \sec \xi - (\sigma_x A) \cos \xi - (\tau_{xy} A) \sin \xi - (\sigma_y A \tan \theta) \sin \xi - (\tau_{yx} A \tan \xi) \cos \xi = 0 \dots \dots \dots (\text{Eq. 2.23})$$

$$\sum F_{y_1} = (\tau_{x_1 y_1} A) \sec \xi - (\sigma_x A) \sin \xi - (\tau_{xy} A) \cos \xi - (\sigma_y A \tan \xi) \cos \xi - (\tau_{yx} A \tan \xi) \sin \xi = 0 \dots \dots \dots (\text{Eq. 2.24})$$

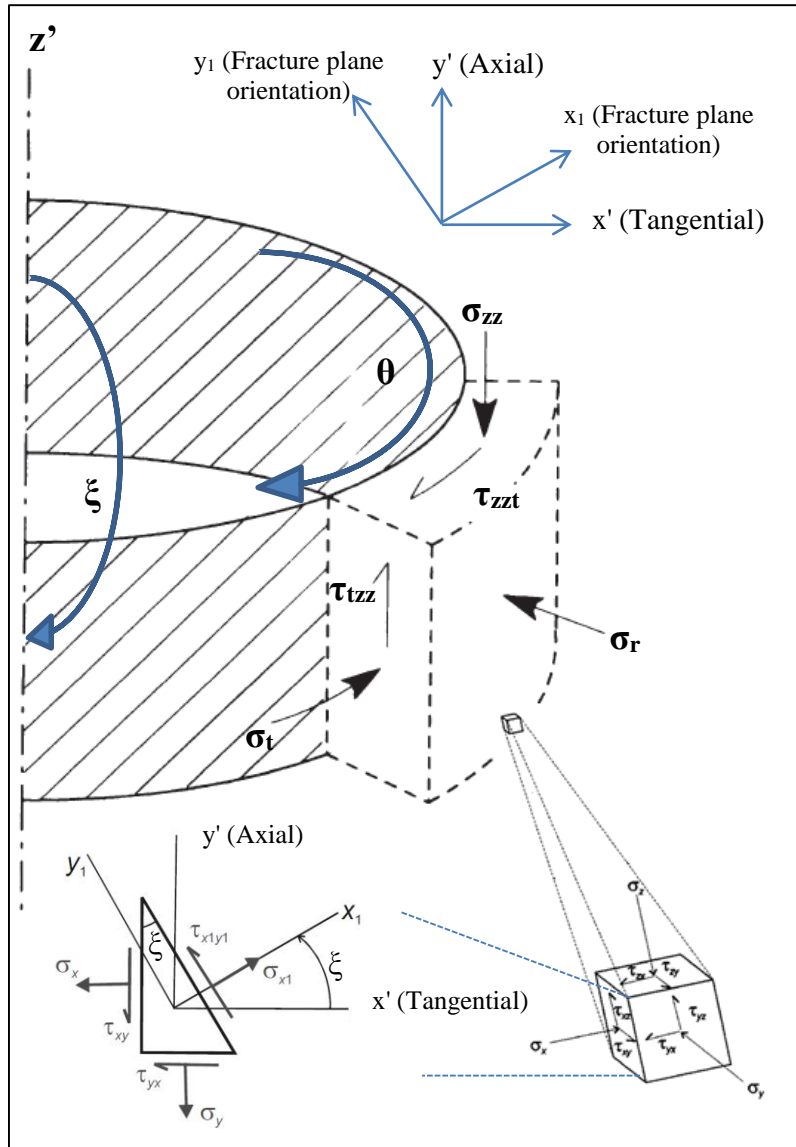


Fig. 9 - The relationship between the induced stresses reference frame and the plane stresses reference frame.

Adjusting the force summation for the wellbore by denoting the x direction as the tangential direction, the y direction as the axial direction, factoring out the area and, using the following simplification:

$$\tau_{xy} = \tau_{yx} = \tau_{tzz} \dots \dots \dots \text{(Eq. 2.25)}$$

The force summation can be stated as follows:

$$\sigma_{x_1} = \sigma_t \cos^2 \xi + \sigma_{zz} \sin^2 \xi + 2 \tau_{tzz} \sin \xi \cos \xi \dots \dots \dots \text{(Eq. 2.26)}$$

$$\tau_{x_1 y_1} = -(\sigma_t - \sigma_{zz}) \sin \xi \cos \xi + \tau_{tzz} (\cos^2 \xi - \sin^2 \xi) \dots \dots \dots \text{(Eq. 2.27)}$$

Using trigonometric identities leads to the following form:

$$\sigma_{x_1} = \frac{\sigma_t + \sigma_{zz}}{2} + \frac{\sigma_t - \sigma_{zz}}{2} \cos 2\xi + \tau_{tzz} \sin 2\xi \dots \dots \dots \text{(Eq. 2.28)}$$

$$\tau_{x_1 y_1} = -\frac{\sigma_t - \sigma_{zz}}{2} \sin 2\xi + \tau_{tzz} \cos 2\xi \dots \dots \dots \text{(Eq. 2.29)}$$

For the y_1 (axial) direction, ξ is replaced by $\xi + 90^\circ$ as follows:

$$\sigma_{y_1} = \frac{\sigma_t + \sigma_{zz}}{2} - \frac{\sigma_t - \sigma_{zz}}{2} \cos 2\xi - \tau_{tzz} \sin 2\xi \dots \dots \dots \text{(Eq. 2.30)}$$

These equations transform the plane stresses affecting the wellbore, which are the tangential, the axial, and the shear stress, to a specified circumferential borehole position. Through these stresses, the principle (fracture) plane can be defined. One important point regarding these stresses is that, according to plane stress transformation rules, the sum of transformed plane stresses in both directions (x_1 and y_1) is equal to the sum of the pretransformed stresses, which are, in this case, the tangential stress and the axial stress. This relationship is expressed as follows:

$$\sigma_{x_1} + \sigma_{y_1} = \sigma_t + \sigma_{zz} \dots \dots \dots \text{(Eq. 2.31)}$$

This relationship will be of use when the principle stresses need to be determined.

The principle stress plane or fracture plane can be defined by an angle from the wellbore axis given by $2\xi_p$. According to Hibbler, this angle is obtained by differentiating the plane stress transformation equations with respect to the borehole position angle ξ in the direction of x_1 and setting the derivative to zero as follows:

$$\frac{d\sigma_{x_1}}{d\theta} = \frac{\sigma_t - \sigma_{zz}}{2} (-2 \sin 2\xi_p) + \tau_{tzz} (2 \cos 2\xi_p) = 0 \dots\dots\dots (\text{Eq. 2.32})$$

Solving equation 2.32 for $2\xi_p$ gives:

$$2\xi_p = \tan^{-1} \frac{2\tau_{tzz}}{\sigma_t - \sigma_{zz}} \dots\dots\dots (\text{Eq. 2.33})$$

The angle $2\xi_p$ has two values over the 360° range starting from the wellbore axis and separated by 180° as illustrated in **Fig. 10**.

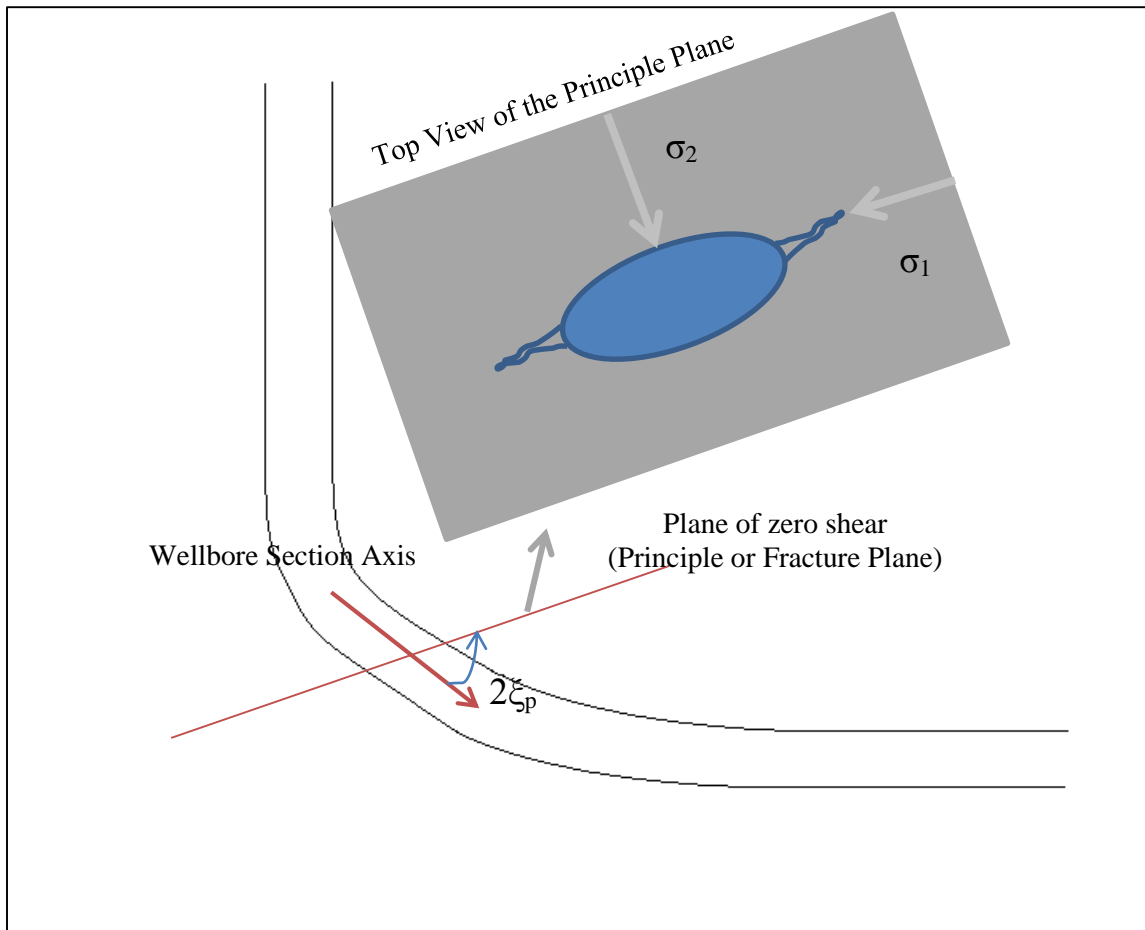


Fig. 10 - Illustration of the resulting principle stresses acting on the plane of zero shears containing the induced fractures.

Now that the principle or fracture plane has been clearly defined, the principle stresses acting directly on this plane can be determined. To determine these stresses, simple geometry in relation to the principle plane angle is applied according to **Fig 11**.

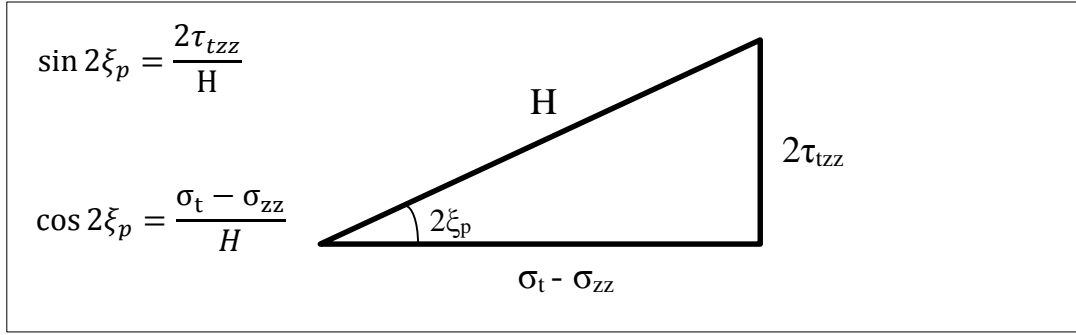


Fig. 11 - The geometry used to derive the equation for the principle stresses acting directly on the fracture plane.

Using Pythagorean's theorem and simple geometry, the first principle stress is determined by substituting the principle angle in the plane stress transformation, equation 2.28, in the direction of x_1 (σ_{x1}) as follows:

$$H^2 = (2\tau_{tzz})^2 + (\sigma_t - \sigma_{zz})^2 \dots\dots\dots (\text{Eq. 2.34})$$

$$\sigma_1 = \frac{\sigma_t + \sigma_{zz}}{2} + \frac{\sigma_t - \sigma_{zz}}{2} \cos 2\xi_p + \tau_{tzz} \sin 2\xi_p \dots\dots\dots (\text{Eq. 2.35})$$

Substituting the parameters described in **Fig 11** in this equation yields:

$$\sigma_1 = \frac{\sigma_t + \sigma_{zz}}{2} + \frac{\sigma_t - \sigma_{zz}}{2} \left(\frac{\sigma_t - \sigma_{zz}}{H} \right) + \tau_{tzz} \left(\frac{2\tau_{tzz}}{H} \right) \dots\dots\dots (\text{Eq. 2.36})$$

Substituting the value for the hypotenuse (H) yields the following equation:

$$\sigma_1 = \frac{\sigma_t + \sigma_{zz}}{2} + \frac{\sigma_t - \sigma_{zz}}{2} \left(\frac{\sigma_t - \sigma_{zz}}{(2\tau_{tzz})^2 + (\sigma_t - \sigma_{zz})^2} \right) + \tau_{tzz} \left(\frac{2\tau_{tzz}}{(2\tau_{tzz})^2 + (\sigma_t - \sigma_{zz})^2} \right) \dots\dots\dots (\text{Eq. 2.37})$$

Rearranging the terms results in the next expression:

$$\sigma_1 = \frac{\sigma_t + \sigma_{zz}}{2} + \sqrt{\left(\frac{\sigma_t - \sigma_{zz}}{2}\right)^2 - \tau_{tzz}^2} \dots \dots \dots (\text{Eq. 2.38})$$

This is the expression for the maximum wellbore principle plane stress acting perpendicular to the fracture plane as described in **Fig. 10**. To determine the second principle stress, the relationship between transformed plane stresses in both directions (x_1 and y_1) and the pretransformed stresses must be recalled (Eq. 2.31). The same relationship applies to wellbore principle plane stresses; i.e., the sum of the wellbore principle plane stresses is equal to the sum of the pretransformed stresses (σ_t and σ_{zz}) and expressed as follows:

$$\sigma_1 + \sigma_2 = \sigma_t + \sigma_{zz} \dots \dots \dots (\text{Eq. 2.39})$$

Therefore, the following two equations follow:

$$\sigma_2 = \sigma_t + \sigma_{zz} - \sigma_1 \dots \dots \dots (\text{Eq. 2.40})$$

$$\sigma_2 = \frac{\sigma_t + \sigma_{zz}}{2} - \sqrt{\left(\frac{\sigma_t - \sigma_{zz}}{2}\right)^2 - \tau_{tzz}^2} \dots \dots \dots (\text{Eq. 2.41})$$

Eq 2.41 is the expression for the minimum wellbore principle plane stress acting parallel to the fracture on the fracture plane as described in **Fig. 10**.

In many references, the expression for the maximum wellbore principle plane stress (σ_1) is denoted as the “maximum tensile stress” (Amadei 1997b; Watson et al. 2003). The reason for this denotation is that the maximum wellbore principle plane stress is the deciding factor in the process of determining the initial fracture-pressure gradient, which means that the applied pressure must exceed this value for the fracture to

initiate. However, a complication arises from the fact that this principle stress changes value around the circumference of the borehole. This complication means that the model cannot advance until a critical value of the maximum wellbore principle plane stress is defined.

The role of the model is to determine the location of the borehole wall where the maximum wellbore principle plane stress is at its minimum value. Determining the location of this critical value requires that the model run the calculations at all points around the borehole circumference until the minimum value is determined. Then, this borehole location is denoted as the critical borehole position angle (θ_c) as illustrated in **Fig. 12**. The model will then run the calculation at this critical angle with ascending values of the wellbore pressure. The purpose of this step is to determine the value of the wellbore pressure sufficient to reduce the maximum wellbore principle plane stress to zero, which means that the wellbore pressure exerted by the drilling fluid has exceeded the maximum tensile stress of the formation. Therefore, the fracture will be initiated and the value of the targeted fracture pressure is equal to the wellbore pressure that was capable of reducing the maximum tensile stress to zero.

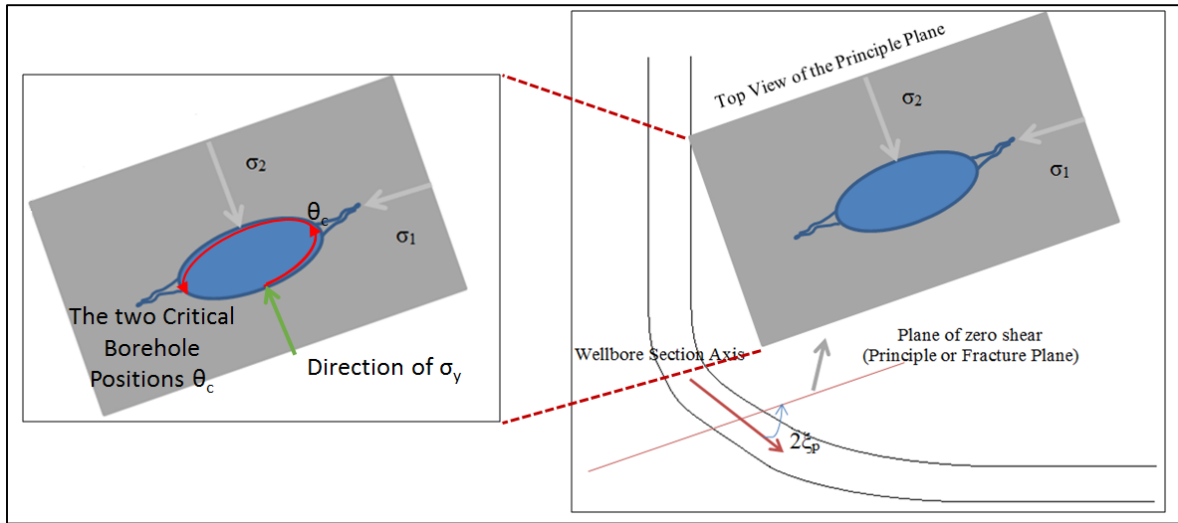


Fig. 12 - The location of the critical angle θ_c .

The concept of plane stress transformation used here is for 2D situations; hence, the transformation produces only two wellbore principle plane stresses. For the purpose of consistency and to comply with the 3D model, a third principle stress needs to be defined. This stress is the equivalent of the radial stress defined in equation 2.15. Thus, the third principal stress is given by:

$$\sigma_3 = \sigma_r = P_w \dots \dots \dots (\text{Eq. 2.42})$$

2.5 Model Assumptions and the Corresponding Implications and Corrections

The model is based on the assumptions that include:

- Linear elasticity and poroelasticity theory
- Perfectly round borehole face
- Perfectly impermeable borehole wall
- Isothermal conditions in the borehole

While the first assumption is reasonable and common in borehole rock mechanics (Fjaer 2008), the other assumptions will result in inaccuracies. In linear elasticity theory, it is assumed that the rock strain tensor is linear relative to the stress tensor. Although there is no rock that can be accurately specified as a linear elastic material, this assumption provides sufficiently accurate results. The reliability of these results stems from the observation that a rock can behave in accordance with the linear elasticity theory when the applied stress is in small increments (Jaeger et al. 2007). Some important aspects of poroelasticity were also considered in the model. Relying simply on linear elasticity to describe the deformation of formation rock material would imply that the formation rock is a homogeneous and completely solid material. However, due to the presence of pore spaces and the formation fluids occupying them (oil, gas, and water), the rock material is certainly not homogeneous. These spaces and fluids in the formation rock play an important role in defining the rock failure. Therefore, considering the poroelasticity of the formation is essential for a model when attempting to define the fracture-pressure gradient and its response to different wellbore strengthening techniques. That is why concepts such as Terzaghi's principle of effective stress, to be discussed later, pertaining to the poroelasticity theory were considered in developing the model.

As for the error-producing assumptions, corrections need to be made to the model to account for them. Starting with the second assumption, obtaining a perfectly round borehole during drilling is realistically possible; however, it is not guaranteed. In many cases, the borehole shape deviates from the circular form due to several reasons, including borehole breakouts (commonly and inaccurately called washouts), irregular formation of mud cake, and poor borehole cleaning. Furthermore, the in-situ earth stress field has an effect on the shape of the borehole as described by (Duffadar et al. 2013) and shown in **Fig. 13**. As was discussed in the in-situ stress section, the earth stress field can cause borehole ovality due to stress asymmetry. Even though the assumption of a perfectly round borehole is not always obtainable in a practical environment, it is not expected to affect the results of the model in a substantial fashion considering the purpose of the model. The reason for the minimal effect is that none of the parameters considered in this model is particularly affected mathematically by the shape of the borehole; therefore, no measures were taken to correct for this particular assumption.

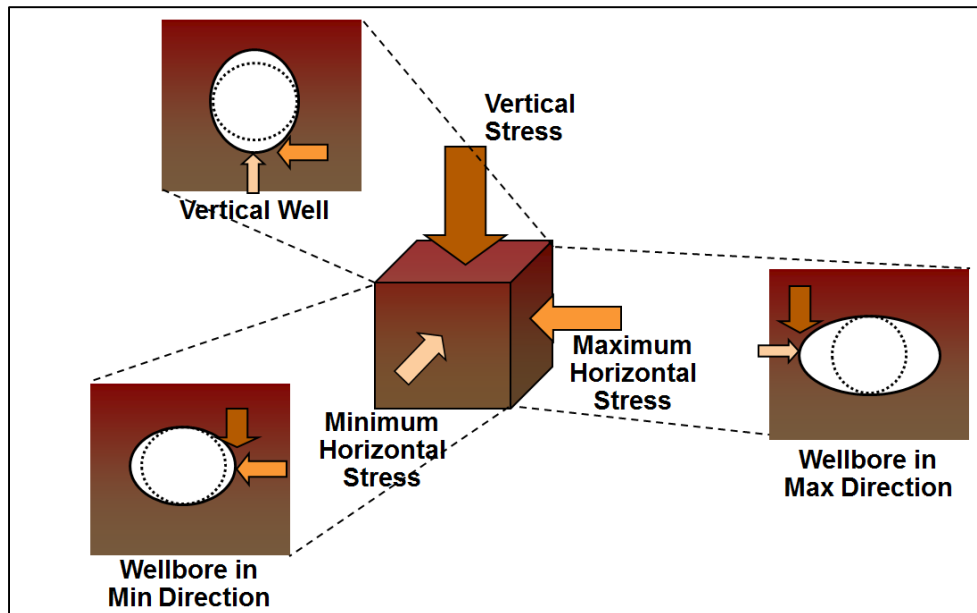


Fig. 13 - The effect of in-situ earth stress field on the shape of the borehole (Duffadar et al. 2013).

However, the same cannot be said about the perfectly impermeable borehole wall assumption because the situation is entirely different. Unless the formation being drilled contains very low-permeability shale or the drilling is being performed underbalance, the borehole wall is expected to be permeable in most practical situations. Filtration and formation of mudcake due to overbalance is expected to occur. The implication of this occurrence is a local change in the pore pressure of the area surrounding the borehole in the formation rock (Watson et al. 2003). **Fig. 14** shows the local change in the pore pressure due to mud filtration. As can be seen, the local pore pressure reaches a maximum value at the wellbore radius. This pore pressure value decreases significantly

farther away from the wellbore wall until it reaches the original undisturbed value of formation pore pressure.

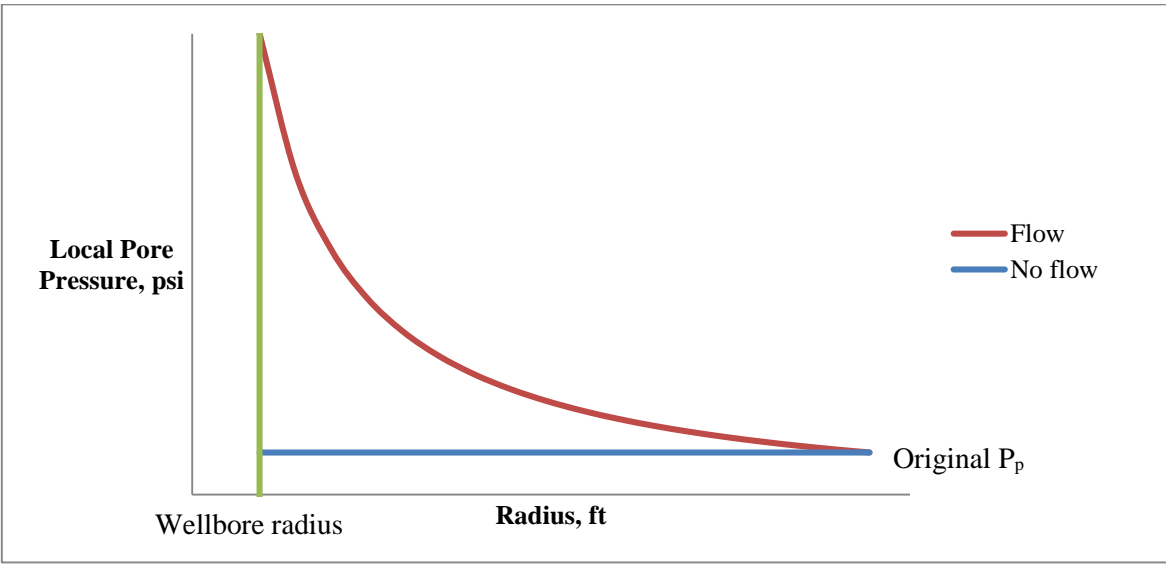


Fig. 14 - The local change to the pore pressure due to mud filtration (Watson et al. 2003).

As a consequence to the increase of the local pore pressure around the borehole and by considering to the following Terzaghi’s principle of effective stress (Terzaghi 1936), the effective stress of the rock surrounding the borehole will decrease. This condition will relieve the stress concentration surrounding the borehole and reduce the initial fracture-initiation pressure. Terzaghi’s principle of effective stress is given by the following equation where the Biot’s constant (α) can be assumed as 1:

$$\sigma_e = \sigma - \alpha P_p \dots \dots \dots (\text{Eq. 2.43})$$

The resulting reduction in the initial fracture-initiation pressure is the main issue regarding the third assumption requiring a correction in the model. One way to achieve this correction is by considering the change in the effective tangential stress of the wellbore. The model uses a relationship that models the reduction of the effective tangential stress in a porous elastic rock due to an overbalance in pressure and continuous flow (Mouchet et al. 1989) given by the following equation:

$$\Delta\sigma_{te(q)} = \frac{1-2\nu}{1-\nu} (P_p - P_w) \dots\dots\dots(\text{Eq. 2.44})$$

Depending on the Poisson's ratio of the rock and on the magnitude of the overbalance between the drilling fluid and the pore pressure, the reduction in effective tangential stress and, consequentially, the reduction in the initial fracture initiation pressure can be quantified. **Fig. 15** shows the effective hoop stress change as a result of a flow through the wellbore wall due to overbalance. The relationship used to describe the tangential stress in a radial direction is as follows (Deily et al. 1969):

$$\sigma_t = \frac{\sigma_H + \sigma_h}{2} \left(1 + \frac{r_w^2}{r^2}\right) - \frac{\sigma_H - \sigma_h}{2} \left(1 + 3 \frac{r_w^2}{r^2}\right) \times \cos 2\theta - P_w \frac{r_w^2}{r^2} \dots\dots\dots(\text{Eq. 2.45})$$

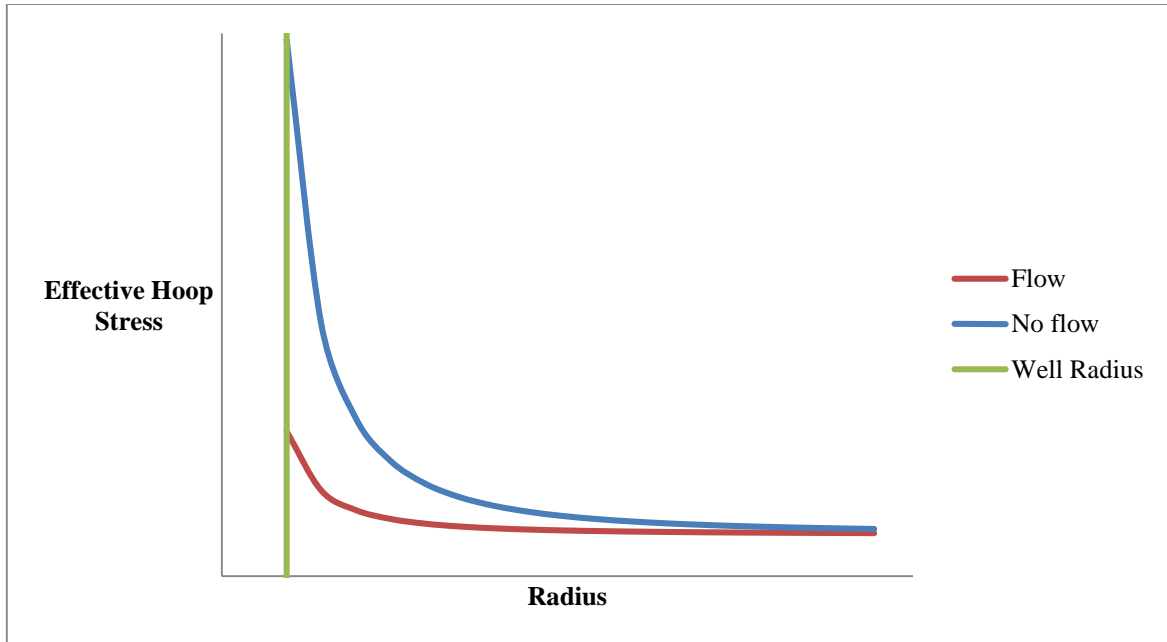


Fig. 15 - Illustration of the change undergone by the effective hoop stress as a result of wellbore wall flow due to overbalance.

One more aspect of the filtration process to be considered is the buildup of filter-cake. The buildup of filter-cake causes a significant pressure drop from the wellbore to the sand face due to its impermeable nature as shown in **Fig. 16**. As a result of the formation of filter-cake, the tangential stress is reduced less by mud filtration. This process of controlling excess filtration results in the reduction of the damaging effect of flow through the wellbore wall due to overbalance of the fracture-pressure gradient. The filter-cake effect is taken into account in the model by adjusting the correction to the effective tangential stress. The adjustment is made by considering the overbalance between the wellbore and the sand face and not the overbalance between the wellbore and the filter-cake, which forces the model to include the positive effect of filter-cake.

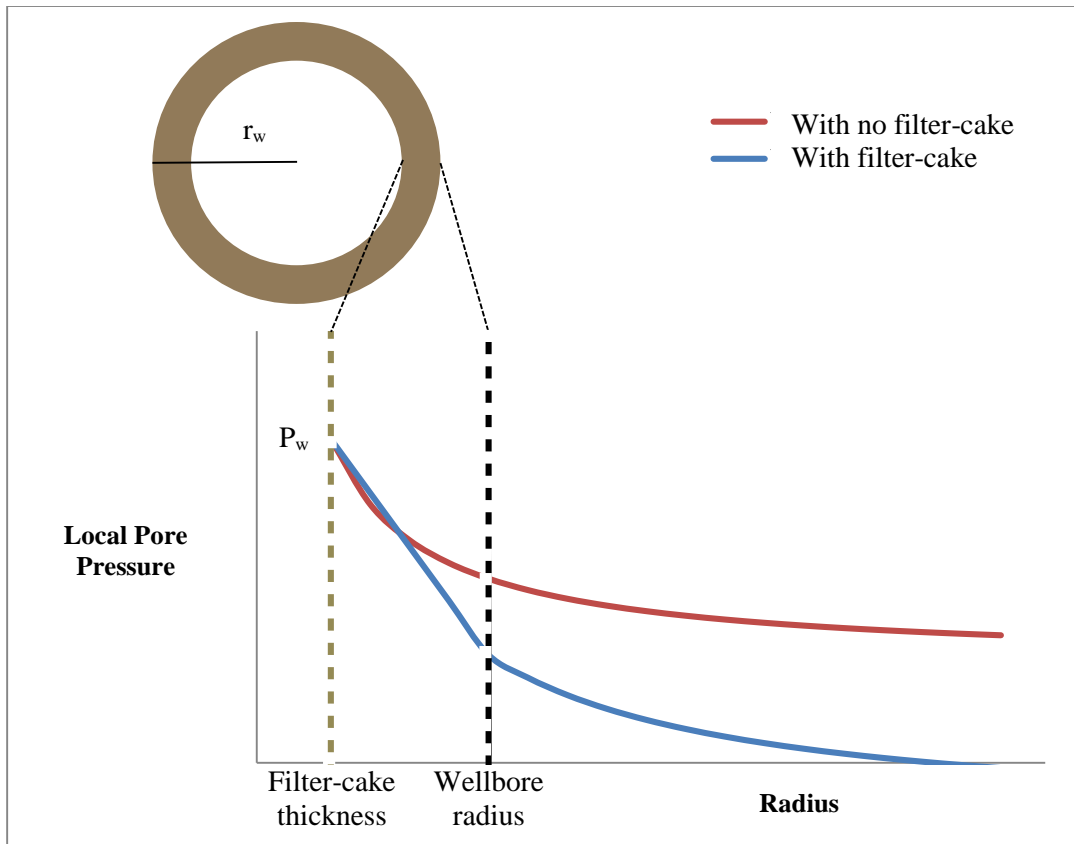


Fig. 16 - Illustration of the effect of the buildup of filter-cake as a drop in pressure from the wellbore to the sand face due to its impermeable nature.

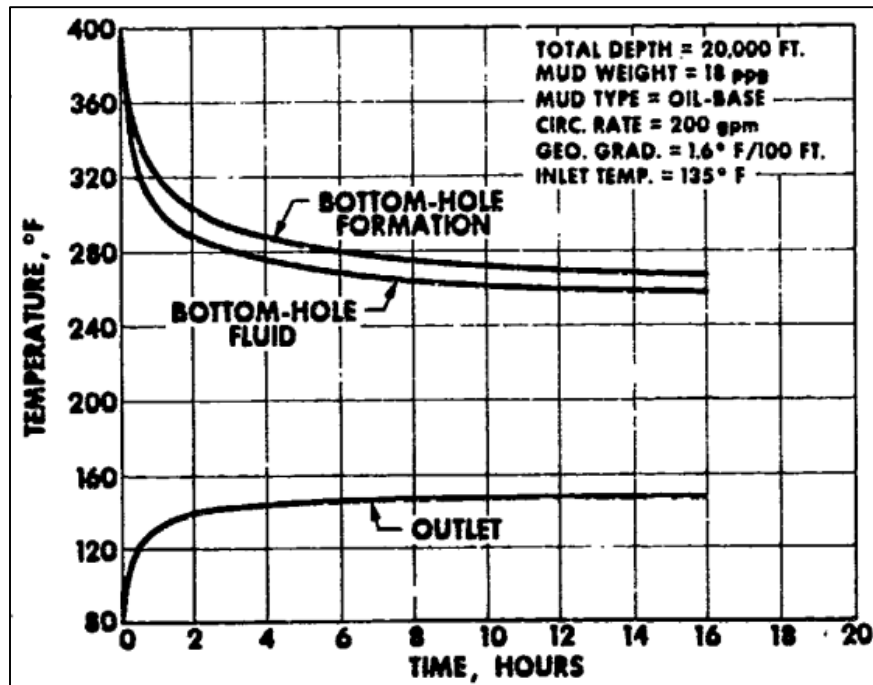


Fig. 17 -The contrast between the bottomhole formation and bottomhole fluid temperatures and the temperature of the drilling fluid (Raymond 1969).

Finally, the last assumption of the model is also an assumption that results in a correction to the model. Assuming isothermal conditions in the wellbore is not an accurate assumption during the drilling process. Due to the depths of the formations being drilled, the formation temperatures will reach high enough values so as to affect the model's results. The formation temperatures are typically significantly higher than those of the drilling fluids pumped from the surface. **Fig. 17** shows the contrast between the bottomhole formation and bottomhole fluid temperatures and the temperature of the drilling fluid. Due to the temperature difference, an exchange of heat occurs at the wellbore wall. The temperature of the drilling fluid is elevated due to its exposure to the

formation rock and, most importantly, the formation rock temperature decreases due to its exposure to the colder fluid. The formation rock exposure to the lower temperature can alter its stress state. This change in the rock stress state is logical when considering the physical effect a sudden temperature change can have on material such as rocks. The resulting physical expansion or contraction in the rock is the driving force behind the change of the stress state. In the case of deep wells where the geothermal gradient causes the formation rock to be of higher in temperature than the drilling fluid, the drilling fluid will act to cool the formation rock with circulation time. The result of this interaction will be contraction of the formation rock over time due to cooling, which will have a detrimental effect on fracture-pressure gradient in the form of a decrease. In the opposite case of shallow wells or of high-temperature drilling fluid, the colder formation rock will absorb heat from the drilling fluid. This will cause an expansion of the formation rock volume and an increase in the fracture-pressure gradient.

To consider the effect of temperature changes on the initial fracture-pressure gradient in the model, a closed form solution based on an analytical expression is used. The solution considers the effective tangential stress change in an elastic cylindrical zone around the wellbore that undergoes temperature change. This expression can be stated according to (Perkins et al. 1984) as follows:

$$\Delta\sigma_{te(T)} = \frac{E}{1-\nu} \alpha_T (T_{\text{drilling fluid}} - T_{\text{formation}}) \dots\dots\dots (\text{Eq. 2.46})$$

As expected, a positive change in temperature will produce an increase in the effective tangential stress. This increase in tangential stress will be considered as an

incremental gain to the total fracture-pressure gradient in the model. Likewise, a negative change in temperature will decrease the effective tangential stress. This reduction of the tangential stress will be considered a reduction in the total fracture-pressure gradient in the model.

2.6 The Evaluation of Fracture-Pressure Gradient Enhancement

Due to the continuous maturation and depletion of reservoirs worldwide, the drilling window is narrowing significantly in many fields. The reduction in the drilling window can be attributed to falling pore pressures and the consequent decrease in the minimum horizontal in-situ stress as described by this relationship:

$$\sigma_H = \frac{\nu}{1-\nu}(\sigma_V - P_p) + P_p \dots\dots\dots(\text{Eq. 2.47})$$

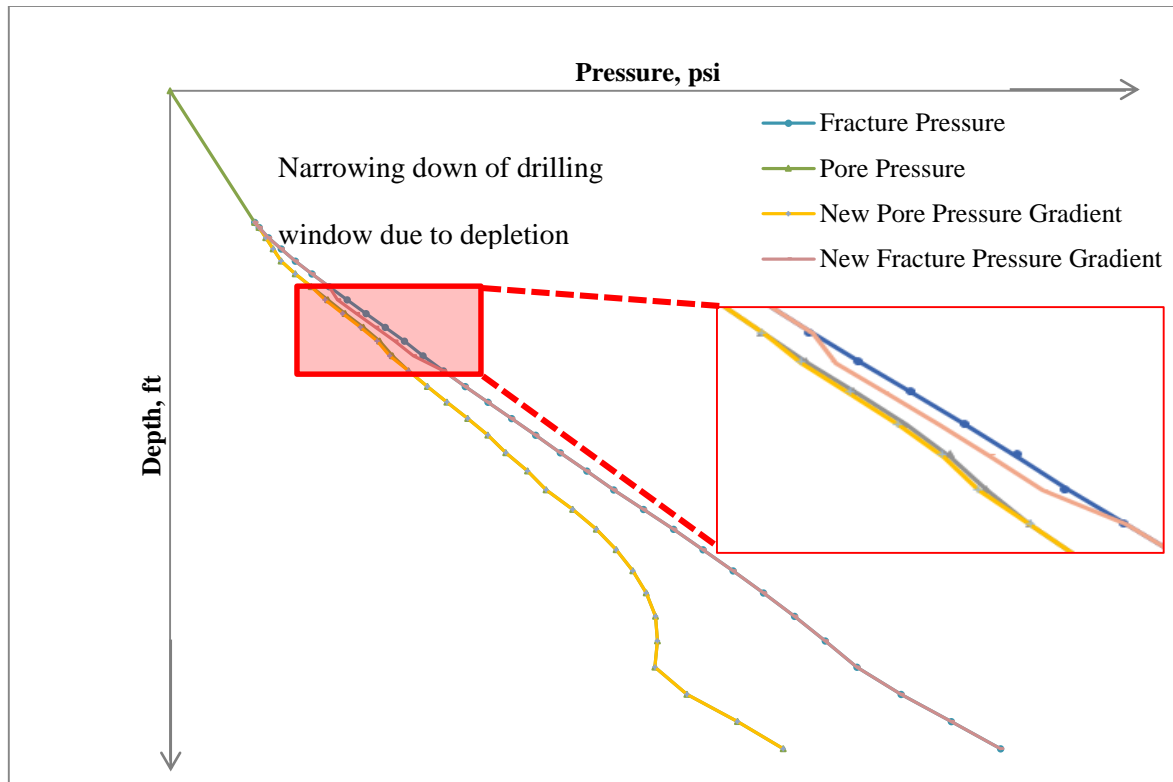


Fig. 18 - The resulting narrower drilling window due to reservoir depletion.

The decrease in the minimum horizontal stress leads to a reduction in the fracture-pressure gradient. The resulting narrower drilling window, as described in **Fig. 18**, presents various challenges to drilling operations. A drilling fluid can typically be designed to accommodate both the fracture gradient and the pore pressure gradient in static conditions. However, in dynamic conditions where the equivalent circulation density is higher than the static mud weight due to annular friction pressure, the fracture gradient can easily be exceeded resulting in lost circulation. Plus, there is no guarantee that such a drilling fluid, which was designed for the restriction condition of the narrow

drilling window, can provide wellbore stability. One tool which can give a wider drilling window is wellbore strengthening techniques.

Over the years, various wellbore strengthening techniques were developed to increase the fracture-pressure gradient and widen the drilling window. The benefits of these techniques could also include the elimination of lost circulation and sand production. The wellbore strengthening techniques can be classified according to the type of their interaction with targeted formation rock as follows (Barrett et al. 2010):

1. Physical methods—reduce the fluid rock interaction by means of plastering
2. Chemical methods—chemical grouting, dictating the dynamics of the formation fluid through osmotic mechanisms, and using deformable, viscous, and cohesive systems (DVC)
3. Thermal methods—increase the temperature of the rock in the wellbore wall through heat transfer from the drilling fluid to cause rock expansion and an increase in the tangential stress.
4. Mechanical methods—enhance the tangential stress of the wellbore by inducing fractures and plugging or sealing them in what is known as “stress caging” (Aston et al. 2004)

The focus of this work will be on techniques that deal directly with rock stresses as the driving force for enhancing the fracture-pressure gradient. Those techniques include the wellbore strengthening techniques that stabilize the rock's existing or induced fractures either by plugging or sealing to change the stress state around the wellbore.

They also include the techniques that use wellbore temperature variations to alter the stress around the wellbore.

2.6.1 Evaluation of Wellbore Strengthening Techniques from Basic Rock Mechanics

The model requires a mathematical representation of the induced stress alteration due to the action of the different wellbore strengthening techniques. Building the model on an analytical or exact solution would be the ideal case; however, there is no such solution available where the stress state alteration is quantified due to the effects of different wellbore strengthening techniques as reported in the literature. Therefore, the model relies on an approximate solution to achieve this. This solution was developed by Nobuo Morita (Morita et al. 2012) as a closed-form solution based on a boundary element model. According to Morita's laboratory work, the model accuracy in its different variations ranges from 0.2% to 5%; hence, it was deemed suitable for the purpose of the model being developed for this work.

The main advantage of the selected solution is that it relies on basic rock mechanics principles to determine the enhancement to the fracture-pressure gradient. These basic rock mechanics principles make the solution more accessible from an operation point of view. The data used to describe these principles are easily obtainable through the cooperation of the drilling engineer and the field geologist. Also, this solution is particularly useful for the purpose of the model being constructed by applying it to actual field data. Morita's approach to addressing the evaluation of wellbore

strengthening is the introduction of the fracture theory and to the stress around the wellbore. According to fracture mechanics, a fracture tip undergoes three types of loadings or opening modes as described in **Fig. 19**.

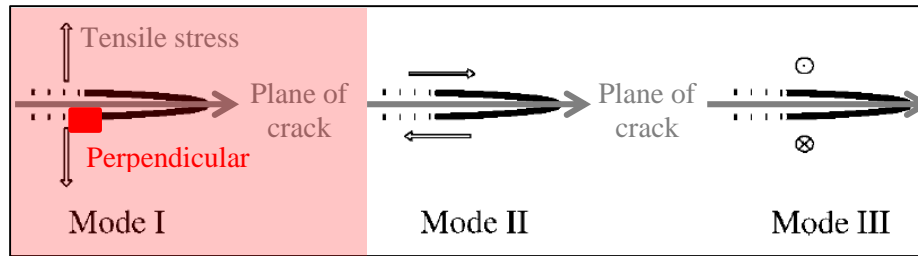


Fig. 19 - The three mode of fracture loadings or openings according to fracture mechanics (Jaeger et al. 2007).

The mode of interest in this work is the mode where the tensile stress is normal to the plane of the crack, which is mode I. The direction of the tensile stress in mode I is similar to the direction of the stress applied in strengthening by the solid particles on the wellbore fractures. In his solution, Morita based his solution on the integral of stress intensity factor for mode I and solving it for various scenarios. Those scenarios or different classifications on which the numerical solution was derived are as follows:

1. Enhancing the wellbore fracture pressure by the means of temperature variation of 0- to 0.1-in. fractures.
2. Enhancing the wellbore fracture pressure by plugging or sealing microfractures (0.1 to 1 in.) with the drilling fluid solid particles.

3. Enhancing the wellbore fracture pressure by plugging or sealing macrofractures (1 to 2 ft) with the drilling fluid solid particles in what is known as the stress cage method.
4. Enhancing the wellbore fracture pressure by plugging or sealing large fractures (more than 10 ft) with the drilling fluid solid particles in what is known as the tip screening method.

Based on those scenarios, mathematical relationships of fracture-pressure enhancement were derived. These relationships were added to the model to quantify the change to the initial virgin fracture-pressure gradient in a specific section of the well when different wellbore strengthening techniques are implemented.

The first scenario of wellbore strengthening in the model deals with the resultant fracture-pressure enhancement when a naturally existing or induced microfracture is purposely sealed at the fracture mouth by solid particles from a “designer mud”. This scenario can be considered as a branch of the “stress cage” method. In the “stress cage” method, an induced fracture is created and kept open by solid particles from a “designer mud” for the purpose of increasing the hoop stress of the wellbore. Field applications showed that applying this method does indeed enhance the fracture pressure in the wellbore section where it is applied (Aston et al. 2004). However, there is no clear physical evidence of what the nature of the interaction between the solid particles from the “designer mud” and the induced fracture actually is. For this reason, the model takes into account these different scenarios to examine this particular wellbore strengthening technique. For the purpose of the model, this scenario of fracture and solid particle

interaction is denoted as the “sealed fracture”. Based on the solution employed by Aston, et al, two fractures are sealed in the wellbore section being considered. **Fig. 20** describes this scenario.

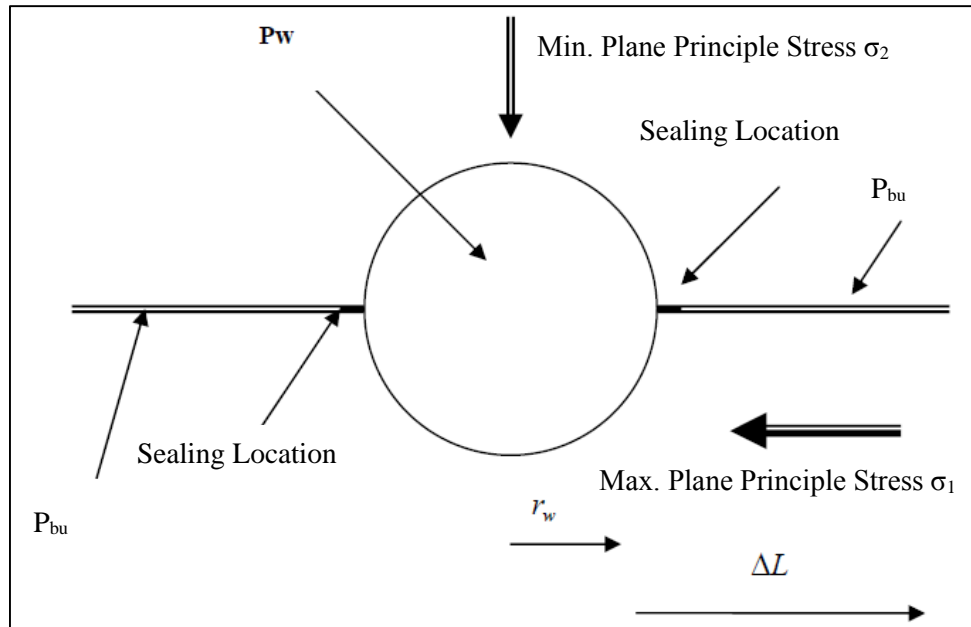


Fig. 20 – The description of the sealed fracture scenario of particle and fracture interaction in wellbore strengthening (Morita et al. 2012).

To be able to integrate this solution with the model described thus far, minor adjustments were made for the purpose of improving the solution’s compatibility with rest of the model and improving the results. The first and most important adjustment is replacing the in-situ stresses by the fracture plane principle stresses calculated in a previous section of the model. The solution originally uses the magnitudes of the earth in-situ stresses as the stresses acting in the perpendicular and parallel direction of the

fractures. The model seeks to improve the use of this particular aspect of the solution by considering the principle stresses acting on the specific plane of the fractures (the plane of zero shear) as the stresses acting in the perpendicular and parallel direction of the fractures. As such, the model will take the magnitude of these stresses in the solution instead of the magnitude of the earth in-situ stresses, which means that the minimum fracture plane principle stress will act in the perpendicular direction to the fracture and prevent its propagation.

The second change to the solution is made for the sole purpose of its compatibility with the rest of the model. In the original solution, the signs for the stresses were assigned as positive for tension and negative for compression. This sign assignment will not work with the rest of the model. Nevertheless, all of the stresses being considered in all of the previous sections of the model were compressive; thus, the solution was adjusted so that all of the stresses used will be a positive value for compression.

In **Fig. 20** describing this first scenario of wellbore strengthening, P_{bu} is the pressure inside of the fracture or the buildup pressure. This value will be equal to the pore pressure in the majority of cases. The reason for this condition is that one of the main requirements for applying the “stress cage” method is high-rock permeability. The high permeability is required because it will allow the “designer mud” filtrate to flow into the formation and prevent further and unwanted fracture propagation. Therefore, the high permeability will aid in arresting the fracture growth to a desired length and will dissipate the pressure inside of the fracture until it reaches the original pore pressure of

the rock. In the less probable case of a low-permeability rock, the filtrate is expected to create a pressure buildup in the fracture. The result would be a higher pressure inside of the fracture than the original pore pressure of the rock.

After making the required adjustments to the solution, the final equation for the enhanced fracturing pressure for the first scenario that will be used in the model will be as follows:

$$P_{f-enhanced} = \frac{\frac{k^c}{\sqrt{\pi\Delta L}} + \sigma_2 F_\lambda(s) - P_{bu}[1 + (1-s)(-0.137 + 0.258(1-s)^2 - 0.4s^2(1-s))]}{(1-s)[0.637 + 0.485(1-s)^2 + 0.4s^2(1-s)]} \dots\dots\dots (\text{Eq. 2.48})$$

Where:

$$\Delta L = \frac{W_c E}{4(1-\nu^2)(\sigma_2 - P_{bu})} \dots\dots\dots (\text{Eq. 2.49})$$

$$\lambda = \frac{\sigma_1}{\sigma_2} \dots\dots\dots (\text{Eq. 2.50})$$

$$s = \frac{\Delta L}{(r_w + \Delta L)} \dots\dots\dots (\text{Eq. 2.51})$$

$$\omega = \frac{P_{bu}}{\sigma_2} \dots\dots\dots (\text{Eq. 2.52})$$

$$F_1(s) = 1 + (1-s)[0.5 + 0.743(1-s)^2] \dots\dots\dots (\text{Eq. 2.53})$$

$$F_o(s) = 0.5(3-s)[1 + 1.243(1-s)^3] \dots\dots\dots (\text{Eq. 2.54})$$

$$F_\lambda(s) = (1-\lambda)F_o(s) + \lambda F_1(s) \dots\dots\dots (\text{Eq. 2.55})$$

The second scenario considers a different type of solid particle and fracture interaction. Instead of assuming that the solid particles from the “designer mud” seal the

fracture at the fracture mouth, it assumes that the particles are plugging the fracture at a certain distance from the fracture mouth. Again, due to the ambiguity in the nature of the interaction between the fracture and the designer mud solid particles, this scenario can be considered as a branch of the “stress cage” method. This scenario is denoted as the plugged fracture technique in the model as opposed to the sealed fracture techniques discussed previously. The closed-form solution used in the model for the plugged fracture scenario is similar to the sealed-fracture scenario in that it also considers two fractures created in the wellbore section being considered as shown in **Fig. 21**.

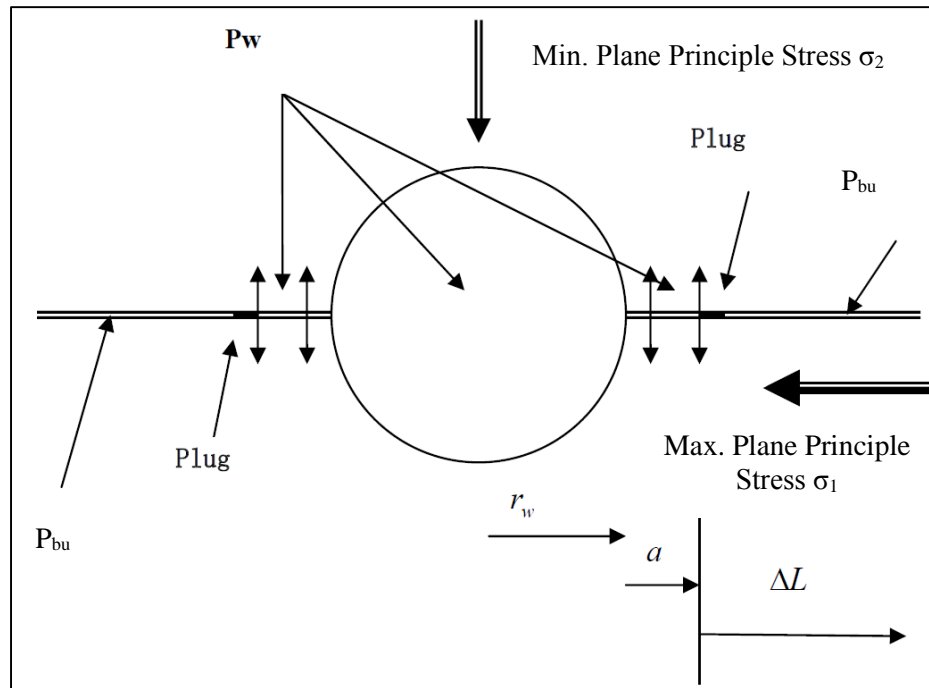


Fig. 21 - The description of the plugged fracture scenario of particle and fracture interaction in wellbore strengthening (Morita et al. 2012).

The same changes that were applied to the sealed-fracture scenario solution were also applied to the plugged-fracture solution to ensure its compatibility with the rest of the model and to achieve the desired improvements. However, there are some notable differences between the descriptions of the two scenarios. In this scenario, the parameter “a” defines the distance at which the solid particles plug the fracture and the parameter ΔL defines the length of the fracture, excluding the plugging distance. In the sealed-fracture scenario, ΔL defines the length of the fracture as a whole. Also, the solution considers the pressure buildup, P_{bu} , to be in effect behind the plugging particles only.

After making the required adjustments to the solution, the final equation for the enhanced fracturing pressure for the second scenario that will be used in the model will be as follows:

$$P_{f-enhanced} = \frac{\frac{k^c}{\sqrt{\pi(a+\Delta L)}} + \sigma_2 F_\lambda(s) - 2L \frac{P_{bu}}{\sqrt{\pi(a+\Delta L)\sqrt{\pi L}}} [\arcsin \sqrt{\frac{\Delta L}{2L}} - \arcsin \sqrt{\frac{2L-\Delta L}{2L}} + \frac{\pi}{2}]}{1 + (1-s)(0.5 + 0.743(1-s)^2) - 2L \frac{1}{\sqrt{\pi(a+\Delta L)\sqrt{\pi L}}} [\arcsin \sqrt{\frac{\Delta L}{2L}} - \arcsin \sqrt{\frac{2L-\Delta L}{2L}} + \frac{\pi}{2}]} \dots (\text{Eq. 2.56})$$

Where:

$$\Delta L = \frac{W_c E}{4(1-\nu^2)(\sigma_2 - P_{bu})} \dots (\text{Eq. 2.57})$$

$$\lambda = \frac{\sigma_1}{\sigma_2} \dots (\text{Eq. 2.58})$$

$$s = \frac{a + \Delta L}{(r_w + a + \Delta L)} \dots (\text{Eq. 2.59})$$

$$L = r_w + a + \Delta L \dots (\text{Eq. 2.60})$$

$$\omega = \frac{P_{bu}}{\sigma_2} \dots\dots\dots (Eq. 2.61)$$

$$F_1(s) = 1 + (1 - s)[0.5 + 0.743(1 - s)^2] \dots\dots\dots (Eq. 2.62)$$

$$F_o(s) = 0.5(3 - s)[1 + 1.243(1 - s)^3] \dots\dots\dots (Eq. 2.63)$$

$$F_\lambda(s) = (1 - \lambda)F_o(s) + \lambda F_1(s) \dots\dots\dots (Eq. 2.64)$$

2.7 Model Interface

For the purpose of generating results in a timely manner, a user-friendly interface was created to accompany the model's VBA Excel programming code. The interface accepts the input data from the user that defines the section of the well being targeted for examination, field stress data, rock basic mechanical properties, and wellbore strengthening techniques data. The initial results of the model can be obtained using the command buttons shown in **Fig. 22**.

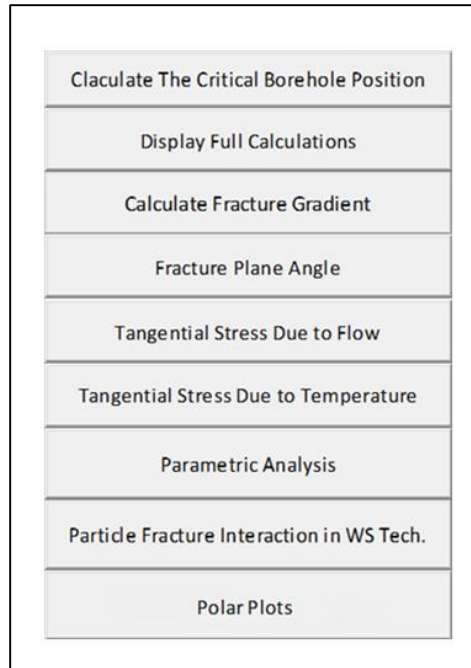


Fig. 22 - The command buttons used in the model to obtain the initial results.

These command buttons perform the initial calculations of the model and display the results in the form of a message box and on an Excel spreadsheet. The commands performed are as follows:

1. Display the value of the critical angle (θ_c), which defines the circumferential position of fracture initiation in the wellbore wall.
2. Display the full calculations performed at every degree of the wellbore circumference.
3. Display the value of the initial fracture gradient (g_{fi}) corresponding to the section of the well being examined.
4. Display the angle of the zero shear plane ($2\xi_p$).

5. Display the correction to the effective tangential stress due to mud filtration ($\Delta\sigma_{te(q)}$) and temperature change ($\Delta\sigma_{te(T)}$).
6. Display the user form that enables generating parametric analysis of the effect of various parameters on the initial fracture-pressure gradient and the temperature- and mud filtrate-affected fracture-pressure gradients.
7. Display the user form that enables the user to enter the data required for each wellbore strengthening scenario.
8. Display the user form that enables the user to generate the ease-of-drilling polar plots.

The model requires specific input data to perform the wellbore strengthening evaluation calculations. The first input is selecting the type or the scenario of solid particles and fracture interaction. After pressing the “Particle Fracture Interaction in WS Tech.”, the user form shown in **Fig. 23** will appear.

Fracture Formation Strengthening Evaluation

Fracture Type

☒ Sealed Fracture ☐ Plugged Fracture

Sealed Fracture

Wellbore Radius, inch

Fracture Aperture, inch

Fracture Toughness, psi.inch^{1/2}

☐ Fracture Pressure Buildup

Fracture Pressure, psi

Plugged Fracture

Wellbore Radius, inch

Fracture Aperture, inch

Fracture Toughness, psi.inch^{1/2}

Plug Placement, inch

☐ Fracture Pressure Buildup

Fracture Pressure, psi

Calculate Fracture Gradient

Parametric Analysis

Polar Plot Data

Fig. 23 - The user form that enables the model to select the particle and fracture interaction scenario and input the data for each scenario.

The user can select the appropriate scenario and enter the required data that can be related to the closed-form solution as follows:

1. Wellbore radius (r_w) in inches
2. Fracture aperture (W_c) in inches
3. Fracture toughness (k^c) in $\text{psi.inch}^{1/2}$

4. Fracture-pressure buildup (P_{ub}) in psi; if left blank, assumed to be zero
5. Plug placement distance from the mouth of the fracture (a) in inches (applies to the plugged fracture option only)

This will enable obtaining the fracture-pressure gradient resulting from applying the selected wellbore strengthening technique.

The “Parametric Analysis” command button shown in **Fig. 22** will prompt the form shown in **Fig. 24**.

Parametric Analysis

Please Select the Parameter You Would Like to Use for the Sensitivity Analysis and Enter the Center of the Range of the Parameter Values:

Parameters

☒ **Poisson Ratio**
Enter the center of the range that will be varied by 0.02 over five increments.

☐ **Young Modulus, psi.**
Enter the center of the range that will be varied by 2×10^6 psi over five increments.

☐ **Wellbore Azimuth, Degrees**
Enter the center of the range that will be varied by 5 deg. over five increments at a constant intermediated in-situ stress direction.

☐ **Wellbore Inclination, Degrees**
Enter the center of the range that will be varied by 5 Deg. psi over five increments. 0-90

Plot the Results

Fig. 24 - The user form that enables selecting the base variable for the initial parametric analysis.

This user form produces different plots that show the effect of the four parameters listed on:

1. The initial fracture-pressure gradient (g_{fi})
2. The temperature-influenced fracture-pressure gradient ($g_{fi(T)}$)
3. The mud filtrate-influenced fracture-pressure gradient ($g_{fi(q)}$)
4. The combined temperature and mud filtrate- influenced fracture-pressure gradient ($g_{fi(qT)}$).

The user form allows for entering a value for a parameter that will be the base for the parametric analysis. This input value will be used as the center of a range of values of the particular parameter. Then, the code will calculate the different types of the fracture-pressure gradient at each value of the parameter and will plot the results graphically in a separate Excel worksheet.

A similar analysis can be performed on the wellbore strengthening influenced fracture-pressure gradient using the form shown in **Fig. 25**.

Parametric Analysis

Please Select the Parameter You Would Like to Use for the Sensitivity Analysis and Enter the Center of the Range of the Parameter Values:

Parameters

- ☒ **Poisson Ratio**
Enter the center of the range that will be varied by 0.02 over five increments.
- ☐ **Young Modulus, psi.**
Enter the center of the range that will be varied by 2×10^6 psi over five increments.
- ☐ **Wellbore Azimuth, Degrees**
Enter the center of the range that will be varied by 5 deg. over five increments at a constant intermediated in-situ stress direction.
- ☐ **Wellbore Inclination, Degrees**
Enter the center of the range that will be varied by 5 Deg. psi over five increments. 0-90
- ☐ **Wellbore Radius, Inches**
Enter the center of the range that will be varied by 0.5 in. psi over five increments.
- ☐ **Fracture Aperture, inch**
Enter the center of the range that will be varied by 0.005 in. over five increments.
- ☐ **Fracture Toughness, $\text{psi} \cdot \text{inch}^{1/2}$**
Enter the center of the range that will be varied by 200 $\text{psi} \cdot \text{inch}^{1/2}$ over five increments.
- ☐ **Plug Placement, inch**
Enter the center of the range that will be varied by 0.2 in. over five increments.
- ☐ **Fracture Pressure Buildup, psi**
Enter the center of the range that will be varied by 100 psi over five increments.

Fig. 25 - The user form that enables selecting the base variable for the final parametric analysis.

This form can be obtained by pressing the command button “Parametric Analysis” in the user form shown in **Fig. 23**, and it performs the same task as the user form shown in **Fig. 24**. The only difference is that this form offers more parameters to be used as the basis of the analysis. These additional parameters are concerned with the

solid particle and fracture interaction type. The produced plots will show the trend exhibited by the following:

1. Initial fracture-pressure gradient, g_{fi}
2. Wellbore strengthening influenced fracture-pressure gradient, g_{fFS}
3. Temperature and wellbore strengthening influenced fracture-pressure gradient, $g_{fFS(T)}$
4. Mud filtrate and wellbore strengthening influenced fracture-pressure gradient, $g_{fFS(q)}$
5. Temperature, mud filtrate and wellbore strengthening combined influenced fracture-pressure gradient, $g_{fFS(qT)}$

For the purpose of analyzing the performance of wellbore strengthening techniques based on the well section placement with respect to the field in-situ stresses, the options shown in **Fig. 26** were created.

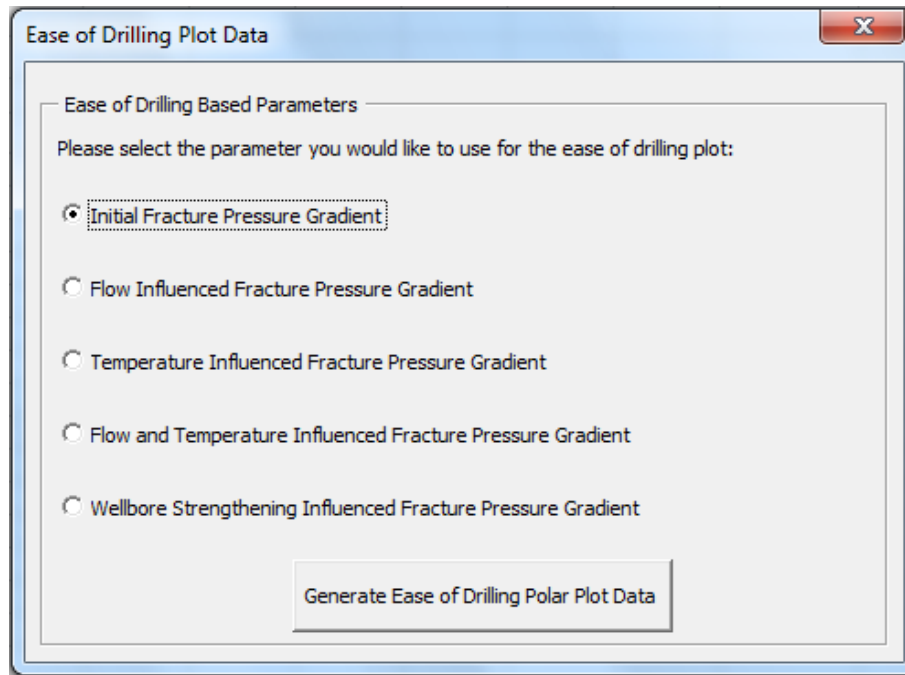
A screenshot of a software window titled "Ease of Drilling Plot Data". The window has a standard Windows-style title bar with a close button (X) in the top right corner. Inside the window, there is a section titled "Ease of Drilling Based Parameters" with a subtitle "Please select the parameter you would like to use for the ease of drilling plot:". Below this, there are five radio button options: "Initial Fracture Pressure Gradient" (which is selected), "Flow Influenced Fracture Pressure Gradient", "Temperature Influenced Fracture Pressure Gradient", "Flow and Temperature Influenced Fracture Pressure Gradient", and "Wellbore Strengthening Influenced Fracture Pressure Gradient". At the bottom of the window, there is a button labeled "Generate Ease of Drilling Polar Plot Data".

Fig. 26 - Ease of drilling data user form.

The user form shown in **Fig. 26** will be used to create polar plots that show the ease of drilling that particular section of the well based on the well surface location and trajectory. The generated plots use the well azimuth angle in polar coordinates to display all of the possible well placement scenarios. In radial coordinates, a parameter that can be called “ease-of-drilling fraction” is calculated and plotted for every possible well placement scenario. The purpose of this parameter is to demonstrate the size of the drilling window compared with a reference window size. The code uses two references for the drilling window size when calculating the ease-of-drilling fraction. The first reference is based on the maximum possible fracture-pressure gradient in the 360° azimuth range for the individual well section and fracture-pressure gradient type in

consideration. Based on this fracture-pressure gradient, the ease-of-drilling fraction will be calculated for each 0.5° of the 360° azimuth as follows:

$$\text{Ease of Drilling Fraction (Based on Maximum } g_f) = \frac{g_f}{\text{Max } g_f} \dots\dots\dots (\text{Eq. 2.65})$$

This calculation is done for all of the different types of fracture-pressure gradients, which include the initial fracture-pressure gradient, g_{fi} , the temperature-influenced fracture-pressure gradient, $g_{f(T)}$, the mud filtrate-influenced fracture-pressure gradient, $g_{f(q)}$, and the temperature and mud filtrate combined influenced fracture-pressure gradient, $g_{f(qT)}$. Because the "ease-of-drilling polar plot" is based on a specific and unique to the plot reference value (the maximum possible fracture-pressure gradient in the 360° azimuth range), two different polar plots cannot be compared to each other to decide which type of fracture-pressure gradient provides the wider drilling window in a certain direction. For that reason, the code calculates the ease-of-drilling fraction with a constant reference value for all the different types of fracture-pressure gradients as follows:

$$\text{Ease of Drilling Fraction (Based on } C \text{ psi/ft)} = \frac{g_f}{C} \dots\dots\dots (\text{Eq. 2.66})$$

The reference value for the ease-of-drilling-fraction is selected to be equal to or greater than the maximum possible value of the fracture-pressure gradient. This assumption will make it possible to compare different ease-of-drilling polar plots, even if they are based on different types of fracture-pressure gradients. For example, using the constant reference in the ease-of-drilling fraction, the ease-of-drilling polar plot for a particular section of the well based on the initial fracture-pressure gradient can be

compared to the ease-of-drilling polar plot for the same section of the well based on the wellbore strengthening influenced fracture-pressure gradient.

Fig. 27 shows a sample of the produced polar plots that will be discussed in more details in the next chapter.

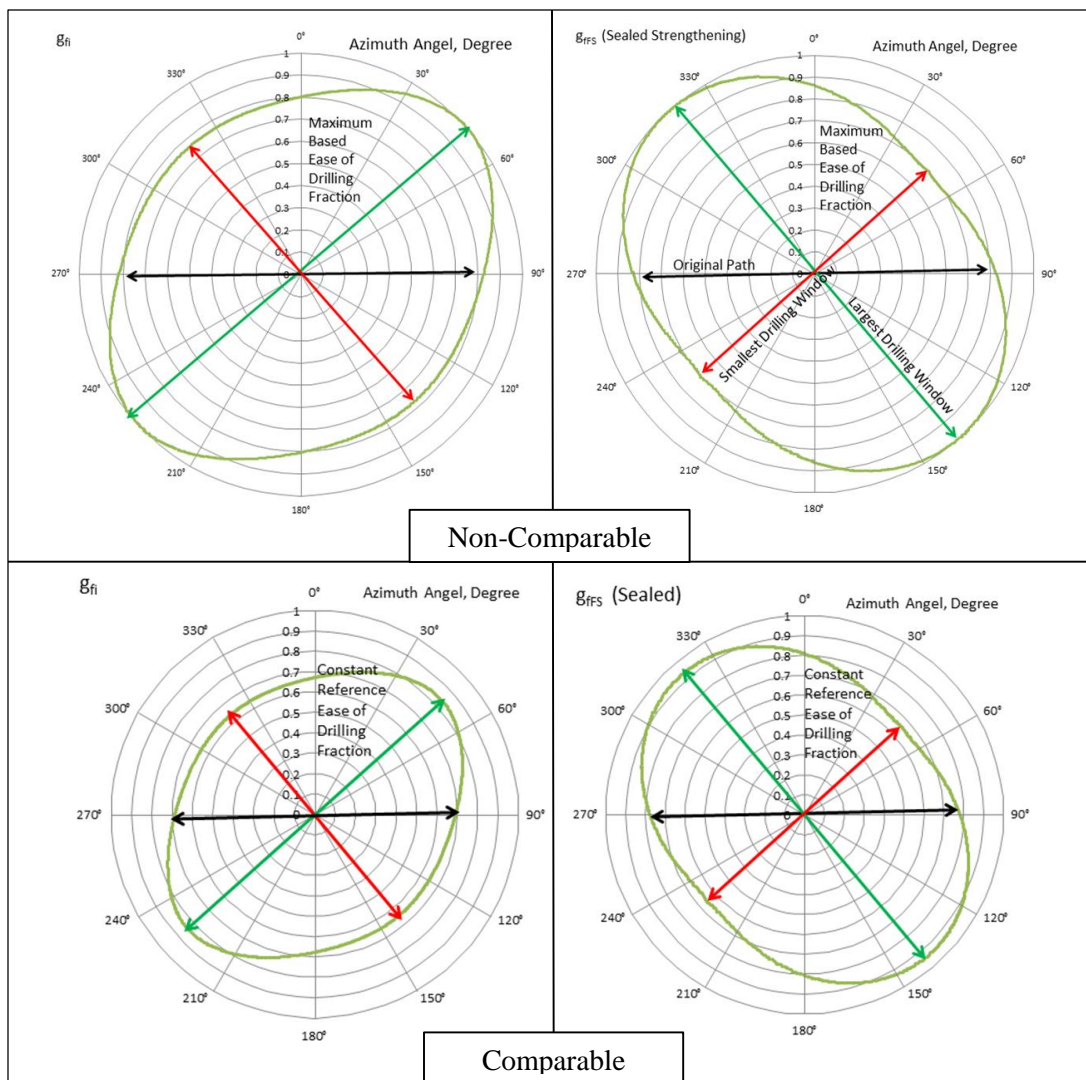


Fig. 27 - Samples of the produced polar plots highlighting the differences between them each type.

3. MODEL RESULTS AND ANALYSIS (CASE STUDY SCENARIO)

3.1 The Case Study Setup

For the model to produce the targeted results, there is a set of input data required. The input data is aimed at defining the following:

- The targeted wellbore section in terms of its position with respect to the field in-situ stresses, trajectory, and depth
- The field in-situ stresses in terms of magnitude and direction
- The targeted formation pore pressure
- The targeted formation basic rock mechanic parameters, including Poisson's ratio, Young's modulus, and the thermal expansion coefficient
- The drilling fluid properties, including the pressure overbalance it provides and the temperature change it brings to the wellbore.

For the purpose of evaluating the general performance of the formation strengthening techniques previously presented, a case study is created based on typical and common input parameter values. The model's code accepts the input values and yields realistic values as long as the input values for each parameter are within a reasonable range.

Table 1 shows the values selected for this particular case study:

Table 1 - The initial input values for the model case study.

Input Depth, ft	14,000
Input Pore Pressure Gradient, ppg	12
Input vertical Stress σ_v Gradient, psi/ft	0.972
Input Poisson's ratio ν	0.25
Input σ_H (max horiz.) Gradient, psi/ft	0.8
Input σ_h (min horiz.) Gradient, psi/ft	0.739
Input Well Azimuth, degree	88
Input Well inclination γ (Between σ_1 and Borehole Axis), degree	70
Input σ_H (max horiz.) direction measured from the north clock-wise, degree	138
Input Beta β (Between σ_H and Borehole Projection on σ_H - σ_h Plane or Azimuth), degree	50
Input Actual Borehole Pressure Gradient for $\Delta\sigma_{te(q)}$ Calculations, ppg	12.1
Input Temperature Increment ΔT , F°	10
Input Young's Modulus E, psi	2500000
Input Coefficient of Thermal Expansion α_T , in/(in -F°)	0.000008

These values represent typical values for a Gulf of Mexico field, showing in-situ stress anisotropy due to a salt dome intrusion (Watson et al 2003). In this case study, the vertical stress or the vertical overburden is the maximum in-situ stress; however, the well section being considered is drilled with a 70° inclination angle. In the model, this inclination angle is interpreted as a 70° deviation of the wellbore section from the maximum in-situ stress direction. Also, the wellbore projection on the σ_H - σ_h plane is located at 50° from the direction of the maximum horizontal stress σ_H , all of which means that the wellbore section does not fall on the same coordinate system as do the in-situ stresses. This condition will necessitate that the model performs the discussed transformation of the in-situ stresses to the wellbore section coordinate system. **Fig. 28**

shows the visual representation of the position of the well section of interest with respect to the in-situ stresses and the two coordinate systems involved in the transformation process of the model.

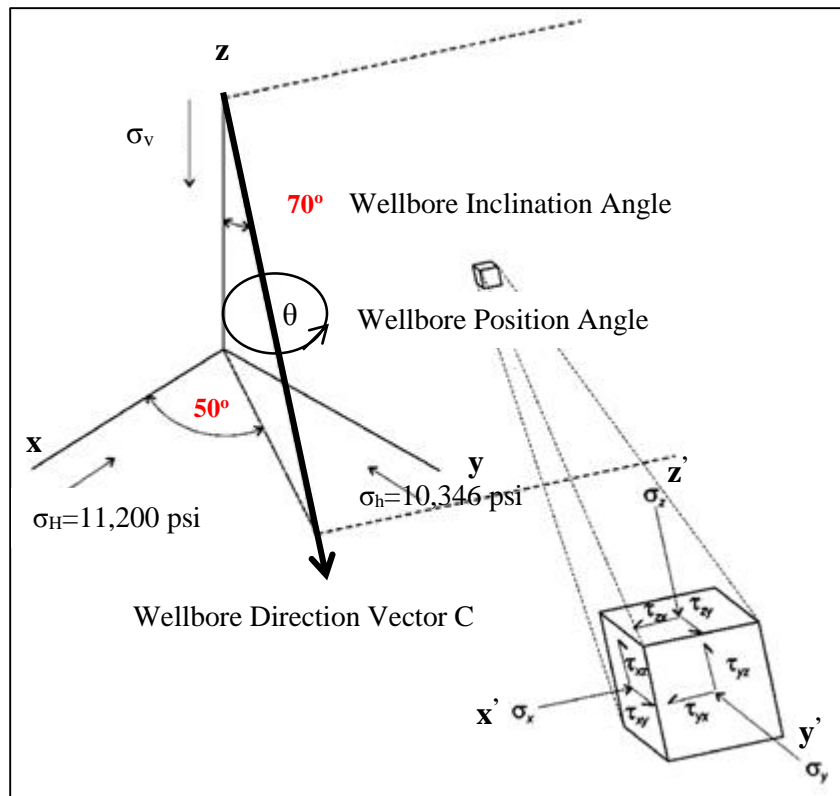


Fig. 28 - Description of the case study well trajectory and position with respect to the in-situ stresses (Watson et al. 2003).

Upon performing the transformation, the model's code will move to the calculation of the induced stresses around the wellbore and eventually determine the two principle stresses acting on the plane of zero shear stress. The next step in the process is

determining the critical angle of the circumferential position of the wellbore, which is defined by the minimum value of the minimum principle stress. The final step that the model performs at this stage is defining the minimum wellbore pressure that has the ability to set the effective minimum principle stress to zero. This value of wellbore pressure will be considered as the initial fracture pressure of formation.

3.2 The Preliminary Results

In preparation for evaluating the wellbore strengthening techniques, the model produces the preliminary results as shown in **Table 2**. These values explain the fracture system in the wellbore before applying any wellbore strengthening procedure. The values also depict the initial reaction of the fracture system to a wellbore pressure overbalance, resulting in mud filtration and to the wellbore wall exposure to drilling fluid resulting in a change in the temperature. The most important value in the preliminary results is the initial fracture-pressure gradient. This is the value that is going to be used as a reference when the model reaches the wellbore strengthening techniques evaluation portion and the well placement and trajectory evaluation portion.

Table 2 - The model preliminary results.

Critical Borehole Position, Degrees	169
Fracture Initiation Gradient Δg_{fi}, psi/ft	0.6957
Incremental Change in Effective Tangential Stress due to Flow $\Delta \sigma_{te(q)}$, psig	-48.5
Recalculated Fracture Initiation Gradient due to Flow $\Delta g_{f(q)}$, psi/ft	0.6922
Incremental Change in Effective Tangential Stress due to Temperature $\Delta \sigma_{te(T)}$, psig	266.7
Recalculated Fracture Initiation Gradient due to Temperature $\Delta g_{f(T)}$, psi/ft	0.7148
Recalculated Fracture Initiation Gradient due to Flow and Temperature $\Delta g_{f(qT)}$, psi/ft	0.7113
Fracture Plane Angel Measured from the Wellbore Axis $2\xi_p$, Degrees	-67.6

By examining the preliminary results, the detrimental effect of the mud filtration flow in the formation on the fracture-pressure gradient is clearly obvious. As previously discussed, the reduction of the fracture-pressure gradient is the result of applying the Biot's principle of effective stress. This fracture-pressure gradient reduction was built into the model by introducing the overbalance and filtration correction relationship discussed in Section 2.5. The beneficial effect of increasing the temperature of the wellbore wall on the fracture-pressure gradient is also obvious. The temperature effect found in the model by introducing the temperature change correction relationship discussed in Section 2.5.

The model set up the transition to the wellbore strengthening techniques evaluation by defining the plane of the fracture or the plane of zero shear stress. The plane of the fracture is defined by an angle measured from the wellbore section axis. Even though this angle has two values, only one value is displayed because the two values are separated by 180° and define the same plane. The principle stress calculations

are performed in this stage of the model. The model analyzes these calculations and defines the value of the two principle stresses acting on the plane of zero shear stress at the defined critical angle. These are the stresses that will be used in evaluating the wellbore strengthening techniques' performance.

3.3 Wellbore Strengthening Evaluation Data and Preliminary Results

Additional input data are required for the evaluation. These data describe the nature of the interaction between the drilling fluid solid particles intended to be used for the treatment and the initiated fractures. A drilling engineer is not expected to have a sufficient knowledge or access to this type data. Therefore, cooperation between a drilling engineer, a field geologist and a rock mechanics lab technician is required. Starting with the fracture aperture parameter, it can be estimated based on the applied stress as discussed in (Kulatilake et al. 2006). As for the fracture toughness, it can be assigned a value based on the type of rock being treated. Zhao et al. and Senseny et al. discuss the process of fracture toughness determination and list typical values for the parameter based on the rock type (Zhao et al. 1993), (Senseny et al. 1984). The plug placement is determined based on the size of the drilling fluid bridging particle, which should be obtainable by the drilling engineer, and the fracture aperture. Finally, pressure buildup behind the plug can be estimated based on the permeability of the formation rock. As the rock permeability increases, as the value of the pressure buildup approaches

zero. It is preferable, as will be discussed in the pressure buildup parametric analysis, that the buildup is kept at a minimum to avoid the undesired fracture elongation. That is the reason behind assuming this value to be a zero for both scenarios in this particular case scenario.

As discussed previously, there are two scenarios for the interaction between the drilling fluid solid particles. For this case study, typical values will be used for the required parameters for each scenario. These values are the same values used by (Morita et al. 2012) in their paper that discuss the closed form solution to the integral of the stress intensity factor. **Table 3** shows these values for each scenario.

Table 3 - Input data describing the interaction between the induced fractures and the solid particles for the wellbore strengthening part of the model case study.

Scenario	Fracture Plugged at the Mouth (Sealed)	Fracture Plugged at a Distance
Wellbore Radius r_w , inch	4.25	4.25
Fracture Aperture W_c , inch	0.02	0.02
Fracture Toughness k^c , psi.inch ^{1/2}	500	500
Plug Placement a , inch	0	0.5
Pressure Build up Behind the Plug P_{bu} , psi	0	0

The results from applying these parameters in the model are shown in **Table 4**. In this particular case, the model shows that the fracture-pressure gradient is enhanced by 11% when considering the first scenario and by 3% when considering the second

scenario. This is of course favorable; however, it does not present a complete picture of the performance of the wellbore strengthening techniques.

Table 4 - The initial result of the wellbore strengthening performance evaluation from the model case study.

Strengthening Technique Scenario	Initial Fracture Pressure Gradient, psi/ft	New Fracture Pressure Gradient, psi/ft	Improvement Percentage, %
Sealed Fracture Strengthening Scenario	0.6957	0.7723	11%
Plugged Fracture Strengthening Scenario	0.6957	0.7175	3%

3.4 Parametric Analysis

To examine the effect of certain parameters on the performance of the wellbore strengthening techniques, the model calculates the different fracture-pressure gradients resulting from varying the value of a single parameter while holding the other parameters constant. This procedure is also used to gain a more complete understanding of the wellbore strengthening techniques effect on the fracture-pressure gradient when using values that are different from the values used in the previous case study. In addition, this parametric analysis provides a reliable process for determining the optimal value for each parameter. One final and significant reason for performing this parametric analysis is to use the analysis as a form of validation and evaluation to the model final

results. There are typical trends in the fracture-pressure gradient which can be found in literature and published field experience. This analysis should provide a tool for a preliminary evaluation of the model performance and eventually highlight its weaknesses.

The analysis is performed in two stages, first before and then after applying the wellbore strengthening techniques. In the first stage, a sensitivity analysis will be performed for the following parameters

1. Poisson's ratio
2. Young's modulus
3. Wellbore placement with respect to the in-situ stresses and azimuth
4. Wellbore section inclination and trajectory

This is to examine their effect on the:

1. The initial fracture-pressure gradient (g_{fi})
2. The temperature-influenced fracture-pressure gradient ($g_{fi(T)}$)
3. The mud filtrate-influenced fracture-pressure gradient ($g_{fi(q)}$)
4. The combined temperature and mud filtrate- influenced fracture-pressure gradient ($g_{fi(qT)}$).

In the second stage, a sensitivity analysis will be performed for the following selected parameters that include the parameters used to describe the nature of interaction between the drilling fluid solid particles:

1. Poisson's ratio
2. Young's modulus
3. Wellbore placement with respect to the in-situ stresses and azimuth
4. Wellbore section inclination and trajectory
5. Wellbore diameter
6. Fracture aperture
7. Fracture toughness
8. Plug placement
9. Fracture-pressure buildup

In this stage, the following will be examined:

1. Initial fracture-pressure gradient, g_{fi}
2. Wellbore strengthening influenced fracture-pressure gradient, g_{fFS}
3. Temperature and wellbore strengthening influenced fracture-pressure gradient, $g_{fFS(T)}$
4. Mud filtrate and wellbore strengthening influenced fracture-pressure gradient, $g_{fFS(q)}$
5. Temperature, mud filtrate and wellbore strengthening combined influenced fracture-pressure gradient, $g_{fFS(qT)}$

3.4.1 First Stage Parametric Analysis

The purpose of this stage is to gain a better understanding of the effect of the selected parameters on the model results before taking into consideration the effect of the fracture and particle interaction. Comparing the results produced in this stage to the

results produced in the next stage will be beneficial to the process of strengthening candidate selection. This is because the comparison will highlight the main characteristics of a well that has the potential to undergo a successful strengthening treatment.

3.4.1.1 First stage Poisson's ratio analysis

The first sensitivity analysis is performed to examine the change in the fracture-pressure gradients as the Poisson's ratio value is varied. Poisson's ratio is one of the two parameters that govern the formation rock mechanical response to applied stress in the model along with the Young's modulus. Considering that the definition of the Poisson's ratio is "the ratio of lateral expansion to longitudinal contraction for a rock under a uniaxial stress condition." (Fjaer et al. 2008), the model uses this parameter to translate the formation rock response to the combined effect of the in-situ stresses and the existence of a wellbore. The model also uses this parameter to translate the formation rock response to changes in effective stress as a result of the temperature variation or mud filtration. The sensitivity analysis is performed over a range of Poisson's ratio values commonly encountered in formations as shown in **Table 5**. The result of the Poisson's ratio sensitivity analysis using the model is shown in **Fig. 29**.

Table 5 - The range of Young's modulus and Poisson's ratio used for the parametric analysis (Fjaer et al. 2008).

Rock Type	Young's Modulus psi	Poisson's Ratio
Unconsolidated Sand	1.45E+03-1.45E+04	0.45
Sandstone	1.45E+04-4.35E+06	0-0.45
Clay	8.70E+03-2.18E+04	0.4
Shale	5.80E+04-1.02E+07	0-0.3
High Porosity Chalk	7.25E+04-7.25E+05	0.05-0.35
Low Porosity Chalk	7.25E+05-4.35E+06	0.05-0.3
Basalt	7.25E+06-1.45E+07	0.2-0.3
Granite	7.25E+05-1.23E+07	0.1-0.34
Dolomite	1.45E+06-1.45E+07	0-0.5
Limestone	2.90E+05-1.45E+07	0-0.3
Gneiss	5.80E+06-1.45E+07	0.1-0.3
Marble	7.25E+05-1.31E+07	0-0.3

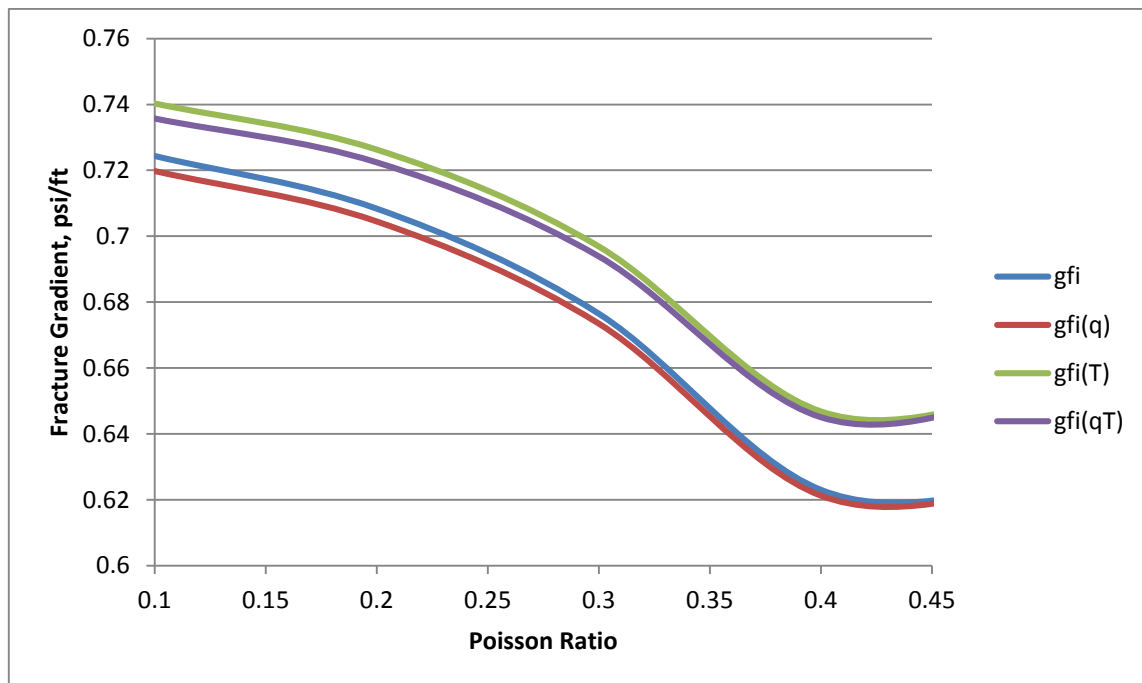


Fig. 29 - The results of the Poisson's ratio first stage parametric analysis showing a decrease in the fracture gradient with the increasing Poisson's ratio values.

The same trend is shown by all of the different fracture-pressure gradients calculated. At lower Poisson's ratio values, the gradients exhibit higher values. The gradient values decrease as the Poisson's ratio value increases until the gradient values reach a plateau. The reason for this trend is that the Poisson's ratio plays a predominant role in translating the formation rock response to the combined effect of the in-situ stresses and the existence of a wellbore. This trend means that Poisson's ratio is a major factor in determining the effect of the induced stresses on the resulting value of the fracture-pressure gradient. One important observation is the diminished effect of mud filtration as Poisson's ratio increases. The implication of this trend is that the formation rock will be less affected by mud filtration at high-Poisson's ratio values, which consequently will limit the detrimental effect of filtration on the fracture-pressure gradient at those values. On the contrary, the temperature influences increase with an increase in the Poisson's ratio. This result shows that formations with a Poisson's of 0.4 or higher will yield better results when the formation is strengthened by heating.

3.4.1.2 First stage Young's modulus analysis

Because the effect of Young's modulus in the model is based on a single empirical relationship, this model is not sufficiently reliable to be used for the Young's modulus sensitivity analysis. However, the analysis is performed through the model and the results are displayed here for two reasons. First, to gain a basic understanding of the types of rocks most affected by formation temperature strengthening. Second, to highlight this particular weakness of the model in terms of its reliance on an empirical relationship to show the effect of Young's modulus.

As with the Poisson's ratio analysis, the Young's modulus analysis was carried out over a range of Poisson's ratio values commonly encountered in the field as shown previously in Table 5. Young's modulus is a measure of the formation rock stiffness and is defined as "the ratio of stress to strain for uniaxial stress." (Fjaer et al. 2008) as shown in **Fig. 30**. The result of the Young's modulus sensitivity analysis from the model is shown in **Fig. 31**.

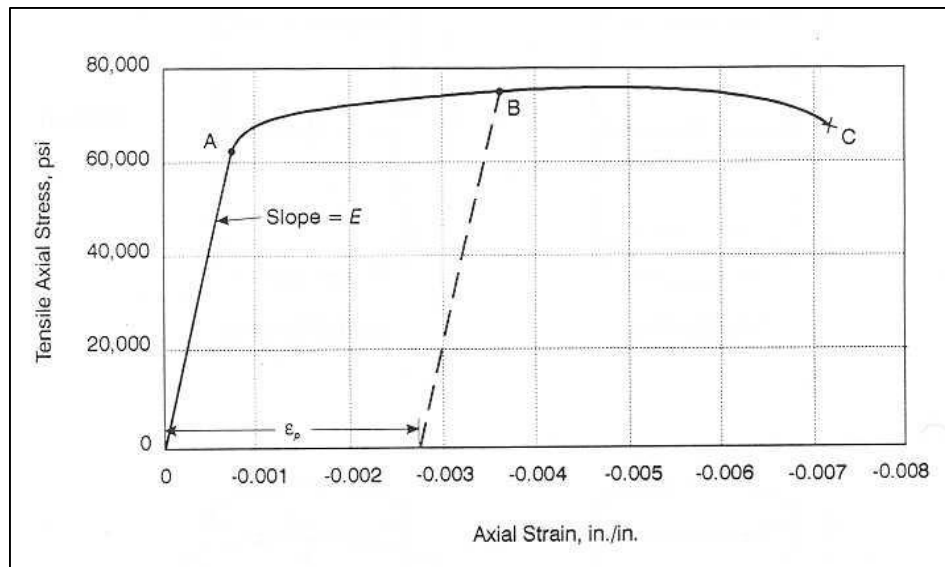


Fig. 30 - The definition of the Young's modulus as the slope of the stress versus strain plot (Watson et al. 2003).

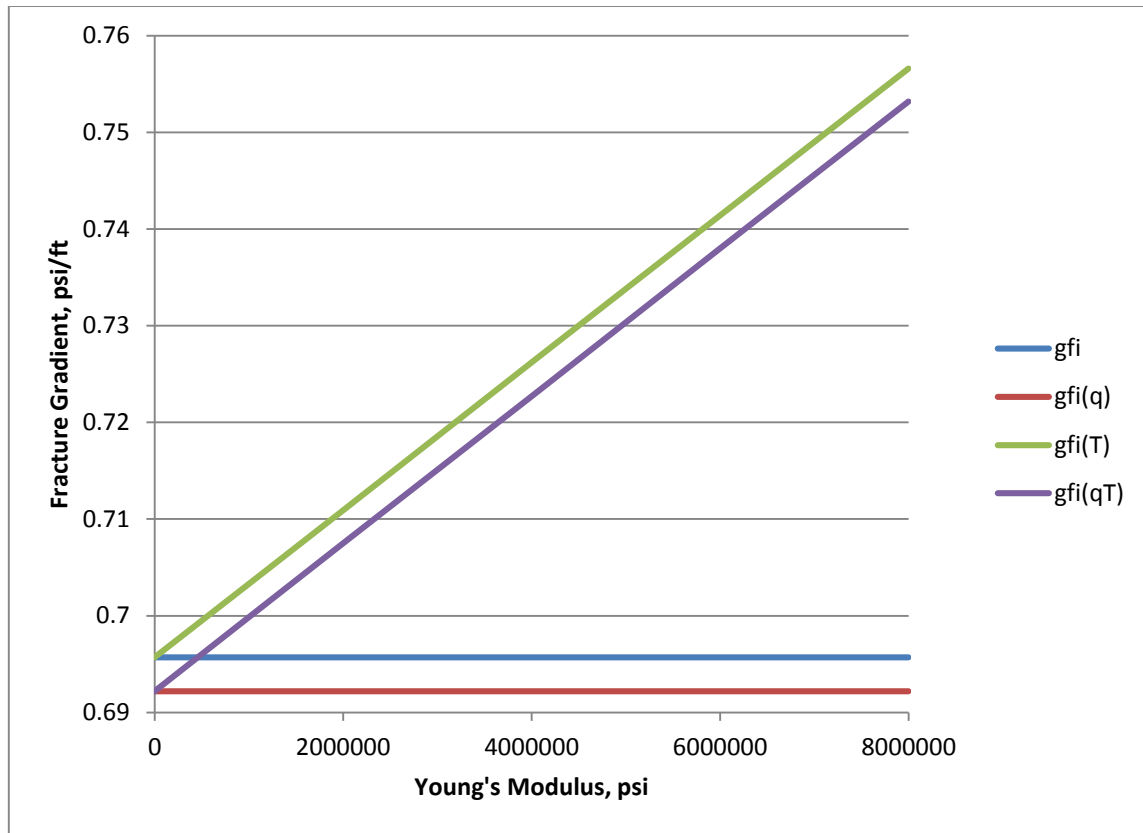


Fig. 31 - The results of the Young's modulus first stage parametric analysis showing an increase in the fracture gradient with the increasing Young modulus values.

Because the effect of Young's modulus in the model is based on a single empirical relationship, the initial and the mud filtrate-influenced fracture-pressure gradients are not affected by the change in Young's modulus. The main result from this analysis is that rocks with higher stiffness values will yield enhanced results when strengthened by heating. However, it should be noted that this conclusion is not entirely accurate because it ignores the change in the coefficient of thermal expansion of the rock.

3.4.1.3 First stage wellbore azimuth analysis

The next analysis focuses on the well azimuth angle. The purpose of this analysis is to examine the size of the drilling window in all of the possible orientations of the wellbore section. The results of this analysis are shown in **Fig. 32**.

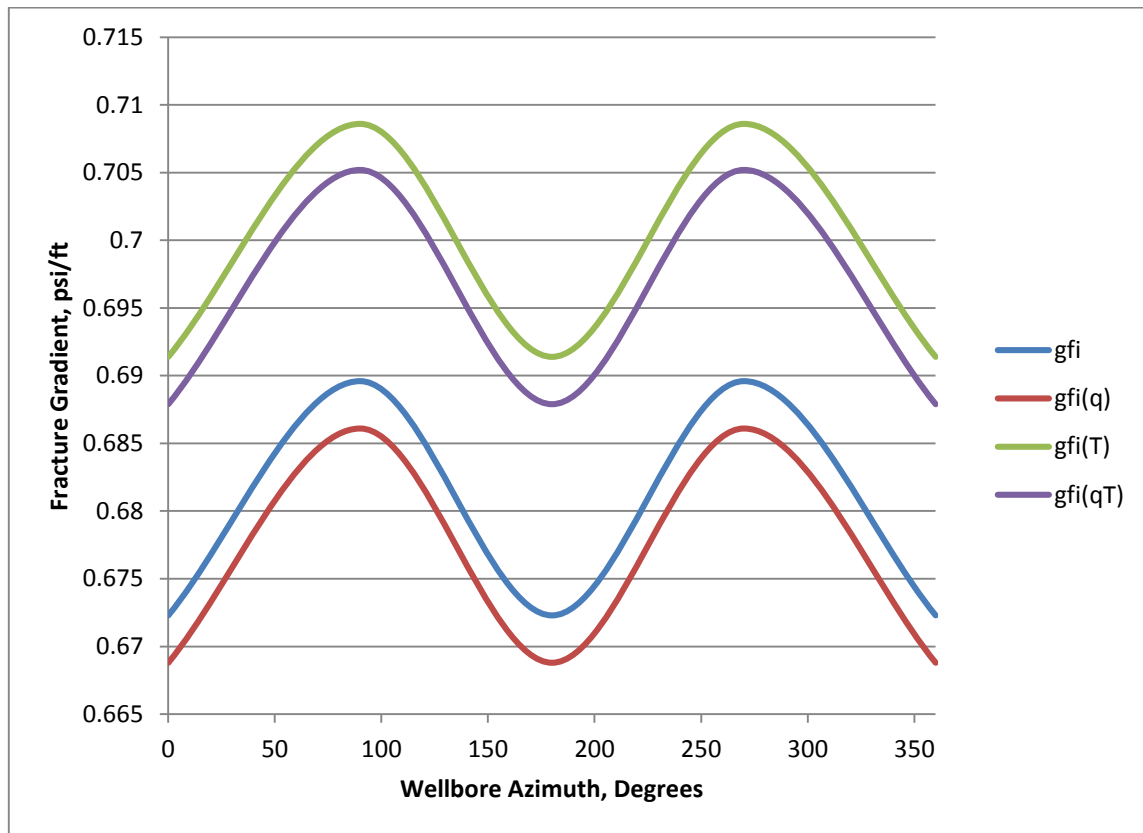


Fig. 32 - The results of the wellbore azimuth angle first stage parametric analysis.

The fracture-pressure gradients in the wellbore azimuth angle analysis are calculated every 90° of the 360° range. While the results shown illustrate the effect of the

wellbore orientation with respect to the in-situ stresses direction, it is not the best way to depict this effect in terms of accuracy and clarity. The preferred method is to create a polar plot that represents similar results in a more comprehensive fashion. The implications of this analysis will be discussed more thoroughly in the polar plots section.

3.4.1.4 First stage wellbore inclination analysis

The final sensitivity analysis at this pre-wellbore strengthening stage is the analysis of the wellbore section inclination angle. As discussed in the in-situ stress transformation section, the wellbore inclination angle is defined as the deviation of the wellbore from the maximum in-situ stress, which is the vertical overburden stress in this case. The results of this analysis are shown in **Fig. 33**.

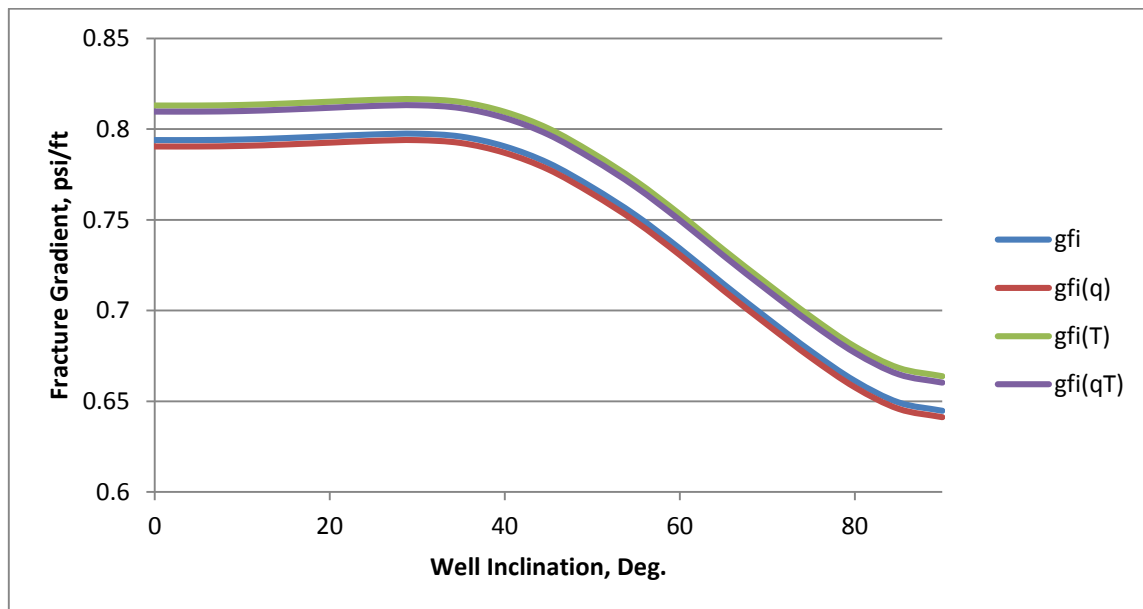


Fig. 33 - The results of the wellbore inclination angle first stage parametric analysis showing a decrease in the fracture gradient with the increasing inclination angle.

The different fracture-pressure gradient trends show that the changing wellbore inclination angle is greatly affected by the orientation of the in-situ stresses. As expected, the fracture gradients show a substantial decrease at the higher inclination angles. The decrease continues until the fracture gradients reach their minimum value at the horizontal wellbore. This result is typical as the horizontal sections of a well show a narrower drilling window, frequent lost circulation and hole stability problems due to the reduced fracture pressure. In this particular case, the gradients show a very slight and practically insignificant but interesting increase as the wellbore inclination shifts from the vertical to approximately 29° where they reach their maximum value. **Fig. 34** shows a magnified version of that trend.

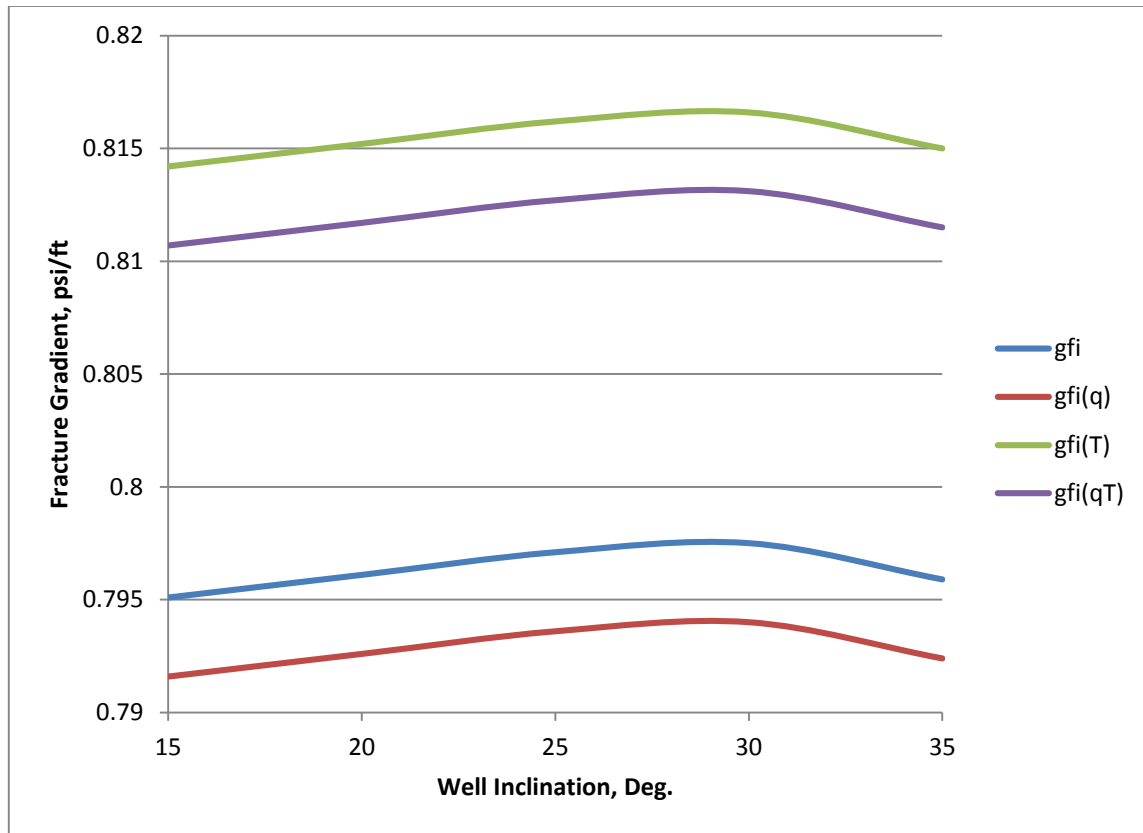


Fig. 34 - A magnified section of the graph of the results of the wellbore inclination angle first stage parametric analysis showing a slight increase in the fracture gradient with the increasing inclination angle.

The declining fracture gradient at high-inclination angles is the result of the vertical overburden stress. In vertical wells, the wellbore axis is aligned with the direction of the vertical overburden; therefore, the overburden does not contribute to wellbore-induced stresses as significantly as the two horizontal stresses. This conclusion means that the stress anisotropy is based on the difference between the two horizontal stresses in vertical sections. On the other hand, in inclined and horizontal wells, the overburden effect increases because it creates a larger stress anisotropy on the wellbore

as described previously in **Fig. 4**. The result of that trend is a decrease in fracture pressure.

The slight increase in the fracture gradients, which is around 0.0035 psi/ft in this particular case, at the beginning of the inclination is more complicated. A possible explanation is that the stress anisotropy changes favorably at the beginning of the inclination because the contribution of the overburden stress is still minimal compared with the two horizontal stresses. This favorable change in stress anisotropy continues until the inclination angle reaches a critical value, which is approximately 29° in this case. At this critical value, the fracture gradient reaches its maximum value. This critical inclination angle can be used to adjust the trajectory of a well to avoid exceeding this inclination if possible in problematic sections such as depleted formations where lost circulation and hole stability are concerns.

The conclusion of the parametric analysis at this stage is that the type of formation producing the widest drilling window is one with a low-Poisson's ratio and high-Young's modulus. This conclusion means, according to the values displayed in **Table 4**, that shale is least favorable option, while limestone is the most favorable. From the operational perspective, to maximize the fracture gradient through adjusting the well trajectory, optimally the suspect region will be drilled at a 29° inclination. This type of analysis can be carried out for any well during the well planning phase to evaluate whether applying these parameters is an economically sound decision.

3.4.2 Second Stage Parametric Analysis

The purpose of performing sensitivity analysis in the second stage is to examine the effect the different parameters have on the performance of the stress-related wellbore strengthening techniques. The same parameters used in the previous stage will be used in this analysis in addition to the parameters describing the interaction between the fracture and the mud solid particles. This analysis will help define the optimum value for each parameter to achieve the best possible result from the formation strengthening process.

3.4.2.1 Second stage Poisson's ratio analysis

The first sensitivity analysis is focused on the Poisson's ratio. The analysis was performed over the same range described in the previous stage, and the results of this analysis for the two wellbore strengthening scenarios described in **Fig. 20** and **Fig. 21** are shown in **Fig. 35** and **Fig. 36**. The initial fracture-pressure gradient is shown with formation strengthening gradients to illustrate the contrast in the effect of the Poisson's ratio on the gradients before and after applying the formation strengthening technique.

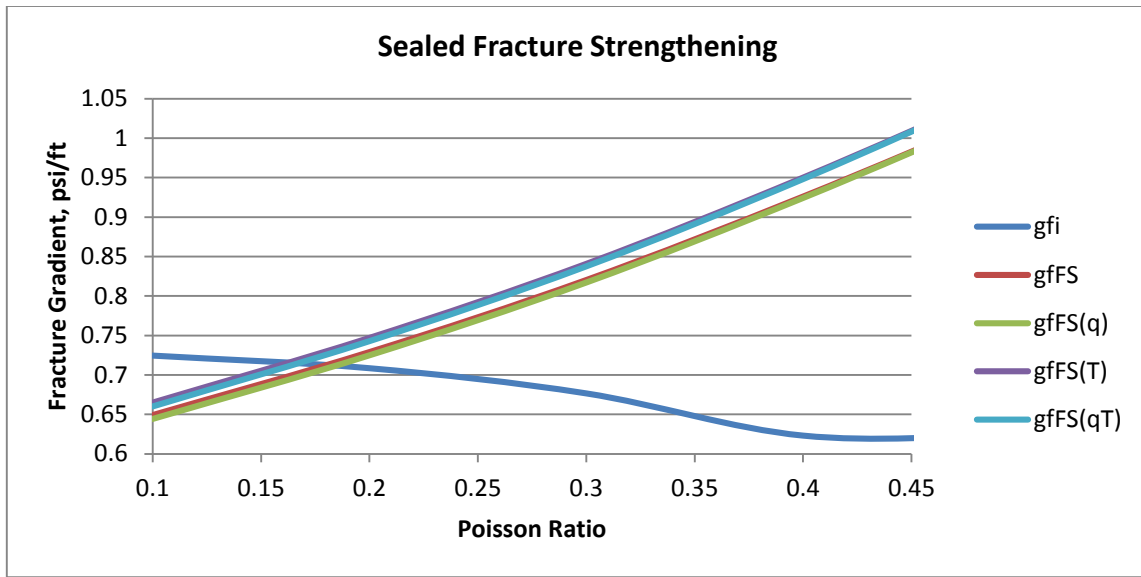


Fig. 35 - The results of the Poisson's ratio second stage sealed fracture strengthening parametric analysis showing an increase in the fracture gradient with the increasing Poisson's ratio values.

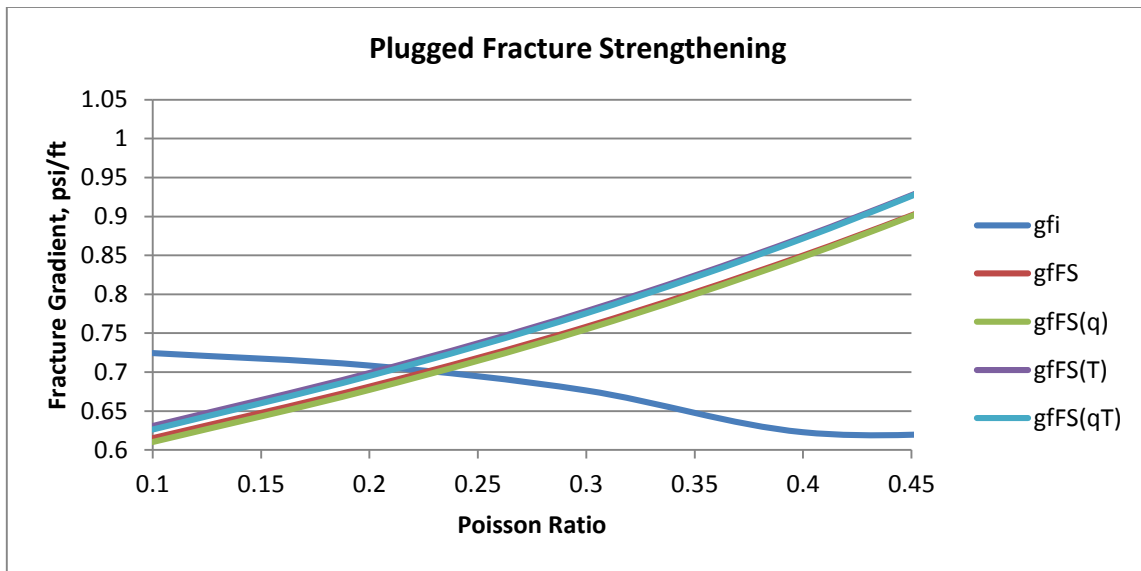


Fig. 36 - The results of the Poisson's ratio second stage plugged fracture strengthening parametric analysis showing an increase in the fracture gradient with the increasing Poisson's ratio values.

The model shows that the Poisson's ratio effect on the gradients is reversed after applying both of the strengthening techniques. As discussed in the previous stage, in the model, Poisson's ratio translates the axial induced stresses into the transverse direction, which means it translates the axial- and the tangential-induced stresses into a direction perpendicular to the respective stresses. That result explains why the fracture gradient decreases as Poisson's ratio increases because this conversion is reduced at higher Poisson's ratio values, leading a decrease in fracture resistance. After applying the strengthening technique, this process is reversed. In the wellbore strengthening case, the reversal occurs when the radial load is now acting on the sand face tangentially due to the intentional plugging of the fracture by the solid particles. The load reversal process is illustrated in **Fig. 37**. Another very important finding is that in this stage, the Poisson's ratio controls the fracture length and aperture. A higher Poisson's ratio leads to larger fracture aperture, which will lead to a more substantial enhancement of the tangential stress. This means that even though the low Poisson's ratio will produce the most favorable fracture gradient, a rock with a high Poisson's ratio has the most to gain from a strengthening technique. As a result of the enhancement of the tangential stress, higher fracture pressure will now be required to overcome the enhanced tangential stress and initiate a new fracture. Also, the higher values of Poisson's ratio lead to a smaller fracture length, which is the main reason supporting the importance of arresting the fracture length. The fracture length is arrested in several techniques such the "stress cage" method through limiting the "designer mud" filtration volumes and applying the

techniques in sufficiently permeable formations where the excess filtration will dissipate into the formation pores instead of elongating the fracture.

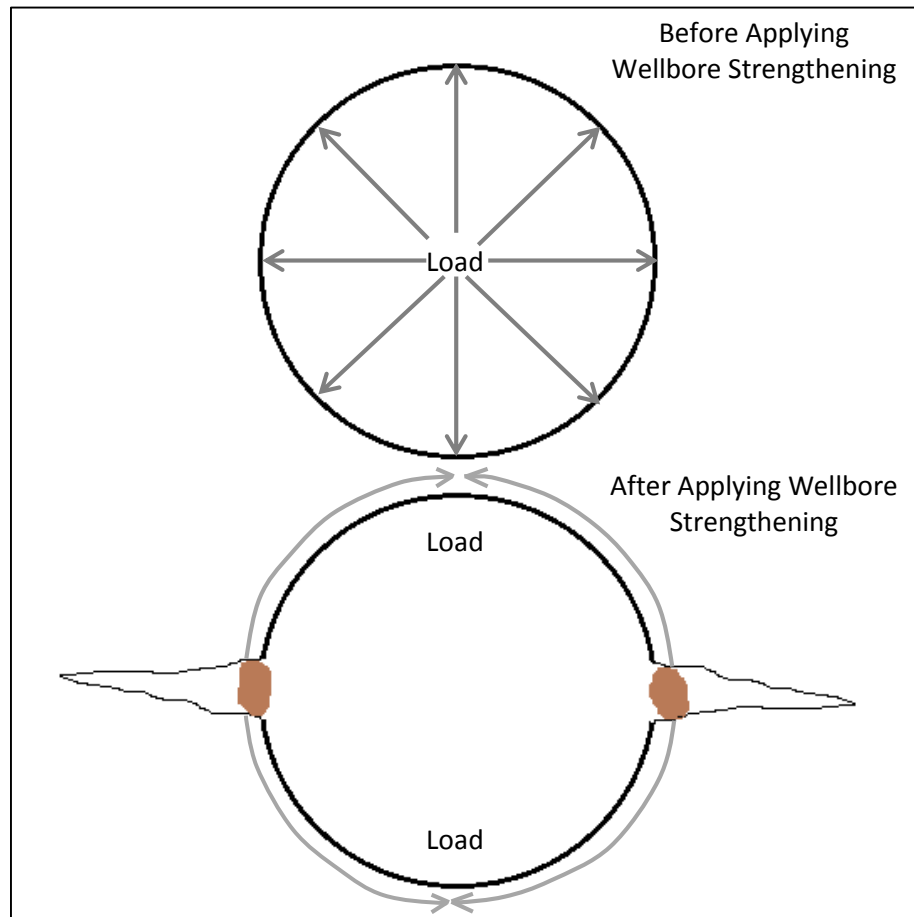
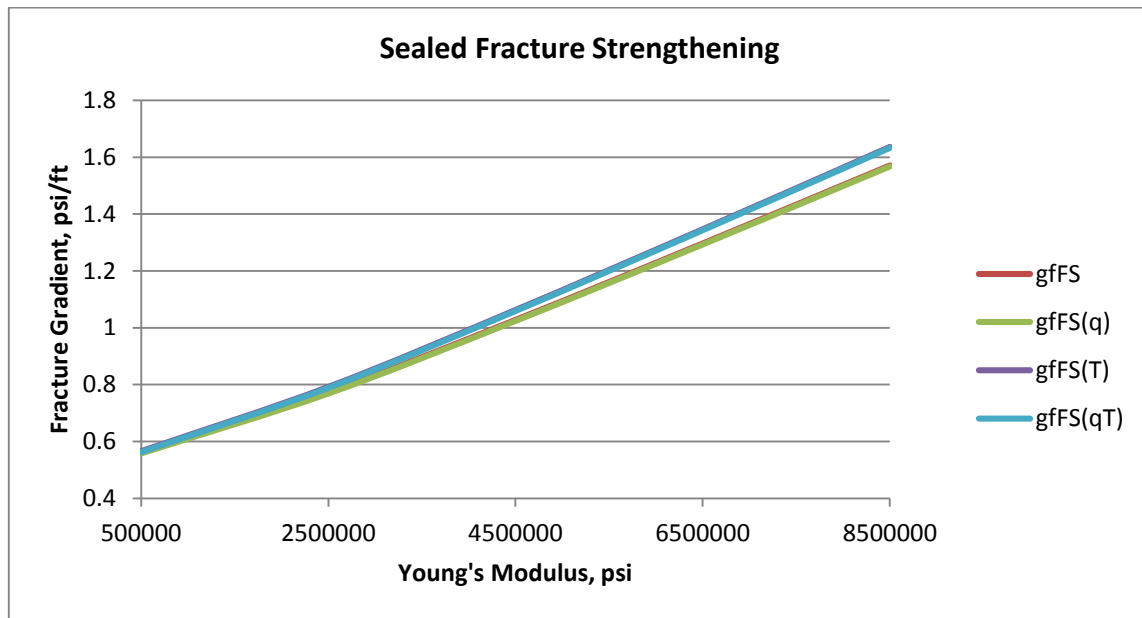


Fig. 37 - The illustration of the load reversal after applying the wellbore strengthening technique due to the action of the Poisson ratio.

3.4.2.2 Second stage Young's modulus analysis

The next analysis is performed for the Young's modulus over the same range specified in the pre-wellbore strengthening stage. The results of this analysis for two wellbore strengthening scenarios are shown in **Fig. 38** and **Fig. 39**.



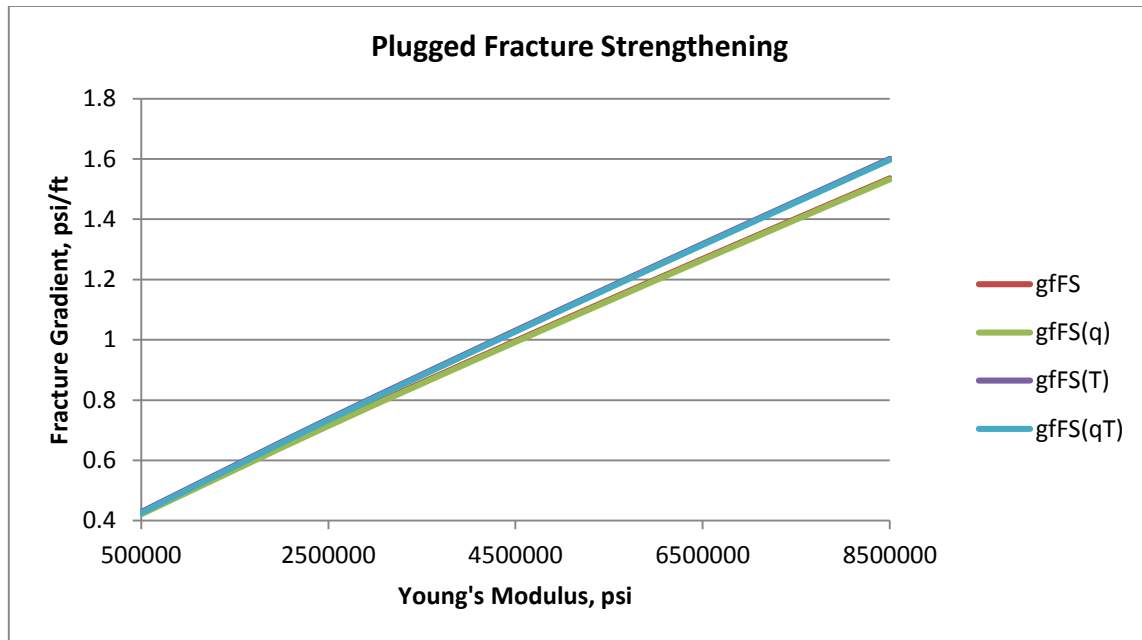


Fig. 39 - The results of the Young's modulus second stage plugged fracture strengthening parametric analysis showing an increase in the fracture gradient with the increasing Young modulus values.

The effect Young's modulus has on the fracture gradients is the same after applying the wellbore strengthening techniques. This is because, unlike the Poisson's ratio, the Young's modulus effect is not reversed due to the creation of a fracture and applying the load on the sand face tangentially. The only difference is that after the strengthening, Young's modulus now governs the nature of the created fracture, an opposite influence to that of the Poisson's ratio. Because Young's modulus is a measure of the formation rock stiffness, a larger Young's modulus will lead to smaller fracture aperture and larger fracture length. Although this means that a large Young's modulus will produce undesirable fracture geometry for the purpose of strengthening, the adverse effect of the large Young's modulus is not shown here as the fracture geometry is

introduced to the model as an independent user input. However, the supplied fracture geometry parameters are expected to be based on actual measurement specific to the formation rock that includes the influence of the Young's modulus. Therefore, assuming favorable fracture geometry, higher Young's modulus will result in a higher fracture gradient.

3.4.2.3 Second stage wellbore inclination analysis

The third sensitivity analysis is focused on the wellbore section inclination angle. The results of this analysis for two wellbore strengthening scenarios are shown in **Fig. 40** and **Fig. 41**. The initial fracture-pressure gradient is shown in addition to the formation strengthening gradients to illustrate the contrast between the two stages.

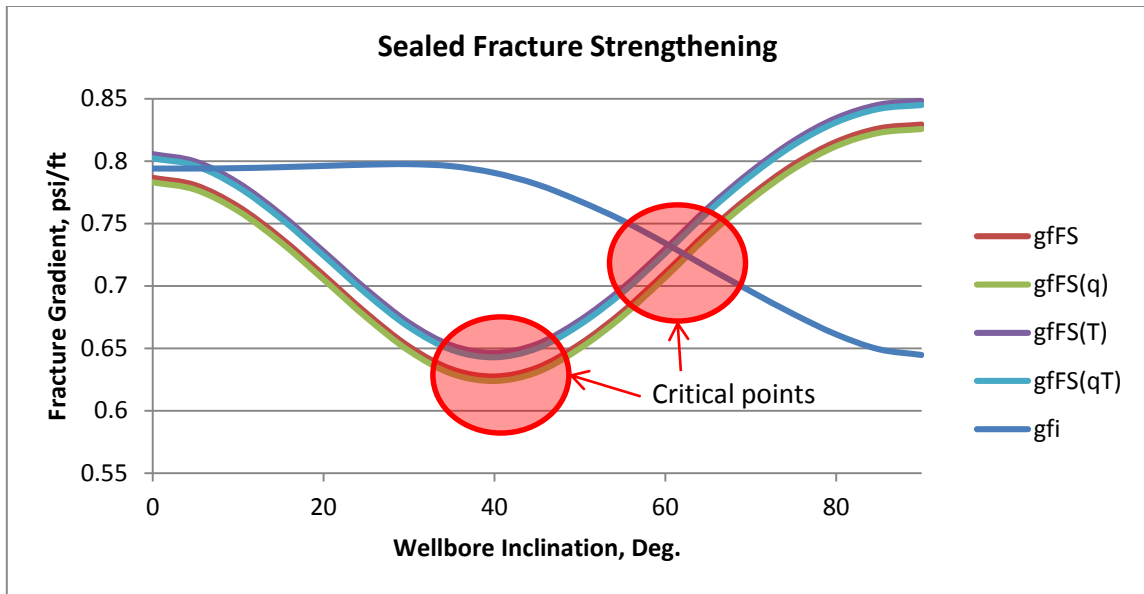


Fig. 40 - The results of the wellbore inclination angle second stage sealed fracture strengthening parametric analysis.

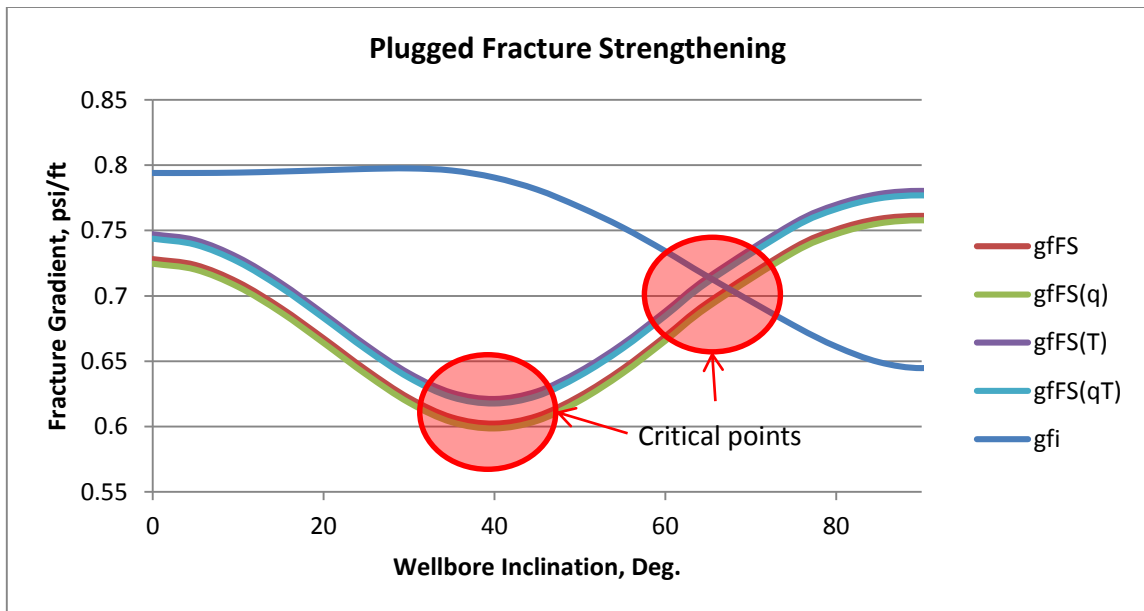


Fig. 41 - The results of the wellbore inclination angle second stage plugged fracture strengthening parametric analysis.

When observing the trend of the different fracture gradients with the changing wellbore inclination in the sealed fracture strengthening scenario shown in **Fig. 40**, it can be seen that the fracture gradients all follow the predicted decreasing paths with increasing inclination. However, this trend reverses itself at a certain critical point, 40° in this case. This change in trend is caused by the change in in-situ stress anisotropy working in favor of the strengthening process. Another important observation is that when comparing the pre-wellbore strengthening or initial fracture gradient to the strengthened gradients, it can be seen that applying this strengthening technique at low-inclination angles, lower than the critical point of 65° in this case, will actually be detrimental by reducing the fracture gradient.

In the plugged fracture strengthening scenario shown in **Fig. 41**, the same trends are observed; however, there are two important differences. First, this strengthening technique begins to show beneficial results only at inclination angles greater than 75° compared with 65° in the sealed fracture strengthening scenario. Second, the detrimental effect that this strengthening technique has on the fracture gradient at low-inclination angles is more exacerbated when compared with the sealed fracture strengthening scenario.

Based on this analysis, it can be concluded that the strengthening techniques discussed here are only suitable for highly inclined and horizontal wellbores.

3.4.2.4 Second stage wellbore diameter analysis

The fourth sensitivity analysis focuses on the wellbore section diameter. The results of this analysis for the two wellbore strengthening scenarios are shown in **Fig. 42** and **Fig. 43**.

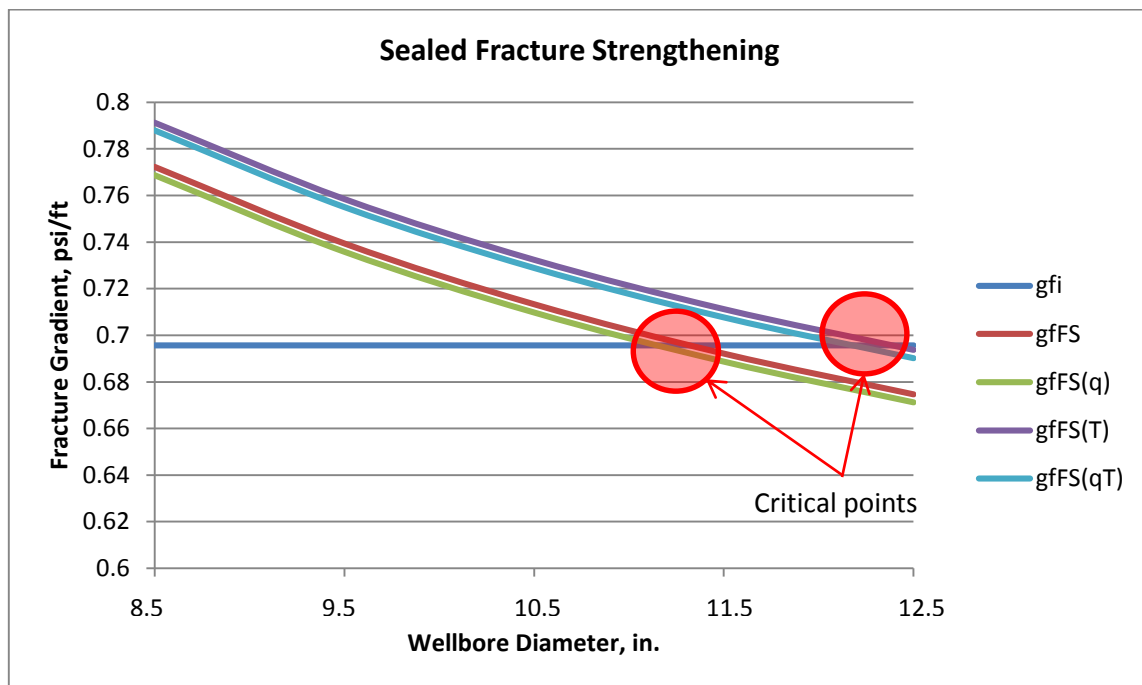


Fig. 42 - The results of the wellbore diameter second stage sealed fracture strengthening parametric analysis showing a decrease in the fracture gradient with the increasing wellbore diameter.

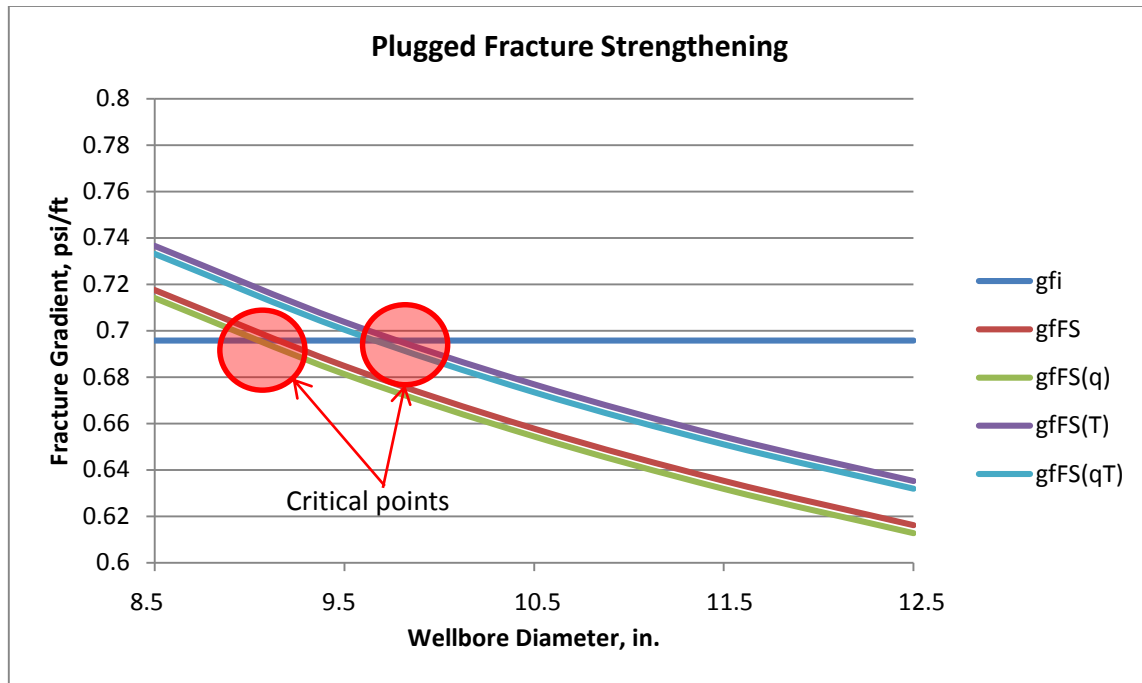


Fig. 43 - The results of the wellbore diameter second stage plugged fracture strengthening parametric analysis showing a decrease in the fracture gradient with the increasing wellbore diameter.

In calculating the initial fracture gradient, the wellbore diameter was not a contributing factor in the model. For that reason, the wellbore diameter appears in these figures as a constant value and is included as a reference to evaluate the performance of the strengthening techniques. In the sealed fracture strengthening scenario shown in **Fig. 42**, performance of the strengthening technique declines uniformly as the borehole size increases. In fact, the model results in this case show that applying this strengthening technique on borehole sizes of the critical value 11.3-inch diameter or larger will actually have a reverse effect because it will cause the fracture gradient to decrease from its initial pre-strengthening value. In the plugged fracture strengthening scenario

presented in **Fig. 43**, the same trend is shown. The positive effect of the strengthening technique will reverse itself at a smaller hole size. In this case, the strengthening technique will be detrimental in hole sizes of the critical value 9.1-inch diameter or larger. The result of this analysis is that smaller borehole sizes are preferable, and in some occasions, essential when performing wellbore strengthening.

3.4.2.5 Second stage fracture aperture analysis

The fifth sensitivity analysis is that of an induced fracture aperture. The results of this analysis for the two wellbore strengthening scenarios are shown in **Fig. 44** and **Fig. 45**.

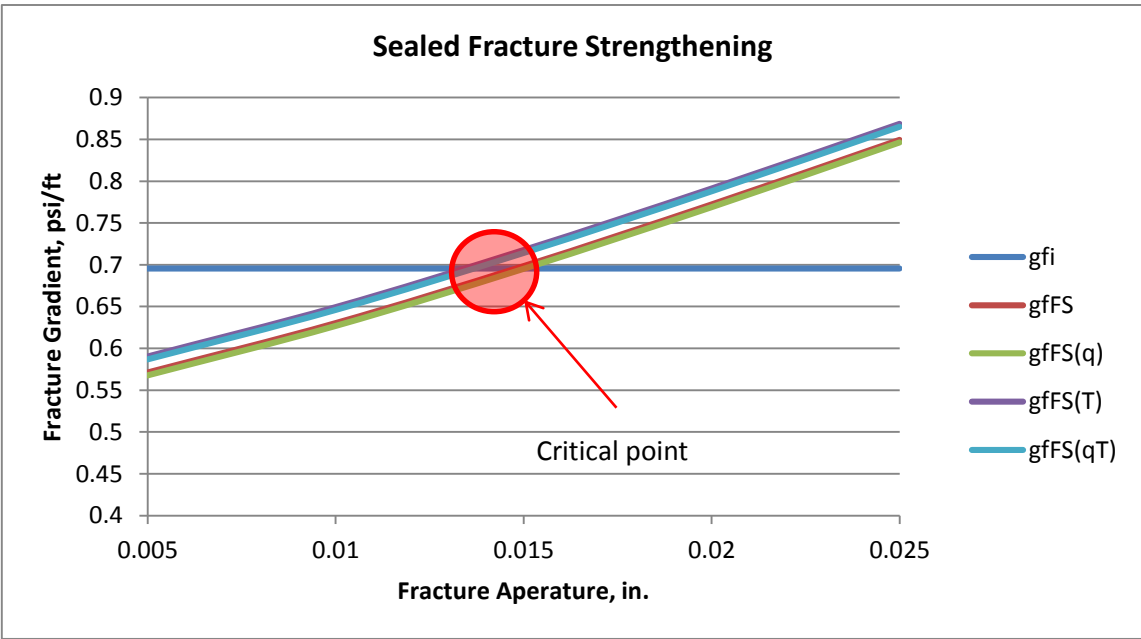


Fig. 44 - The results of the fracture aperture second stage sealed fracture strengthening parametric analysis showing an increase in the fracture gradient with the increasing fracture aperture.

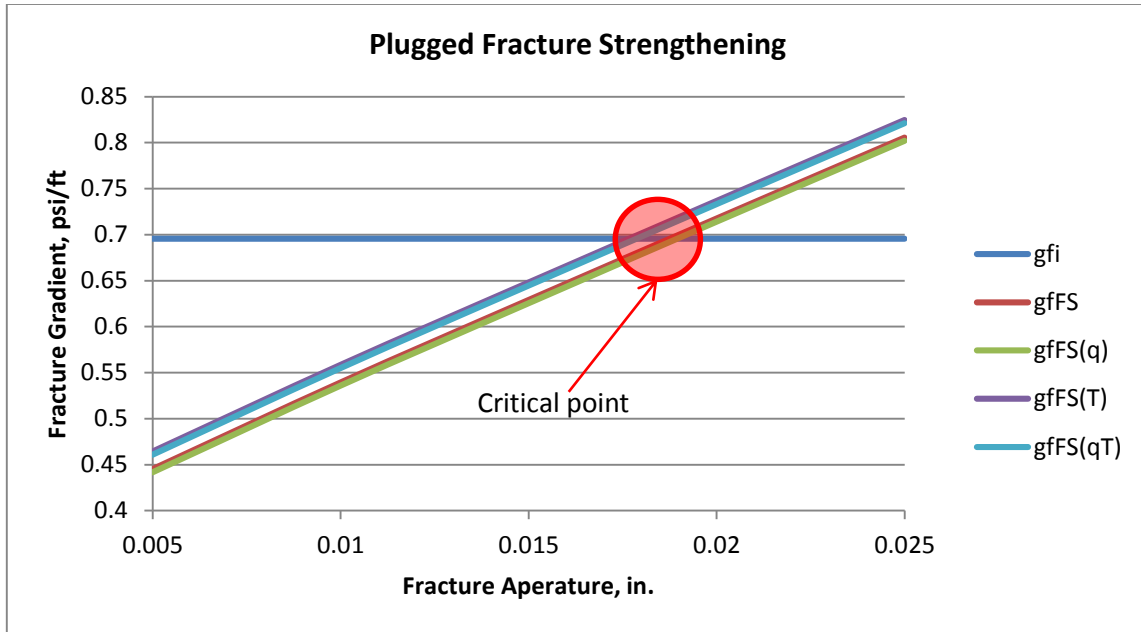


Fig. 45 - The results of the fracture aperture second stage plugged fracture strengthening parametric analysis showing an increase in the fracture gradient with the increasing fracture aperture.

The fracture aperture is directly coupled to the enhancement of the tangential stress. As shown in **Fig. 46**, a larger induced fracture aperture will result in a larger enhancement of the tangential stress. The reason behind this effect is that the large fracture aperture will increase the load applied on the rock grains in the tangential direction. The increased load will push the rock grains more closely together around the circumference of the wellbore. As a result, the closely packed rock grains will offer greater resistance to fracture initiation. Consequently, this condition will lead to a higher fracture gradient of the wellbore. The finite element analysis shown in **Fig. 47** performed by (Duffadar et al. 2013) further illustrates this effect. This analysis clearly shows the increase of the tangential compressive stress with the increase of the fracture aperture,

which explains the trend shown by the fracture gradient in both strengthening scenarios. The sealed fracture scenario again shows the superior performance as it will start producing positive results at a fracture aperture of 0.015 inch or larger. The plugged fracture scenario requires a fracture aperture of at least 0.019 inch to produce a fracture gradient greater than the initial fracture gradient.

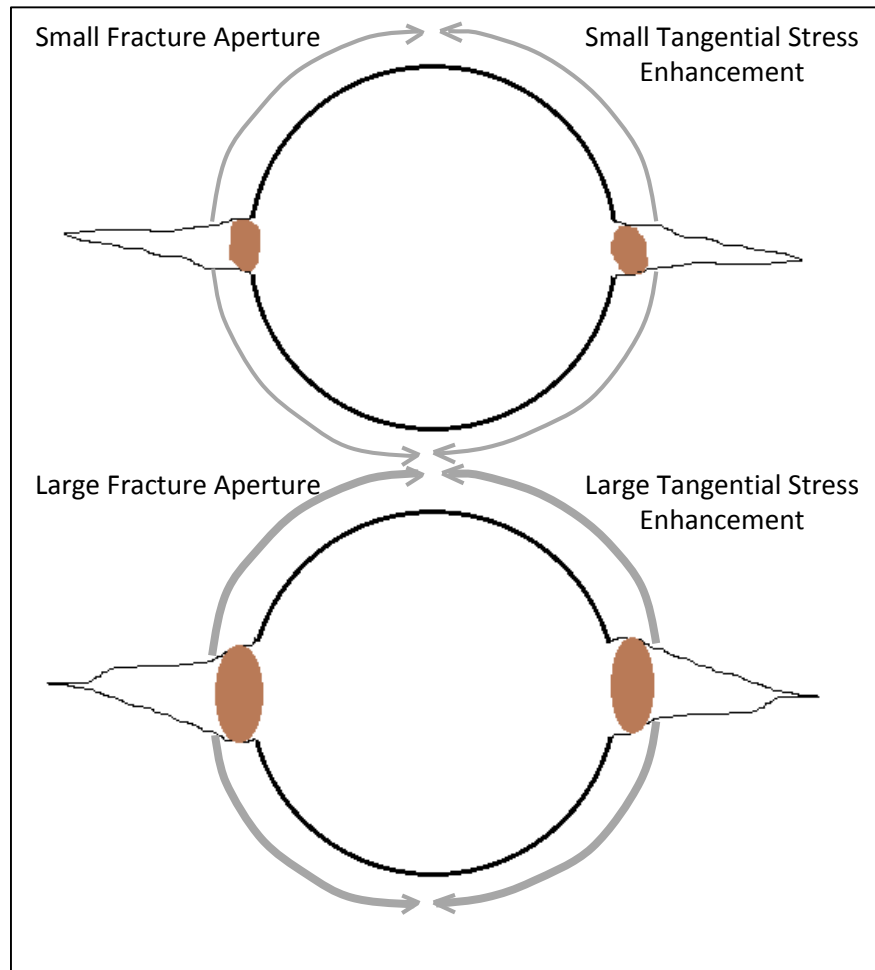


Fig. 46 - The effect of fracture aperture and particle size on the enhancement of tangential stress.

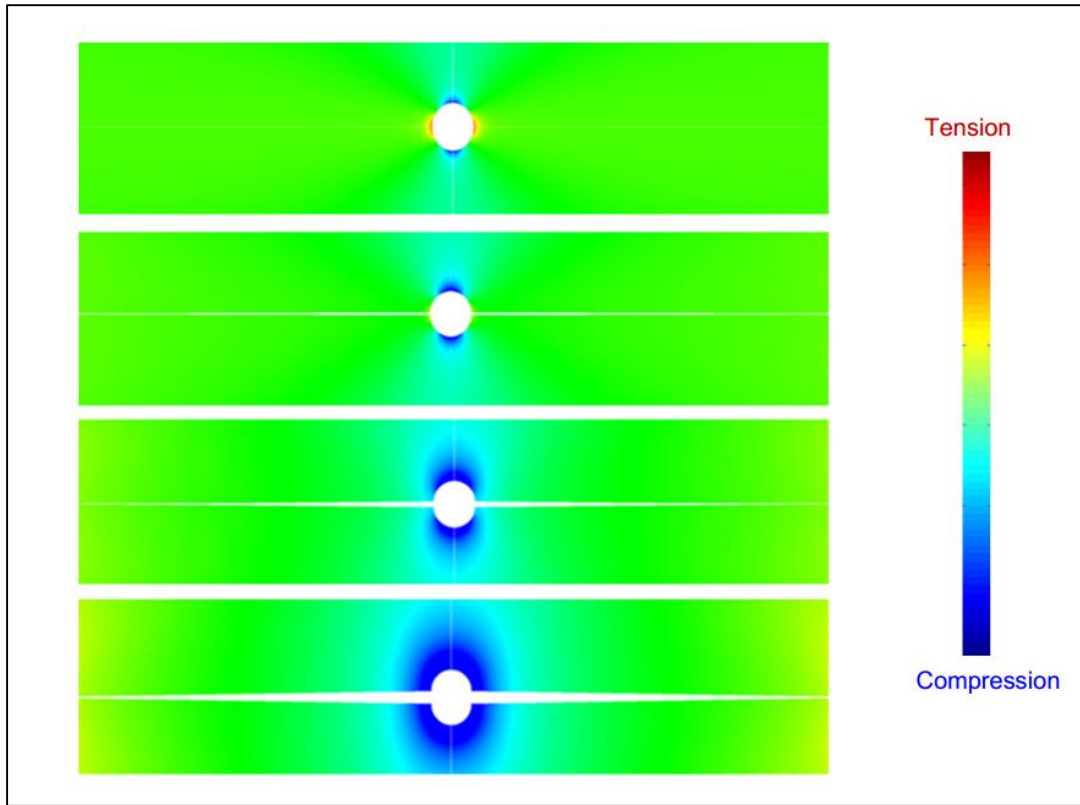


Fig. 47 - The effect of fracture aperture and particle size on the enhancement of tangential stress illustrated by finite element analysis (Duffadar et al. 2013).

3.4.2.6 Second stage fracture toughness analysis

The sixth sensitivity analysis deals with the fracture toughness. The results of this analysis for the two wellbore strengthening scenarios are shown in **Fig. 48** and **Fig. 49**.

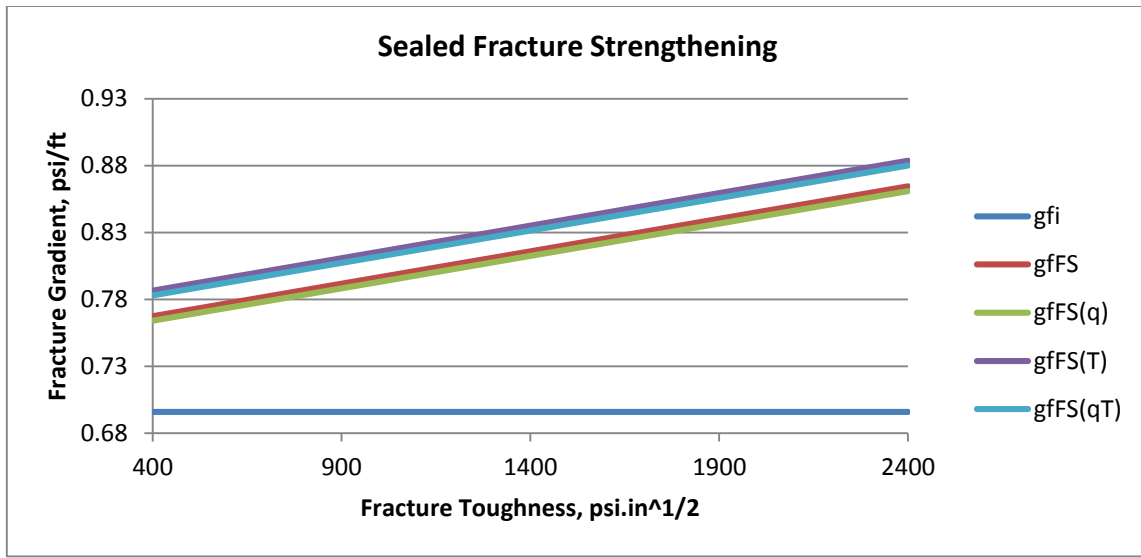


Fig. 48 - The results of the fracture toughness second stage sealed fracture strengthening parametric analysis showing an increase in the fracture gradient with the increasing fracture toughness.

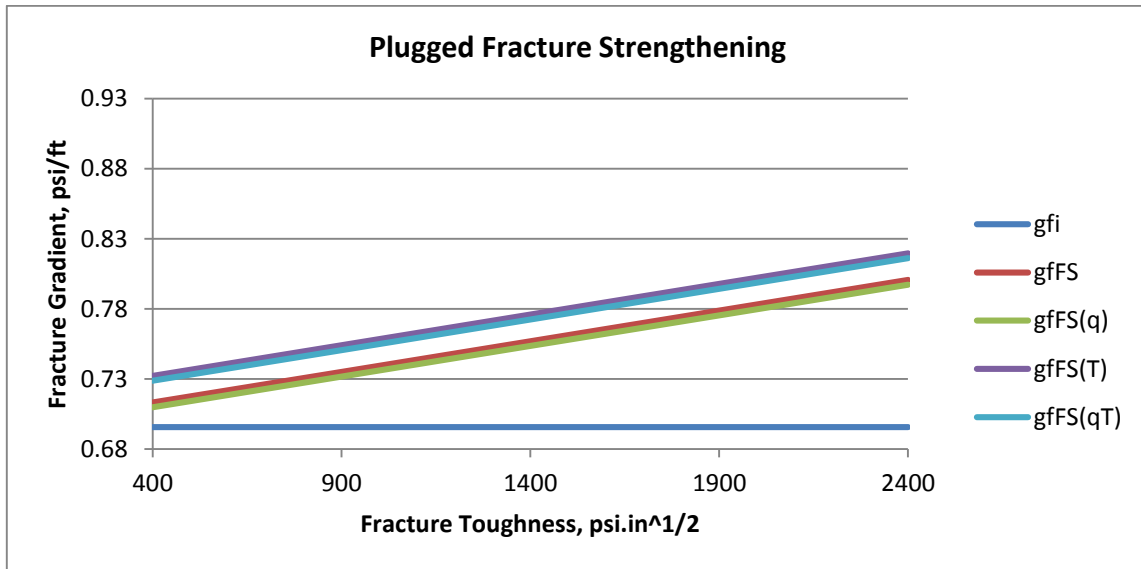


Fig. 49 - The results of the fracture toughness second stage plugged fracture strengthening parametric analysis showing an increase in the fracture gradient with the increasing fracture toughness.

The fracture toughness in this case is the critical value of the mode I stress intensity factor that will lead to fracture propagation (Thiercelin et al. 1989). This definition is confirmed by the model response to the change in the fracture toughness value. In a rock with a large fracture toughness value, higher loads are required to create a fracture; hence, the increasing fracture gradients with the increasing fracture toughness.

3.4.2.7 Second stage fracture plug placement analysis

The seventh sensitivity analysis is focused on the fracture plug placement. The result of this analysis is shown in **Fig. 50**.

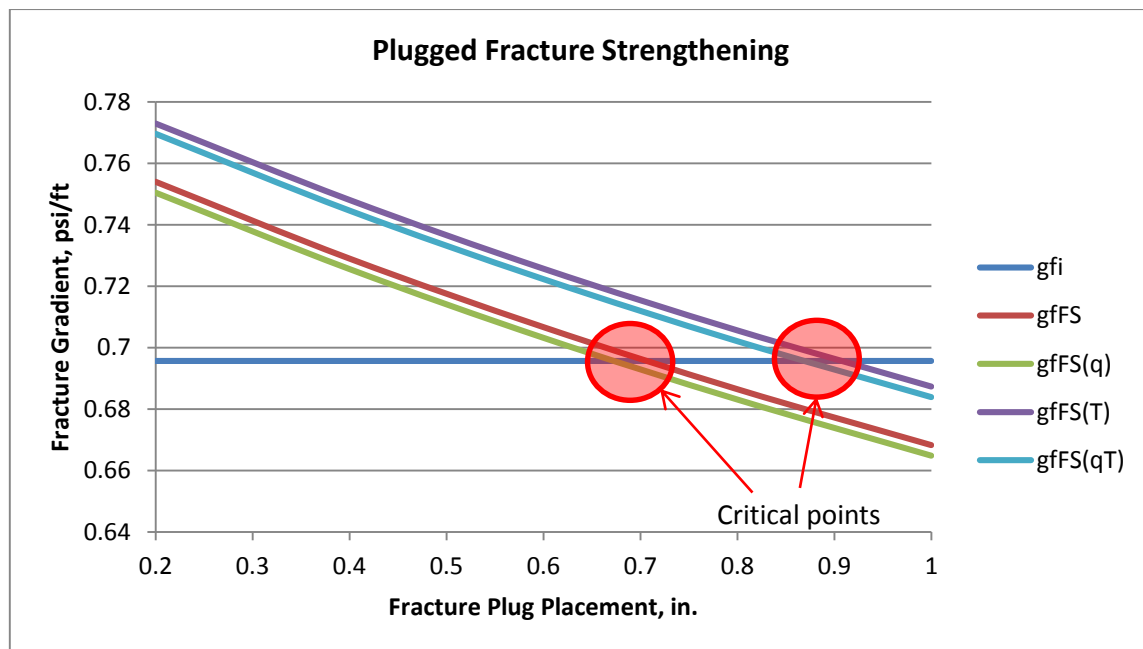


Fig. 50 - The results of the fracture plug placement second stage plugged fracture strengthening parametric analysis showing a decrease in the fracture gradient with the increasing fracture plug placement.

The placement of the drilling fluid plugging particle in the fracture is a major factor in determining the results of a fracture-related wellbore strengthening technique. From the previous analyses, it is clear that a fracture plugged at the mouth leads to improved wellbore strengthening. There are many factors that determine the placement of a fracture plug, including but not limited to the following:

1. Size of the designed solid plugging particle
2. Induced fracture aperture
3. Induced fracture length
4. Designer mud filtration rate
5. Magnitude of the wellbore overbalance pressure

There is no analytical solution available for determining the influence these factors have on the plugging particle placement. However, there are many experimental studies done to examine the effect of these factors. One of the most prominent and common study is the study of the influence of the size distribution of the bridging particles. The general goal of those studies is to select the optimum bridging particle size distribution to minimize formation damage (He et al. 2011; Dick et al. 2000). A more specific study that relates to the wellbore strengthening technique known as “the stress cage” (Aston et al. 2004) uses a “designer mud” to create bridging particles at the fracture mouth. The reason for selecting this placement of the bridging particles is clear when observing the analysis shown in **Fig. 44**. The resulting fracture-pressure gradient decreases as the plugging particle is placed farther from the fracture mouth.

One likely explanation of this relationship between the plugging particle placement and the fracture gradient is that the plugging particle is supposed to create pressure isolation between the wellbore and the fracture. Placing the plug farther from the fracture mouth exposes a section of the fracture to the wellbore pressure. As the plug placement distance increases, the length of the exposed fracture section increases, which will lead to poorer pressure isolation. The exposed fracture section will undergo continuous pressure buildup from the wellbore. The result of the pressure buildup is increased local pore pressure, which will have an adverse effect on the tangential stress enhancement.

3.4.2.8 Second stage fracture-pressure buildup analysis

The final sensitivity analysis deals with the fracture-pressure buildup. The results of this analysis for the two wellbore strengthening scenarios are shown in **Fig. 51** and **Fig. 52**.

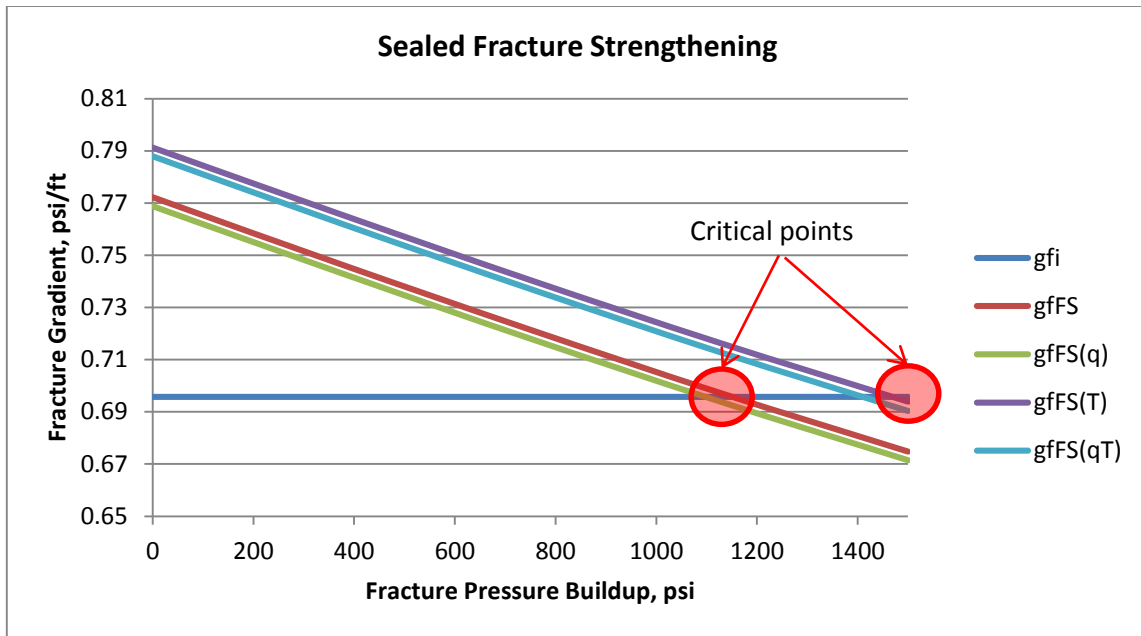


Fig. 51 - The results of the fracture pressure buildup second stage sealed fracture strengthening parametric analysis showing a decrease in the fracture gradient with the increasing fracture pressure buildup.

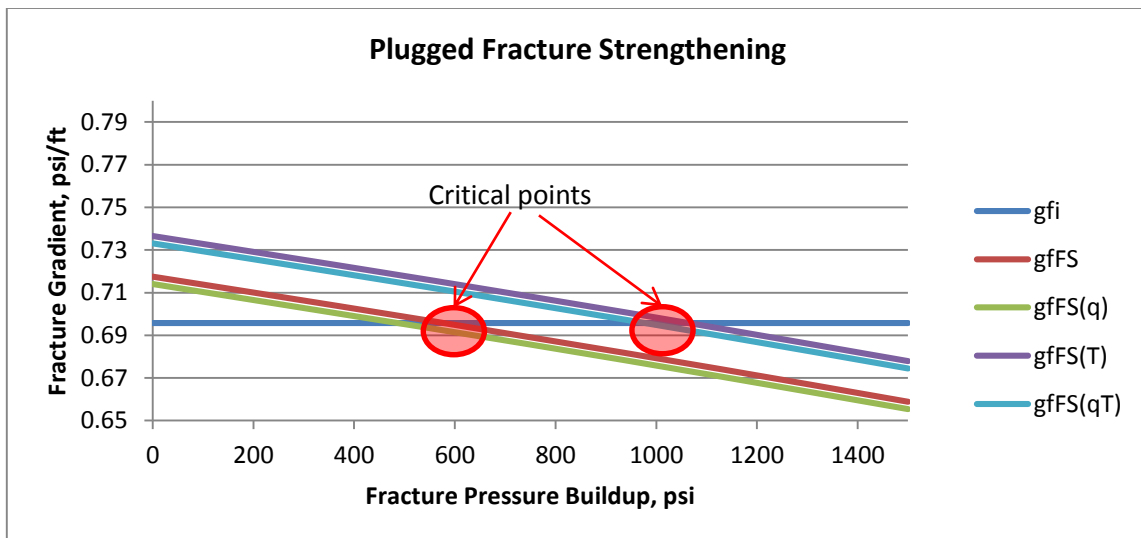


Fig. 52 - The results of the fracture pressure buildup second stage plugged fracture strengthening parametric analysis showing a decrease in the fracture gradient with the increasing fracture pressure buildup.

The pressure buildup being analyzed here is the pressure behind the plugging particle. For the same reasons discussed in the effect of drilling fluid filtration and in the plug placement, increasing the pressure buildup will reduce the fracture gradient. The only difference in this case is that the permeability of the formation rock plays a major role. As mentioned previously, one of the main purposes of the plugging particles is to create pressure isolation between the wellbore and the fracture, which is why the created bridge should be of low permeability. However, the bridging particles will have no effect on the mud filtrate that preceded them to create the fracture. Excessive pressure buildup behind the plug will lead to an increase in the fracture elongation which is, as discussed previously, not undesirable. For that reason, high-rock permeability is a requirement for performing this type of wellbore strengthening technique. The high-formation rock permeability should allow the mud filtrate to flow into the formation and the pressure buildup behind the fracture to dissipate. On the contrary, low-formation rock permeability will trap the filtrate, which will lead to two possible scenarios; i.e., either the filtrate will continue to elongate the fracture, or it will flow back and remove the plug. One solution to this issue was proposed by (Aston et al. 2007) in which the bridging particles solidified the fracture and adhered to the shale, preventing its removal by the flow back from the build pressure

3.4.3 Well Placement Evaluation

Based on the results discussed thus far, it is reasonable to conclude that the placement of the wellbore section with respect to the in-situ stresses is an important factor in determining both the size of the drilling window and the efficiency of the wellbore strengthening techniques that have been presented. For a certain section of a well where the size of the drilling window is a major concern due to various reasons such as low-fracture-pressure gradient resulting from reservoir depletion, adjusting the surface location and trajectory of the well can drastically change the size of the drilling window and improve the performance of the wellbore strengthening techniques. In terms of the model, changing the surface location or trajectory of the well is the practical way to adjust the value of the β angle, which specifies the deviation of the wellbore projection on the two horizontal stress planes from the maximum horizontal stress. For this purpose, polar plots were created using the model to evaluate the resulting fracture gradient and drilling window size over the range of possible well surface location and trajectory.

The effect of β is largely overlooked in the well planning phase. In cases where adjusting the well surface location and trajectory is a viable option such that it will not compromise the target of the well or add substantial footage and cost, optimizing the value of β is an effective tool. The effect of β is even more predominant in wells where applying one of the wellbore strengthening techniques discussed is planned. To illustrate this effect, the model calculates the resulting fracture gradients over the 360° range of β and the wellbore azimuth. To achieve this goal, the model calculates the resulting

fracture gradient in 0.5° increments of β value while specifying the corresponding azimuth angle for each β increment. The model then determines the maximum resulting fracture gradient and uses it to calculate a parameter that can be denoted “the ease-of-drilling fraction” as follows:

$$\text{Ease of Drilling Fraction (Based on Maximum } g_f) = \frac{g_f}{\text{Max } g_f} \dots \dots \dots (\text{Eq. 3.1})$$

The value of this fraction is plotted in polar coordinates with the corresponding azimuth angle to show the direction that will yield the largest possible drilling window or the direction that provide the easiest drilling path; hence, the name ease-of-drilling fraction and plot. However, by using this fraction, two polar plots based on two different types of fracture gradient (e.g., non-strengthened gradient and strengthened gradient) cannot be compared with each other to determine which type of fracture-pressure gradient provides the wider drilling window in a certain direction. For that reason, the model also calculates the ease-of-drilling fraction with a constant reference value for all of the different types of fracture-pressure gradients as follows:

$$\text{Ease of Drilling Fraction (Based on } C \text{ psi/ft)} = \frac{g_f}{C} \dots \dots \dots (\text{Eq. 3.2})$$

The reference value is selected to be equal to or greater than the maximum possible fracture-pressure gradient for all the different types of fracture-pressure gradients. This procedure will allow for a comparison between different ease-of-drilling polar plots, even if they are based on a different type of fracture-pressure gradient. In this particular case study, the value of the constant reference value C is 1.

The resulting plot of the maximum-based ease-of-drilling fraction for the initial fracture gradient (g_{fi}) is shown in **Fig. 53**.

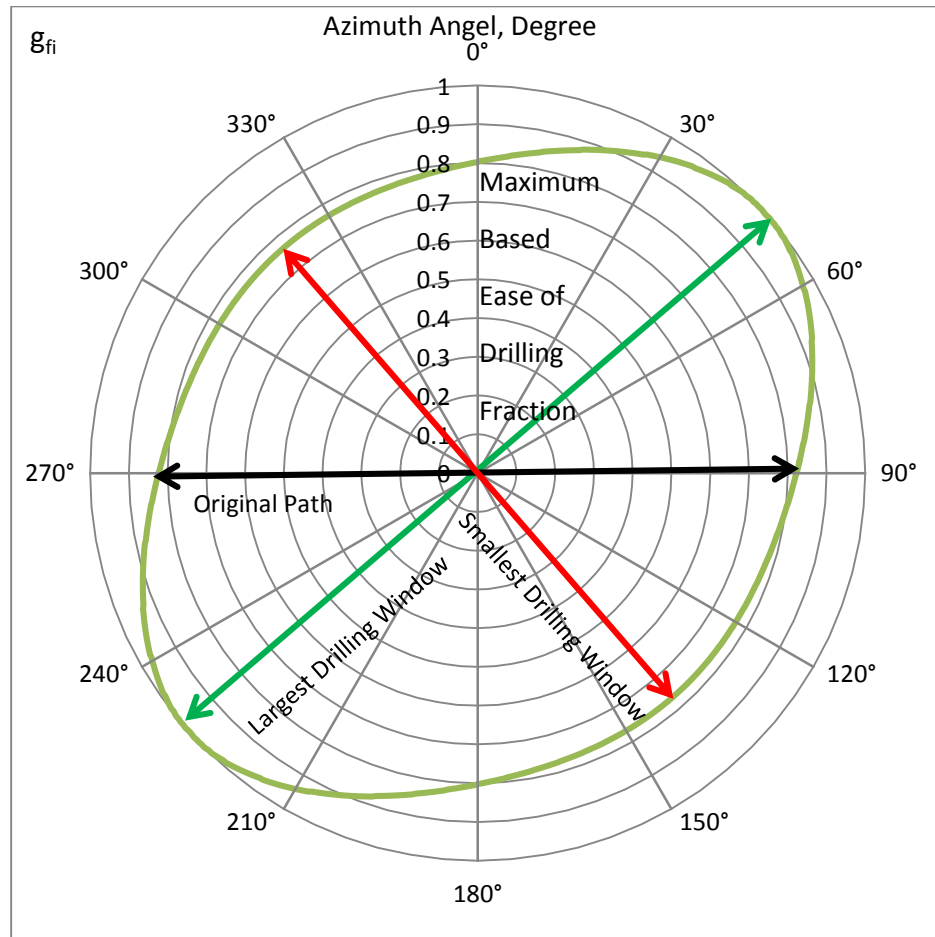


Fig. 53 - The resulting ease of drilling plot based on a maximum gradient for the initial fracture pressure gradient.

According to this polar plot, the path that will provide the largest drilling window for the specified section of the well, or the easiest drilling path, is northeast to southwest.

The original drilling path set for this case is at 88° azimuth. Adjusting the well surface location and trajectory will result an increase of 0.14 psi/ft in fracture gradient, which is a 20.4% improvement on the original fracture gradient and drilling window. Such improvement is sufficiently substantial to eliminate the need for other costly techniques aimed at tackling the issue of a narrow drilling window such as managed pressure drilling. The fracture gradient changes over the 360° azimuth range by a maximum percentage of 30.5%. This result leads to the worst case scenario in which the decision was made to drill the well northwest to southeast without considering the effect of β . In this case, the fracture gradient will decrease 0.05 psi/ft (8.4%) from the original path and by 0.2 psi/ft (30.5%) from the best drilling path. The effect of the wellbore orientation, with respect to the in-situ stress, on the initial fracture gradient proves the significance of considering it in the well planning phase where the well surface location and trajectory are flexible.

The resulting plot of the ease-of-drilling fraction based on the reference value of 1 for initial fracture gradient (g_{fi}) is shown in **Fig. 54**. This plot is created for comparison purposes with the other types of the calculated fracture gradients to be discussed later on.

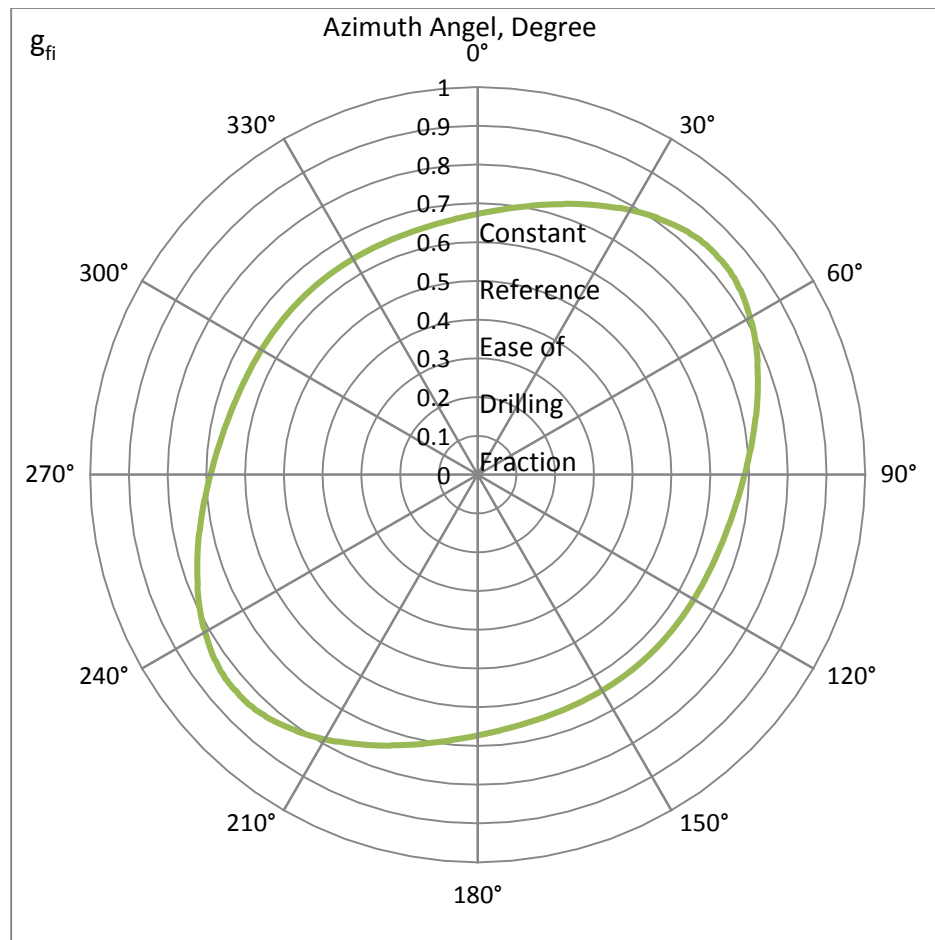


Fig. 54 - The resulting ease of drilling plot based on a constant reference value for the initial fracture pressure gradient.

The resulting plot of the maximum-based ease-of-drilling fraction for mud filtrate and temperature affected fracture gradient (g_{fQT}) is shown in **Fig. 55**.

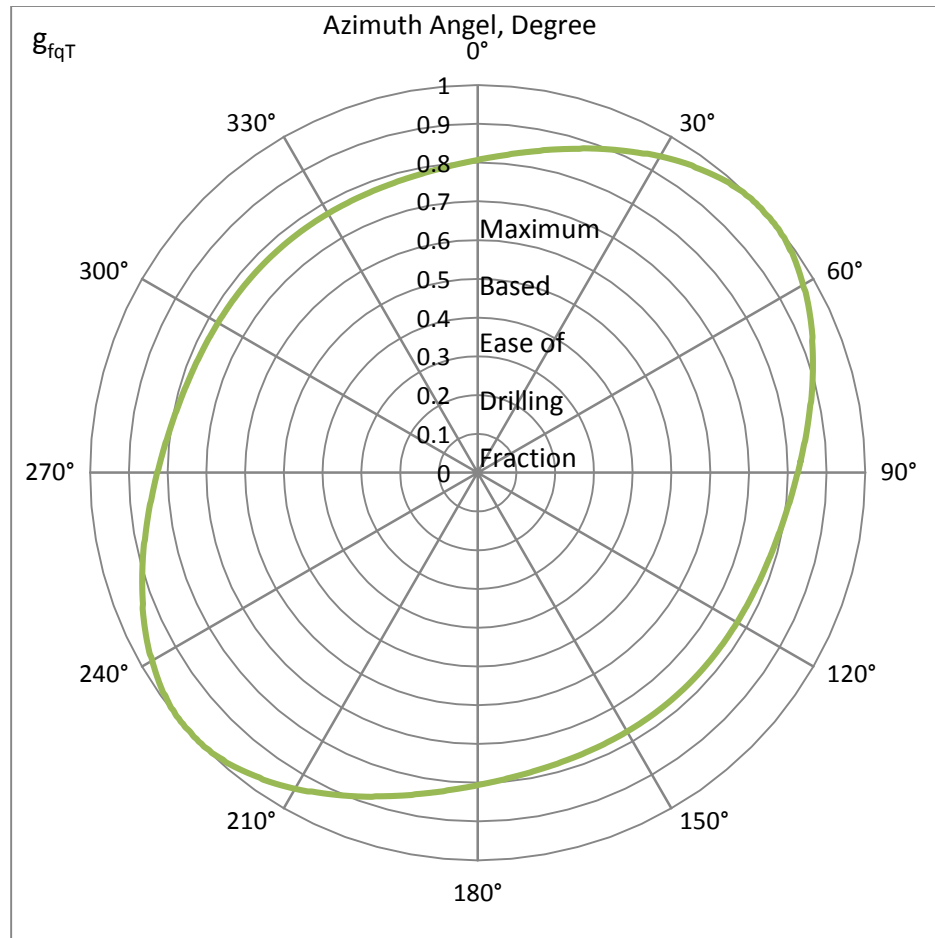


Fig. 55 - The resulting ease of drilling plot based on a maximum gradient for the mud filtrate and temperature affected fracture pressure gradient.

The polar plot for the mud filtrate and temperature-affected fracture gradient shows the same trends and drilling paths as the initial fracture gradient polar plot. The only difference is the overall larger drilling window exhibited due to the combined positive effect of mud filtration and temperature increase.

The resulting plot of the ease-of-drilling fraction based on the reference value of 1 for the mud filtrate and temperature-affected fracture gradient (g_{fqT}) is shown in **Fig.**

56. This plot is created for comparison with the other types of the calculated fracture gradients.

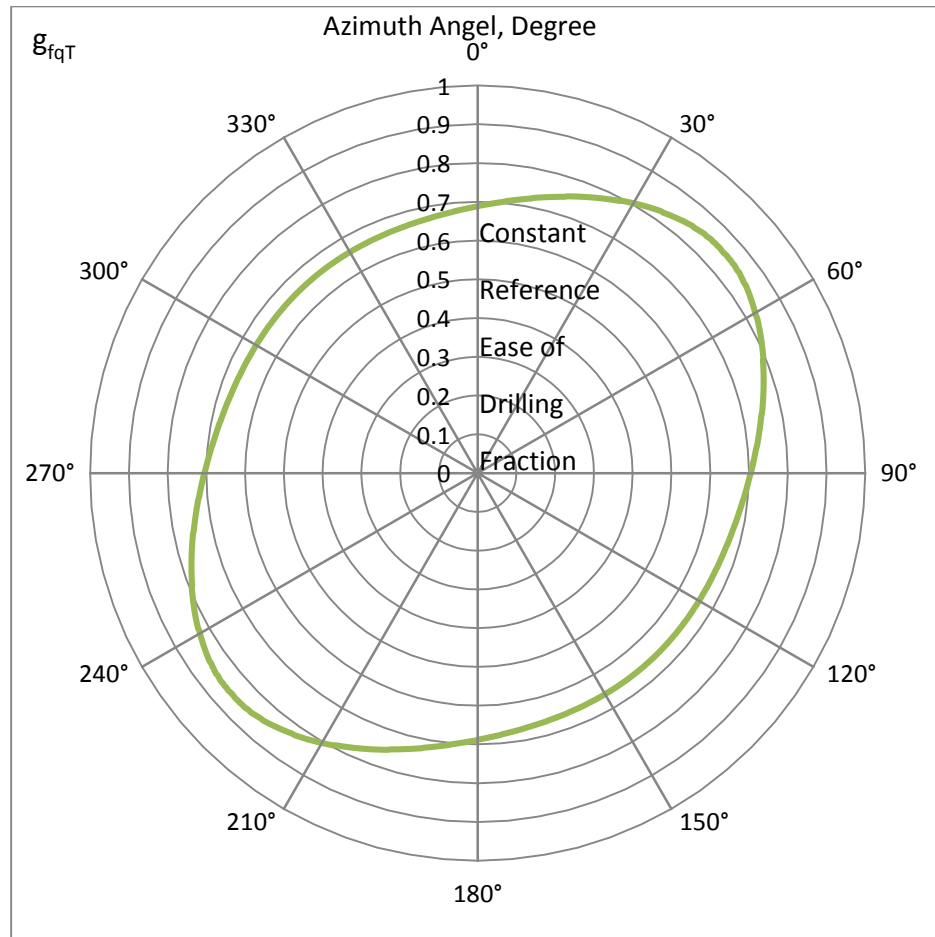


Fig. 56 - The resulting ease of drilling plot based on a constant reference value for the mud filtrate and temperature affected fracture pressure gradient.

The resulting plot of the maximum-based ease-of-drilling fraction for the sealed fracture wellbore strengthening affected fracture gradient (g_{fFS}) is shown in **Fig. 57**.

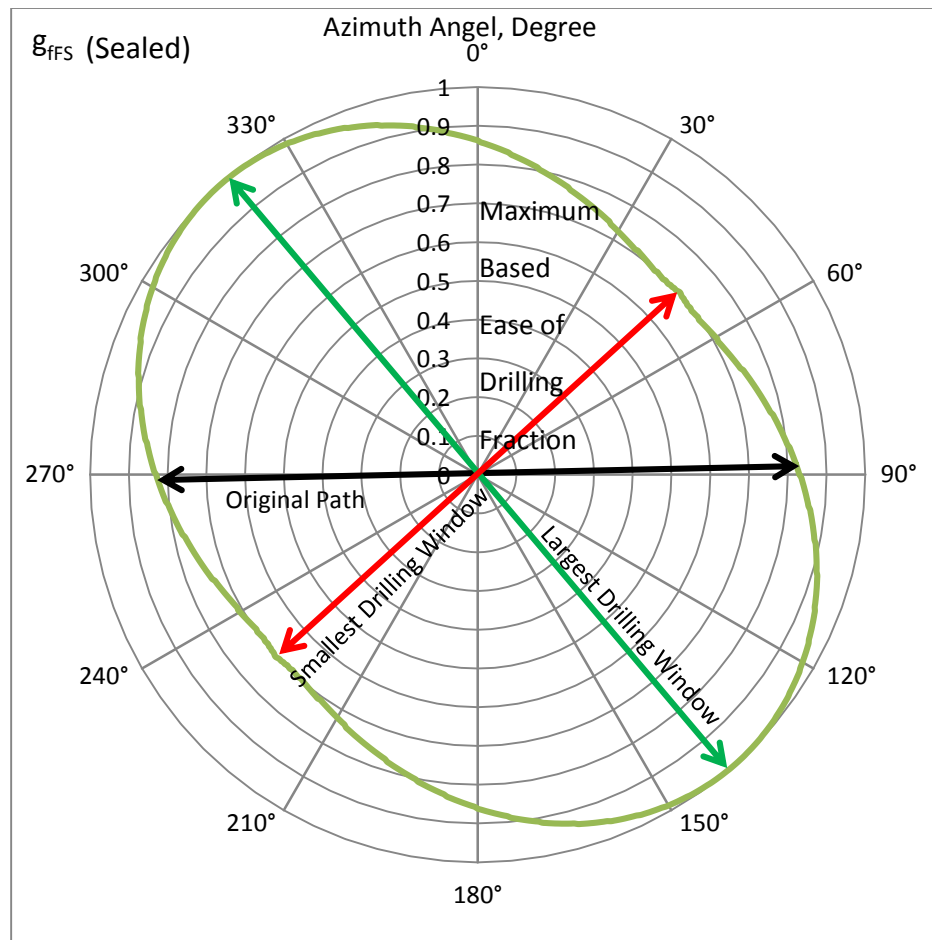


Fig. 57 - The resulting ease of drilling plot based on a maximum gradient for the fracture pressure gradient after applying sealed fracture wellbore strengthening.

This figure uncovers an interesting phenomenon. After applying the wellbore strengthening technique to this wellbore section, the paths of the largest drilling window and the narrowest drilling window switch directions. Originally, and before introducing the wellbore strengthening technique to this wellbore section, the direction that will provide the largest drilling window was northeast to southwest. Now, that same direction will provide the drilling path with the narrowest drilling window. To take this

comparison further, the plot of the ease-of-drilling fraction based on the reference value of 1 for the same fracture gradient (g_{fFS}) is created and shown in **Fig. 58**.

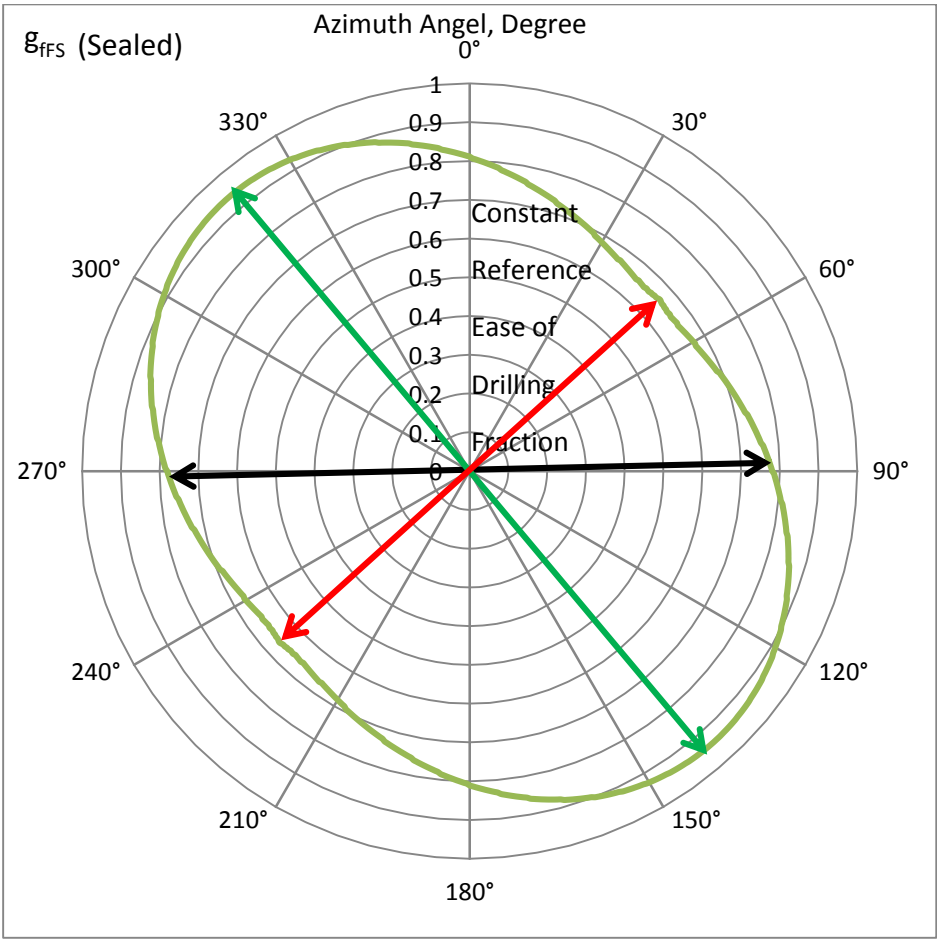


Fig. 58 - The resulting ease of drilling plot based on a constant reference value for the fracture pressure gradient after applying sealed fracture wellbore strengthening.

To understand the difference made by this wellbore strengthening technique, the comparison was made and is shown in **Table 6**.

Table 6 - A comparison to illustrate the varying sealed fracture wellbore strengthening performance in varying wellbore positions.

Fracture Gradient Type	Original Path	Best Case Scenario Path	Worst Case Scenario Path
Initial Fracture Gradient (g_{fi}), psi/ft	0.6957	0.8376	0.6421
Wellbore Strengthened Fracture Gradient (g_{fFS}), psi/ft	0.7723	0.9411	0.6537

There are many important implications from this comparison. Drilling the well section along the initial fracture gradient best-case scenario path will lead to an initial fracture gradient of 0.8376 psi/ft. According to the model results, applying the wellbore strengthening technique to the well in this case will actually create an adverse effect because it will reduce the fracture gradient to 0.6537 psi/ft (22% reduction). On the other hand, drilling the well section along the initial fracture gradient worst-case scenario path will lead to an initial fracture gradient of 0.6421 psi/ft. In this case, applying the wellbore strengthening technique to the well will create the maximum possible and intended strengthening effect because it will enhance the fracture gradient up to 0.9411 psi/ft (46.7% increase). This comparison is represented in **Fig 61**.

The role of well placement in determining the performance of the strengthening technique is significant to the extent that it will determine whether the technique will be extremely beneficial or detrimental. This comparison emphasizes the importance of implicating the angle β analysis and the resulting polar plots in the well planning phase to determine the optimum well surface location and trajectory, especially for wells planned to be subjected to a wellbore strengthening technique.

The resulting plot of the maximum-based and constant reference-based ease-of-drilling fraction for the plugged fracture wellbore strengthening affected fracture gradient (g_{fFS}) are shown in **Fig. 59** and **Fig. 60** respectively.

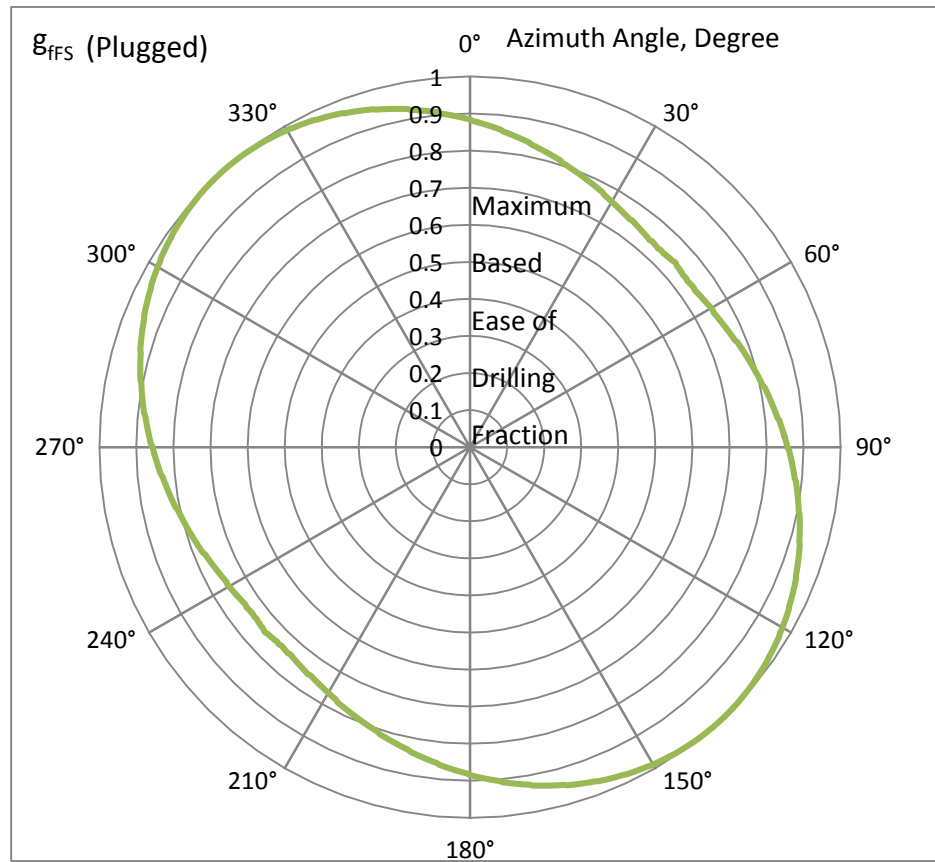


Fig. 59 - The resulting ease of drilling plot based on a maximum gradient for the fracture pressure gradient after applying plugged fracture wellbore strengthening.

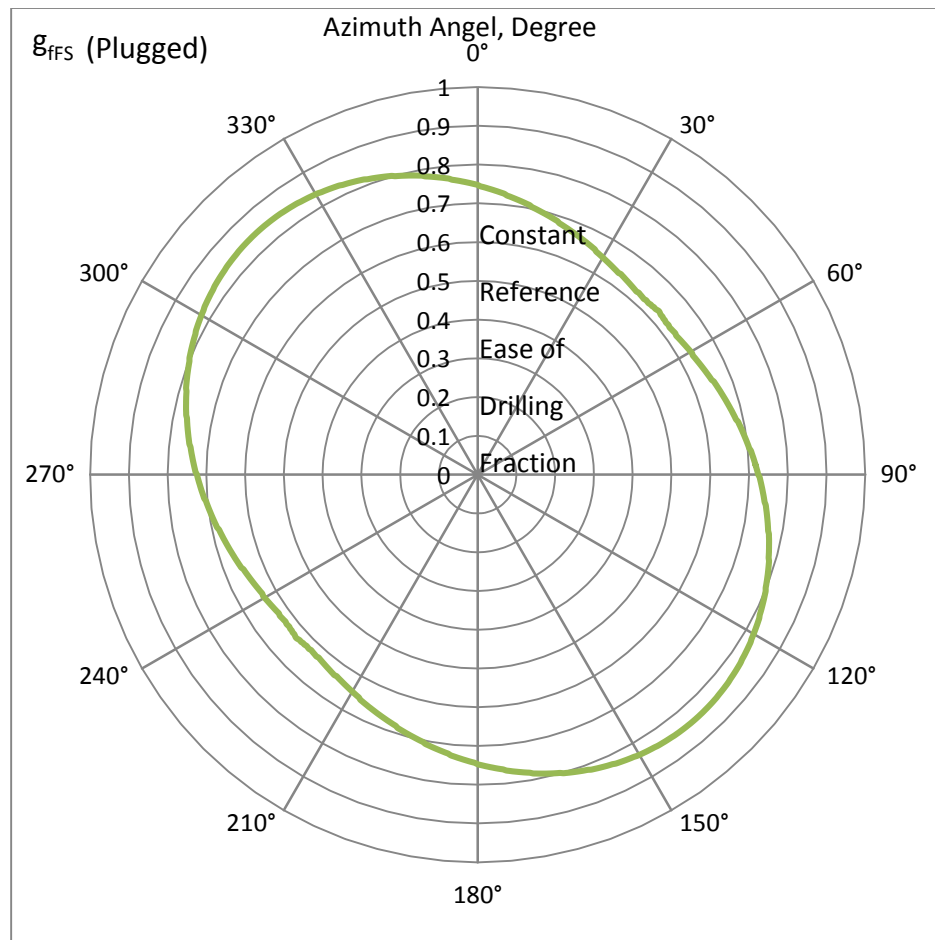


Fig. 60 - The resulting ease of drilling plot based on a constant reference value for the fracture pressure gradient after applying plugged fracture wellbore strengthening.

The polar plot for the plugged fracture strengthening technique shows the same effects as the sealed fracture strengthening technique in addition to the expected lesser performance. The comparison between the initial fracture gradient and the plugged fracture wellbore strengthening gradient is shown in **Table 7**.

Table 7 - A comparison to illustrate the varying plugged fracture wellbore strengthening performance in varying wellbore positions.

Fracture Gradient Type	Original Path	Best Case Scenario Path	Worst Case Scenario Path
Initial Fracture Gradient (g_{fi}), psi/ft	0.6957	0.8376	0.6421
Wellbore Strengthened Fracture Gradient (g_{fFS}), psi/ft	0.7175	0.8452	0.6241

Based on these results, it can be concluded that applying any one of the stress-related wellbore strengthening techniques without analyzing the well section placement is not a recommended practice. A well section already drilled along the path providing the maximum initial fracture gradient has marginal potential for improvement. In fact, the well path has more potential for damage because applying a stress-related wellbore strengthening technique could reduce the fracture gradient according to the model results. Stress-related wellbore strengthening techniques such as “stress cage” have certain requirements. Those requirements include a high-permeability formation rock and a specially designed drilling fluid. Analyzing the well section placement with respect to the in-situ stress in the well planning phase should be considered as another equally important requirement. This comparison is represented in **Fig 61**.

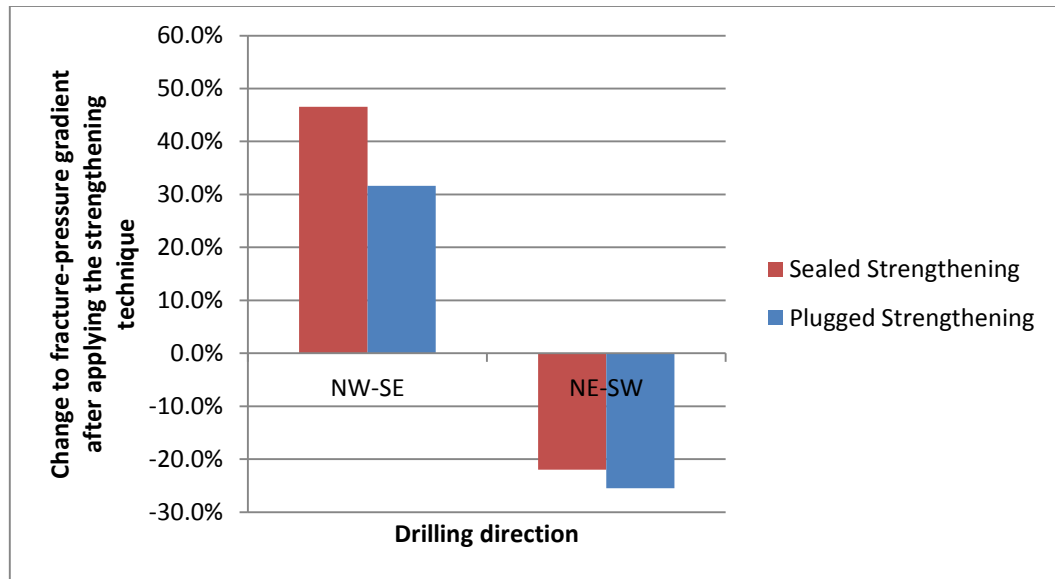


Fig. 61 - A comparison to illustrate the varying fracture wellbore strengthening performance in different drilling directions.

4. CONCLUSIONS

Several aspects of the model can be improved to yield more reliable results. The first area with a potential for improvement is the assumptions on which the model was built. These assumptions can be addressed more thoroughly on an individual basis. Beginning with the isothermal borehole conditions assumption, implementing a more complex heat conduction relationship between the drilling fluid and the formation rock in the model code is expected show the detailed effect of temperature change on the fracture gradient and on the wellbore strengthening performance over a specified period of time. This should result in an improvement in the use of a single correlation for that purpose. Likewise, the same improvement can be achieved regarding the correction for mud filtrate flow in the formation. More advanced hydraulic fracturing modeling principles are required to be added in the model code to show the detailed effect on the fracture gradient and on the wellbore strengthening performance over a specified period of time.

Investigating the nature of the tangential stress enhancement in the wellbore strengthening techniques using computer aided design software is an another topic recommended for future research. Through the use of suitable software, the effect on the tangential stress when the fracture is propped or sealed by different particles varying in size, placement within the fracture, and the nature of their interaction with rock can be monitored to obtain a better understanding of the actual mechanisms behind the wellbore

strengthening effect. This approach can help in determining the more likely cause of the strengthening from two possible explanations. The first of the two explanations is that the strengthening is purely due to an enhancement of the tangential stress. The second explanation is that the strengthening is due to sealing or propping the fracture and which renders initiating a new fracture a more challenging task, effectively working as a lost-circulation material. Gaining this understanding will help in deciding whether applying a wellbore strengthening technique or protecting the tangential stress from wellbore flow and other disturbances is a more viable direction of action.

NOMENCLATURE

A = Area, ft²

a = Plugging particle placement depth in the fracture, inch

$[C]$ = The resultant transformation matrix of the second order transformation for a Cartesian tensor, dimensionless

$[C_x]$ = Rotation matrix about the x-axis by a constant angle, dimensionless

$[C_y]$ = Rotation matrix about the y-axis by a constant angle, dimensionless

$[C_z]$ = Rotation matrix about the z-axis by a constant angle, dimensionless

E = Young's modulus, psi

ECD = Equivalent Circulation Density, ppg

$F_1(s)$ = First function of the ratio of fracture length to fracture length and wellbore radius, dimensionless

$F_0(s)$ = Second function of the ratio of fracture length to fracture length and wellbore radius, dimensionless

$F_\lambda(s)$ = Function of stress anisotropy and the ratio of fracture length to fracture length and wellbore radius, dimensionless

F_{x_1} = Forces resulting from normal and shear stresses acting in the direction of the rotated axis x_1 for principle plane stresses determination, lb

F_{y_1} = Forces resulting from normal and shear stresses acting in the direction of the rotated axis y_1 for principle plane stresses determination, lb

g_f = The fracture pressure gradient, pis/ft

g_{fi} = The initial undisturbed fracture pressure gradient, pis/ft

$g_{fi(T)}$ = The temperature influenced fracture pressure gradient, pis/ft

$g_{fi(q)}$ = The mud filtrate influenced fracture pressure gradient, pis/ft

$g_{fi(qT)}$ = The temperature and mud filtrated combined influenced fracture pressure gradient, pis/ft

g_{fFS} = The wellbore strengthening influenced fracture pressure gradient, pis/ft

$g_{fFS(T)}$ = The temperature and wellbore strengthening influenced fracture pressure gradient, pis/ft

$g_{fFS(q)}$ = The mud filtrate and wellbore strengthening influenced fracture pressure gradient, pis/ft

$g_{fFS(qT)}$ = The temperature, mud filtrated and wellbore strengthening combined influenced fracture pressure gradient, pis/ft

H = Length of the hypotenuse, ft

k^c = Fracture toughness, $\text{psi}\cdot\text{inch}^{1/2}$

- L = Total length of plug placement, fracture length, and wellbore radius, inch
- P_{bu} = Build up pressure in the fracture, psi
- $P_{f-enhanced}$ = Enhanced wellbore fracture pressure, psi
- P_p = Pore pressure, psi
- P_w = Wellbore pressure, psi
- r = Radial distance from the wellbore axis, inch
- r_w = Wellbore radius, in
- s = Ratio of fracture length to fracture length and wellbore radius, dimensionless
- $T_{drilling\ fluid}$ = Temperature of the drilling fluid, F°
- $T_{formation}$ = Temperature of the formation, F°
- ν = Poisson's ratio, dimensionless
- W_c = Fracture aperture, inch
- α = Biot's constant, dimensionless
- α_T = Coefficient of thermal expansion, $in/(in-F^{\circ})$
- β = Wellbore projection angle on the horizontal stresses plane, degree
- ΔL = Fracture length, inch

$\Delta\sigma_{te(q)}$ = Change of the effective tangential stress due to an overbalance in pressure and continuous flow, psi

$\Delta\sigma_{te(T)}$ = Change of the effective tangential stress due to temperature variations, psi

γ = Wellbore inclination angle, degree

λ = Stress anisotropy ratio, dimensionless

ω = Build up pressure to the minimum principle stress ratio, dimensionless

σ = Normal stress, psi

$[\sigma]$ = The stresses in the original coordinate system matrix, psi

$[\sigma_c]$ = The resulting transformed stresses in the wellbore reference coordinate system matrix, psi

σ_1 = Maximum wellbore principle plane stress acting perpendicularly on the fracture plane, psi

σ_2 = Minimum wellbore principle plane stress acting parallel on the fracture plane, psi

σ_3 = Third wellbore principle plane stress acting radially on the fracture plane, psi

σ_e = Effective normal stress, psi

σ_H = Maximum horizontal stress, psi

σ_h = Minimum horizontal stress, psi

- σ_r = Radial induced wellbore stress, psi
- σ_t = Total tangential induced wellbore stress, psi
- σ_{t1} = First component of the tangential induced wellbore stress, psi
- σ_{t2} = Second component of the tangential induced wellbore stress, psi
- σ_{t3} = Third component of the tangential induced wellbore stress, psi
- σ_v = Vertical stress, psi
- σ_x = Normal stress in the x-axis direction of the wellbore reference coordinates, psi
- σ_{x_1} = Normal stress in the direction of the rotated axis x_1 for principle plane stresses determination, psi
- σ_y = Normal stress in the y-axis direction of the wellbore reference coordinates, psi
- σ_{y_1} = Normal stress in the direction of the rotated axis y_1 for principle plane stresses determination, psi
- σ_z = Normal stress in the z-axis direction of the wellbore reference coordinates, psi
- σ_{zz} = Axial induced wellbore stress, psi
- τ = Shear stress, psi
- τ_{rt} = Radial-tangential induced shear stress acting on the axial-tangential (σ_r - σ_t) stresses planes, psi

τ_{rzz} = Radial-axial induced shear stress acting on the axial-tangential (σ_r - σ_{zz}) stresses planes, psi

τ_{tzz} = Tangential-axial induced shear stress acting on the axial-tangential (σ_{zz} - σ_t) stresses planes, psi

τ_{yz} = Shear stress on the yz plane of the wellbore reference coordinates, psi

τ_{xz} = Shear stress on the xz plane of the wellbore reference coordinates, psi

τ_{xy} = Shear stress on the xy plane of the wellbore reference coordinates, psi

$\tau_{x_1y_1}$ = Shear stress on the x_1y_1 plane of the rotated coordinates for principle plane stresses determination, psi

θ = Wellbore circumferential position angle, degree

θ_c = Critical wellbore circumferential position angle, degree

ξ = Angle of deviation from the wellbore axis, degree

ξ_p = Angle of deviation of the principle or fracture plane from the wellbore axis, degree

REFERENCES

- Aadnoy, B. S. 1987. Stresses Around Horizontal Boreholes Drilled In Sedimentary Rocks. Society of Petroleum Engineers. SPE-17119-MS.
- Amadei, B. and Stephansson, O. 1997. Estimating In Situ Stresses. In *Rock Stress And Its Measurement*, first edition, Chap. 2, 23-41. London: Chapman and Hall.
<http://dx.doi.org/10.1007/978-94-011-5346-1>.
- Amadei, B. and Stephansson, O. 1997. Hydraulic Methods. In *Rock Stress And Its Measurement*, first edition, Chap. 4, 157-160. London: Chapman and Hall.
<http://dx.doi.org/10.1007/978-94-011-5346-1>.
- Aston, M. S., Alberty, M. W., Duncum, S. D. et al. 2007. A New Treatment for Wellbore Strengthening in Shale. Paper SPE 110713 presented at the SPE Annual Technical Conference and Exhibition, Anaheim, California, 11-14 November.
<http://dx.doi.org/10.2118/110713-MS>.
- Aston, M. S., Alberty, M. W., McLean, M. R. et al. 2004. Drilling Fluids for Wellbore Strengthening. Paper SPE 87130 presented at IADC/SPE Drilling Conference, Dallas, Texas, 2-4 March. <http://dx.doi.org/10.2118/87130-MS>.
- Attong, D. J., Singh, U. B., and Teixeira, G. 1995. Successful Use of a Modified MWD Tool in a High-Concentration LCM Mud System. *SPE Drilling & Completion* **10** (1): 22-26. SPE-25690-PA. <http://dx.doi.org/10.2118/25690-PA>
- Barrett, S., Manescu, G., Vasquez Cueva, G. E. and Growcock, F. 2010. Wellbore Strengthening: Where Field Application Meets Theory. Paper SPE 139167 presented at the SPE Latin American and Caribbean Petroleum Engineering Conference, Lima, Peru, 1-3 December. <http://dx.doi.org/10.2118/139167-MS>.
- Daneshy, A. A. 1973. A Study of Inclined Hydraulic Fractures. *Society of Petroleum Engineers Journal* **13** (2): 61-68. SPE-4062-PA. <http://dx.doi.org/10.2118/4062-PA>.
- Deily, F. H. and Owens, T. C. 1969. Stress Around A Wellbore. Paper SPE 2557 presented at the Fall Meeting of the Society of Petroleum Engineers of AIME, Denver, Colorado, 28 September-1 October. <http://dx.doi.org/10.2118/2557-MS>.
- Dick, M. A., Heinz, T. J., Svoboda, C. F., & Aston, M. 2000. Optimizing the Selection of Bridging Particles for Reservoir Drilling Fluids. Paper SPE 58793 presented at the

SPE International Symposium on Formation Damage Control, Lafayette, Louisiana, 23-24 February. <http://dx.doi.org/10.2118/58793-MS>

Duffadar, R. D., Dupriest, F. E. and Zeilinger, S. C. 2013. Practical Guide to Lost Returns Treatment Selection Based on a Holistic Model of the State of the Near Wellbore Stresses. Paper SPE 163481 presented at SPE/IADC Drilling Conference, Amsterdam, The Netherlands, 5-7 March. <http://dx.doi.org/10.2118/163481-MS>.

Dupriest, F. E., Smith, M. V. et al. 2008. Method To Eliminate Lost Returns and Build Integrity Continuously With High-Filtration-Rate Fluid. Paper SPE 112656 presented at the IADC/SPE Drilling Conference, Orlando, Florida, 4-6 March. <http://dx.doi.org/10.2118/112656-MS>.

Fjaer, E., Holt R. M., Horsrud P. et al. 2008. *Petroleum Related Rock Mechanics*, second edition. Amsterdam: Elsevier.

He, W. and Stephens, M. P. 2011. Bridging Particle Size Distribution in Drilling Fluid and Formation Damage. Paper SPE 143497 presented at the SPE European Formation Damage Conference, Noordwijk, The Netherlands, 7-10 June. <http://dx.doi.org/10.2118/143497-MS>

Hibbler, R. C. 2011. Stress Transformation. In *Mechanics of Materials*, eighth edition, Chap. 9, 445-460. Boston: Pearson Prentice Hall.

Jaeger, J.C., Cook, N.G.W. and Zimmerman, R. W. 2007. *Fundamentals of Rock Mechanics*, fourth edition. London: Blackwell Publishing.

Kirsch E.G. 1898. *Die Theorie der Elastizität und die Bedürfnisse der Festigkeitslehre. Zeitschrift des Vereines deutscher Ingenieure*, 42, 797–807.

Kulatilake, P., Balasingam, P., Park, J. et al. 2006. Natural Rock Fracture Aperture Properties through Fractals. American Rock Mechanics Association. Paper presented at the Golden Rocks the 41st U.S. Symposium on Rock Mechanics (USRMS), Golden, Colorado, 17-21 June. ARMA-06-936

Mitchell, R. and Miska, S. 2011. *Fundamentals of Drilling Engineering*, Vol.12, 60. Richardson, Texas: Textbook Series, SPE.

Morita, N. and Fuh, G.-F. 2012. Parametric Analysis of Wellbore-Strengthening Methods From Basic Rock Mechanics. *SPE Drilling & Completion* **27** (2): 315-327. SPE-145765-PA. <http://dx.doi.org/10.2118/145765-PA>.

Mouchet, J.P. and Mitchell A. 1989. Quantitative Pressure Evaluation. In *Abnormal Pressures while Drilling - Origins, Prediction, Detection, Evaluation*, Chap. 4, 224-227. Paris: Editions Technip.

Nas, S. W. 2010. Deepwater Managed Pressure Drilling Applications. Paper SPE 132049 presented at the International Oil and Gas Conference and Exhibition in Beijing, China, 8-10 June. <http://dx.doi.org/10.2118/132049-MS>.

Perkins, T. K. and Gonzalez, J. A. 1984. Changes in Earth Stresses Around a Wellbore Caused by Radially Symmetrical Pressure and Temperature Gradients. *Society of Petroleum Engineers Journal* **24** (2): 129-140. SPE-10080-PA. <http://dx.doi.org/10.2118/10080-PA>.

Raymond, L. R. 1969. Temperature Distribution in a Circulating Drilling Fluid. *Journal of Petroleum Technology* **21** (3): 333-341. SPE-2320-PA. <http://dx.doi.org/10.2118/2320-PA>.

Richardson, R. M. 1983. Hydraulic Fracture in Arbitrary Oriented Boreholes: An Analytic Approach. In *Hydraulic Fracturing Stress Measurements*, Chap. 3, 167-175. Washington, D.C.: National Academy Press.

Senseny, P. E. and Pfeifle, T. W. 1984. Fracture Toughness of Sandstones and Shales. Paper presented at the 25th U.S. Symposium on Rock Mechanics (USRMS), Evanston, Illinois, 25-27 June, ARMA-84-0390

Soroush, H., Sampaio, J. H. B. et al. 2006. Investigation into Strengthening Methods for Stabilizing Wellbores in Fractured Formations. Paper SPE 101802 presented at the SPE Annual Technical Conference and Exhibition, San Antonio, Texas, 24-27 September. <http://dx.doi.org/10.2118/101802-MS>.

Terzaghi, K. 1936. The Shear Resistance of Saturated Soils and the angle between the planes of shear. In *Proceedings of 1st International Conference of Soil Mechanics Found. Engineering* **1** (1): 54-56.

Thiercelin, M., Jeffrey, R. G. and Naceur, K. B. 1989. Influence of Fracture Toughness on the Geometry of Hydraulic Fractures. *SPE Production Engineering* **4** (4): 435-442. SPE-16431-PA <http://dx.doi.org/10.2118/16431-PA>.

Tingay, M., Muller, B., Reinecker, J. et al, O. 2006. State and Origin of the Present-Day Stress Field in Sedimentary Basins: New Results from the World Stress Map Project. Paper presented at the Golden Rocks the 41st U.S. Symposium on Rock Mechanics (USRMS), Golden, Colorado, 17-21 June. ARMA-06-1049.

Watson, D., Brittenham, T. and Moore, P. 2003. *Advanced Well Control*, Vol. 10, 98–112. Richardson, Texas: Textbook Series, SPE.

Zhao, X. L. and Roegiers, J. C. 1993. Determination of In-Situ Fracture Toughness. Paper presented at the 34th U.S. Symposium on Rock Mechanics (USRMS), Madison, Wisconsin, 28-30 June, ARMA-93-0668